Wall interactions of spin-polarized atoms

Zhen Wu

Rev. Mod. Phys. **93**, 035006 — Published 9 September 2021

DOI: 10.1103/RevModPhys.93.035006

Wall Interactions of Spin-Polarized Atoms

Zhen Wu*

Department of Physics, Rutgers, the State University of New Jersey, Newark, NJ 07102

Spin-polarized atoms have applications in many areas such as biological magnetic resonance imaging, optical magnetometry, atomic clocks and fundamental symmetry studies. Polarized atoms are often held in a container, most commonly a glass cell. Their interactions with the walls of the container during their collisions with the walls are often the main cause of spin relaxation, which determines the ultimate attainable polarization, and frequency shift, which for example affects the long term frequency stability in atomic clocks. This paper presents a critical review of the studies done in the past six decades of the wall interactions of spin-polarized atoms, including the hydrogen atom, alkali metal atoms, and diamagnetic atoms with $^1S_0$ ground states such as mercury, cadmium and noble gas atoms. It summarizes the progress that has been made in understanding the nature of wall interactions and the physical mechanisms of spin relaxation and frequency shift due to wall collisions. It also points out those issues, particularly in connection with the widely used anti-relaxation coatings, that remain to be understood.

CONTENTS

I. Introduction 1

II. Wall Interactions of Spin-Polarized Diamagnetic Atoms with $^1S_0$ Ground States and Nuclear Spins $I \geq 1$ 2
  A. The nature of the wall interactions 2
  B. Quadrupole wall interaction − theory 3
    1. Boundary condition 3
    2. Perturbation theory 4
  C. Quadrupole wall interaction − experiment 5

III. Wall Interactions of Spin-Polarized Noble Gas Atoms with Nuclear Spins $I = 1/2$ 8
  A. The nature of the wall interactions 8
  B. Wall relaxation of ^{3}He 9
  C. Wall relaxation of ^{129}Xe 11
    1. Mechanisms 11
    2. Theory 12
    3. Experiments 13
  D. Cross polarization 13

IV. Wall Interactions of Spin-Polarized Alkali Metal Atoms 14
  A. The nature of the wall interactions 14
  B. Study of the wall interactions of alkali metal atoms in the time domain 15
    1. Relaxation of Rb on paraffin-coated walls − theory 15
    2. Relaxation of Rb on paraffin-coated walls − experiment 15
  C. Study of the wall interactions of alkali metal atoms in the frequency domain 16
    1. Edge enhanced EPR in optically pumped Rb vapor 16
    2. Study of wall interactions using edge enhanced EPR 18
  D. Spatial distribution of the polarization of the alkali metal atoms near the wall 19
    1. Normal gradient coefficient 19
    2. Zeeman polarization near the wall 19
    3. Hyperfine polarization near the wall 19
  E. Phase shift of hyperfine transitions due to wall collisions 20
  F. Wall interactions on alkali hydride 21
    1. Polarization of alkali hydride walls 21
    2. Phase shift of Zeeman transitions on alkali hydride walls 21

V. The Time Scale of Wall Interactions 22
  A. Correlation time τ_c 22
  B. Average dwell time τ_s on the wall 22
  C. Average dwell time τ_s' at a given site 25

VI. Anti-relaxation Coatings 26

VII. Instrumentation 28
  A. Absorption monitoring 29
  B. Polarization monitoring − Poincaré sphere 29
    1. Photoelastic modulator 29
    2. Wollaston prism 30
  C. Evanescent wave monitoring 30

VIII. Summary 30

Acknowledgments 31

References 31

I. INTRODUCTION

Spin-polarized atoms have found applications in many areas, such as biological magnetic resonance imaging using nuclear spin polarized ^{129}Xe and ^{3}He (Albert *et al.*, 1994; Middleton *et al.*, 1995), optical magnetometry based on polarized alkali metal atoms for measuring static and radio-frequency magnetic fields (Böhi *et al.*, 2010; Böhi and Treutlein, 2012; Budker and Romalis, 2007; Budker *et al.*, 2002, 1998; Cohen-Tannoudji *et al.*, 1969; Dang *et al.*, 2010; Farooq *et al.*, 2020; Kominis *et al.*, 2003; Savukov *et al.*, 2005), atomic frequency standards (Robinson and Johnson, 1982; Vanier and Audoin, 1989), NMR gyroscopes (Kitching *et al.*, 2011), miniature atomic devices (Balabas *et al.*, 2006; Knappe *et al.*, 2004;

---

* zw52@caa.columbia.edu

Schwindt *et al.*, 2004; Zhao and Wu, 2006), polarized ^{3}He as targets for scattering experiments and neutron spin filters (Chupp *et al.*, 1987; Coulter *et al.*, 1990; Heil *et al.*, 1999; Jones *et al.*, 2000; Phillips *et al.*, 1962), fundamental symmetry studies (Bouchiat *et al.*, 1982; Chupp *et al.*, 1989; Hallin *et al.*, 1984; Lamoreaux *et al.*, 1986), search for long-range nuclear spin-dependent forces (Vasilakis *et al.*, 2009), search for an electric dipole moment in polarized ^{129}Xe and ^{199}Hg (Griffith *et al.*, 2009; Rosenberry and Chupp, 2001; Vold *et al.*, 1984), sensitive surface probe using polarized ^{129}Xe atoms (Raftery *et al.*, 1991), measurement of quadrupole moments of radioactive noble gas nuclei (Kitano *et al.*, 1986), squeezed spin states of polarized alkali metal atoms (Kuzmich *et al.*, 2000), quantum memory based on spin-polarized alkali metal atoms (Julsgaard *et al.*, 2004; Schori *et al.*, 2002) and study of Berry's phase using polarized ^{131}Xe (Appelt *et al.*, 1994).

Alkali metal atoms and diamagnetic atoms such as mercury and cadmium are typically polarized by optical pumping (Happer, 1972; Kastler, 1950). The nuclei of the noble gas atoms are polarized by spin exchange with optically pumped alkali metal atoms (Bouchiat *et al.*, 1960; Grover, 1978; Walker and Happer, 1997). The ^{3}He nucleus can also be polarized by optically pumping the metastable state $2\,^3S_1$ followed by a collision with a ground state ^{3}He atom, transferring the excitation energy to the ground state ^{3}He atom while retaining its nuclear polarization (Colegrove *et al.*, 1963; Walters *et al.*, 1962). Polarized atoms are often held in a container, most commonly a glass cell. Their collisions with the cell walls constitute one of the most important and complicated mechanisms for spin relaxation and frequency shift. Two approaches have been used to mitigate these effects. In the first approach used for alkali metal atoms, the cell is filled with buffer gas such as N_2 or other inert gases of a few torr or more to slow down the diffusion of the polarized alkali metal atoms to the glass walls (Brossel *et al.*, 1955). However, the use of buffer gas leads to inhomogeneous line broadening if the magnetic field is inhomogeneous (Watanabe and Robinson, 1977). Also, due to wall interactions, the polarization of the alkali metal atoms is not uniform near the wall (Grafström and Suter, 1995). An alternative approach used for both alkali metal atoms and noble gas atoms is to coat the inner walls of the glass cells with anti-relaxation coatings, which can greatly reduce the relaxation rate and frequency shift of polarized atoms due to wall collisions. The use of anti-relaxation coatings stimulated extensive studies of the wall interactions of spin-polarized atoms. Recent interest in miniature atomic devices makes the wall interactions of polarized atoms even more important because of the high surface to volume ratio in these devices (Kitching, 2018).

Wall interactions of spin-polarized atoms have been studied for more than six decades. An excellent summary of the early studies was given in the classic review by Happer (1972). Much progress has since been made. This paper aims to give a critical review of the studies done in the past six decades of the wall interactions of spin-polarized atoms. Because of the large scope of the field, it will focus on the nature of wall interactions, the physical mechanisms of spin relaxation and frequency shift due to wall collisions, and the determination of the microscopic parameters that characterize wall interactions.

Long-range wall interactions of atoms occurring in the vicinity (1–1000 nm) of the wall have been reviewed by Bloch and Ducloy (2005).

In section II the wall interactions of nuclear-spin polarized diamagnetic atoms with $^1S_0$ ground states and nuclear spins $I \geq 1$ such as ^{201}Hg ($I = 3/2$), ^{109}Cd ($I = 5/2$), ^{131}Xe ($I = 3/2$), ^{83}Kr ($I = 9/2$) and ^{21}Ne ($I = 3/2$) are discussed. In section III the wall interactions of spin-polarized noble gas atoms with nuclear spins $I = 1/2$, ^{3}He and ^{129}Xe, are reviewed. In section IV, the wall interactions of spin-polarized alkali metal atoms are reviewed both in the time domain and in the frequency domain. In section V, we discuss the importance as well as the determination of the microscopic time parameters that characterize wall interactions such as the correlation time τ_c, the average dwell time τ_s that a polarized atom spends on the wall without being depolarized, and the average dwell time τ_s' it stays at a given site on the wall. The widely used anti-relaxation coatings are discussed in section VI. Section VII gives a brief review of some of the instrumentation commonly used in the study of wall interactions. Finally, section VIII concludes this review with a brief summary.

II. WALL INTERACTIONS OF SPIN-POLARIZED DIAMAGNETIC ATOMS WITH $^1S_0$ GROUND STATES AND NUCLEAR SPINS $I \geq 1$

A. The nature of the wall interactions

The nature of the wall interactions of nuclear-spin polarized diamagnetic atoms ($I \geq 1$) with a nuclear quadrupole moment such as ^{201}Hg, ^{109}Cd, ^{131}Xe, ^{83}Kr and ^{21}Ne is elucidated by the following observations. It was found that for ^{201}Hg the relaxation rate for the alignment was twice as fast as for the orientation (Cohen-Tannoudji, 1963). Beats were observed in the free precession signal of ^{201}Hg (Simpson, 1978), and later were also observed for ^{131}Xe, ^{83}Kr and ^{21}Ne, indicating an unequal splitting between the nuclear Zeeman levels. Furthermore, the beat frequency depends on the angle between the symmetry axis of the cell and the magnetic field. The observations of these phenomena, signature characteristics of quadrupole interaction, unambiguously show that the dominant wall interaction of the diamagnetic atoms ($I \geq 1$) with a nuclear electric quadrupole moment is the quadrupole coupling between the nuclear quadrupole moment and the fluctuating electric field gradient at the cell wall. This is also corroborated by the following observations. No beat phenomena are observed for ^{199}Hg ($I = 1/2$) and ^{129}Xe ($I = 1/2$), which do not possess nuclear quadrupole moments. Furthermore, the relaxation rate of ^{201}Hg is almost one order of magnitude larger than that of ^{199}Hg even though their nuclear magnetic moments are approximately the same (Cagnac and Brossel, 1959).

Thus the wall interaction Hamiltonian H_w is given by

$$H_\mathrm{w} = \frac{1}{6}\sum_{i,j} eQ_{ij}\frac{\partial^2 V_\mathrm{w}}{\partial x_i \partial x_j} , \qquad (1)$$

where e is the proton charge and the microscopic electric field gradients $\partial^2 V_\mathrm{w}/\partial x_i \partial x_j$, V_w being the electric potential, couple to the nuclear electric quadrupole moment tensor Q_{ij} of the adsorbed atom. The field gradients are produced by, for example, the polar groups on the walls such as –OH, –ONa, etc. Due to the motions of the adsorbed atom and the atoms of the wall, these field gradients fluctuate in time. The field gradients at the nucleus of the adsorbed diamagnetic atom may also be greatly modified because of the Sternheimer shielding or antishielding by the induced field gradient in the electron shells (Campbell *et al.*, 1981).

The wall interaction between the magnetic moment of the nucleus of the diamagnetic atom and the microscopic local magnetic field is neglected in H_w because as previously mentioned it plays a much less important role in comparison with the quadrupole wall interaction.

B. Quadrupole wall interaction – theory

The theory of the nuclear spin relaxation of diamagnetic ^{201}Hg due to the quadrupole wall interaction was first developed by Cohen-Tannoudji (1963), who, applying the theory of Abragam (1961) for the relaxation in liquids and gases to the quadrupole wall interaction of ^{201}Hg, calculated T_1 and T_2 for ^{201}Hg in quartz cells. The calculation shows that the relaxation rate for alignment is twice as fast as for orientation, one of the signature characteristics of the quadrupole coupling of the nuclear quadrupole moment to the fluctuating electric field gradients. The theory does not consider the shift in the magnetic resonance frequencies of ^{201}Hg due to the quadrupole wall interaction.

Following a suggestion by Happer, Volk *et al.* (1979) and Kwon *et al.* (1981) developed a semiquantitative theory of the coherent quadrupole wall interaction for ^{83}Kr and ^{131}Xe based on perturbation theory. It is assumed that, when the atoms are adsorbed on the wall, they interact through their nuclear electric quadrupole moment with a constant ensemble-averaged electric field gradient with a cylindrical symmetry around the cell symmetry axis. The quadrupole wall interaction is treated as a perturbation. The first order corrections to the Zeeman energy levels explain the beats and confirm the dependence of the beat period on the cell orientation with respect to the external magnetic field. The theory, however, does not explain the dependence of the beat frequency on the cell asymmetry, nor does it address the interplay between wall interactions and diffusion in the gas phase, for example, the important question of how fast the atoms must diffuse throughout the cell to effectively sample the entire inner surface of the cell.

Generalizing the work by Masnou-Seeuws and Bouchiat (1967) for the wall relaxation of alkali metal atoms, Happer developed a perturbative theory of the coherent quadrupole wall interaction for diamagnetic atoms with nuclear spins $I \geq 1$ (Wu *et al.*, 1988), which allows the microscopic parameters of the quadrupole wall interaction to be deduced from the experimental data. The theory will be briefly reviewed here. The boundary condition will be stated in a more general form.

1. Boundary condition

Consider a gas of diamagnetic atoms with a nuclear spin $I \geq 1$ and a nuclear quadrupole moment Q, for example ^{131}Xe, contained in a glass cell in a static magnetic field B_0 along the z-axis. The gas phase interaction Hamiltonian of the atoms is $H_0 = -\hbar\gamma_I B_0 I_z = -\hbar\Omega_0 I_z$, where γ_I is the gyromagnetic ratio and $\Omega_0 = \gamma_I B_0$ is the Larmor frequency. Neglecting gas phase spin relaxation, the evolution of the density matrix of the atoms in the gas phase is given by,

$$\frac{\partial\rho(t)}{\partial t} = \frac{1}{i\hbar}[H_0, \rho(t)] + D\nabla^2\rho(t) , \qquad (2)$$

where D is the diffusion constant. The evolution of the density matrix of the atoms while they are adsorbed on the wall is given by

$$\frac{\partial\rho(t)}{\partial t} = \frac{1}{i\hbar}[H_\mathrm{w}(t), \rho(t)] , \qquad (3)$$

where H_0 is assumed to be small enough to be neglected during the adsorption time τ on the wall. Eq.(3), which describes the wall interaction, can be converted into a boundary condition. Since $H_\mathrm{w}\tau$ is small, one can solve Eq.(3) for $\rho(\tau)$ by iteration. Taking the ensemble average, we obtain

$$\langle\rho(\tau)\rangle = \mathcal{E}\rho(0) = (1 + \epsilon^{(1)} + \epsilon^{(2)} + \cdots)\rho(0) , \qquad (4)$$

where $\langle\rho(\tau)\rangle$ is the density matrix after the collision and $\rho(0)$ the density matrix before the collision. The brackets in $\langle\rho(\tau)\rangle$ represent the ensemble average over the fluctuating $H_{\rm w}$ and also over the adsorption time τ on the wall. The terms in the series expansion of the operator $\mathcal{E}$ are

$$\epsilon^{(1)}\rho(0) = \frac{1}{i\hbar}\left\langle \int_0^\tau dt\,[H_{\rm w}(t),\rho(0)]\right\rangle \ , \tag{5}$$

$$\epsilon^{(2)}\rho(0) = \frac{1}{(i\hbar)^2} \times \left\langle \int_0^\tau dt \int_0^t dt' \Big[H_{\rm w}(t),[H_{\rm w}(t'),\rho(0)]\Big]\right\rangle \ . \tag{6}$$

Let J_+ and J_- be respectively the current of polarized atoms into the wall and out of the wall. From kinetic theory we have

$$J_+(0) = \frac{n\bar{v}}{4}\left(\rho(0) - \frac{2\lambda}{3}\frac{\partial\rho(0)}{\partial n}\right) \ , \tag{7}$$

where n is the density of ^{131}Xe atoms, $\bar{v} = (8kT/\pi m)^{1/2}$ their mean speed, λ the mean free path, and $\partial/\partial n = \boldsymbol{n}\cdot\boldsymbol{\nabla}$, with $\mathbf{n}$ being the normal vector pointing out of the cell wall. We assume that the net current to the wall is given by the law of diffusion:

$$J_+(0) - J_-(0) = -nD\frac{\partial\rho(0)}{\partial n} \ . \tag{8}$$

We also assume that every atom, after colliding with the wall, stays on the wall for an average time τ_s before it leaves the wall as an evolved atom. Thus

$$J_-(\tau_s) = \mathcal{E}J_+(0) \ . \tag{9}$$

From Eqs.(7)−(9) one obtains the boundary condition, after neglecting the term $\partial^2\rho(0)/\partial n\partial t$ and replacing $\partial\rho(0)/\partial t$ by $D\partial^2\rho(0)/\partial n^2$ with $D = \lambda\bar{v}/3$,

$$\frac{\partial\rho}{\partial n} = -\mu\rho - \eta\frac{\partial^2\rho}{\partial n^2} \ , \tag{10}$$

where

$$\mu = -\frac{3}{2\lambda}(\mathcal{E}+1)^{-1}(\mathcal{E}-1) \ , \tag{11}$$

$$\eta = \frac{\tau_s\bar{v}}{2}(\mathcal{E}+1)^{-1} \ . \tag{12}$$

Using the series expansion of $\mathcal{E}$, the operators μ and η are given by, to the lowest two orders,

$$\mu = -\frac{3}{4\lambda}\left(\epsilon^{(1)} + \epsilon^{(2)} - \frac{1}{2}\epsilon^{(1)}\epsilon^{(1)} + \cdots\right) \ , \tag{13}$$

$$\eta = \frac{\tau_s\bar{v}}{4}\left(1 - \frac{1}{2}\epsilon^{(1)} - \cdots\right) \ . \tag{14}$$

The boundary condition (10) embodies the wall interactions of spin-polarized atoms, with μ and η being determined by the wall interactions. When combined with the diffusion equation (2) or the Torrey equation (55), depending on whether the magnetic field is uniform (Sec. II.B, Sec. IV.F.2 and Sec. V.B) or there is a field gradient (Sec. IV.C), the boundary condition (10) gives a full description of the wall interactions as well as their interplay with the diffusion in the gas phase. Depending on the experimental conditions, the second derivative term in (10) is sometimes required (Sec. IV.C and Sec. V.B) and sometimes not (Sec. II.B and Sec. IV.F.2). A discussion of the experimental conditions under which the second derivative term in (10) cannot be neglected is given in Sec. IV.C.1. For some experiments μ and η in (10) are treated as operators (Sec. II.B) while for others they are treated as parameters (Sec. IV.C, Sec. IV.F.2 and Sec. V.B).

The physical meaning of the second derivative term in the boundary condition (10) is that it describes a meniscus-like behavior at the wall (Schaden *et al.*, 2007).

Due to the high solubility of Xe gas in silicone compounds, the Ostwald solubility coefficient being of the order of one (Steinberg and Manowitz, 1959), Xe atoms can readily dissolve in the coating, and consequently have very long dwell times τ_s in coated cells (Driehuys *et al.*, 1995), which in the case of ^{131}Xe leads to a very short relaxation time because of the quadrupole interaction (Wu *et al.*, 1990). Therefore the experimental studies of the quadrupole wall interaction of ^{131}Xe are performed in uncoated cells or cells coated with coatings such as alkali hydride, where τ_s is expected to be short. Thus the second derivative term in the boundary condition (10) can be neglected, and we have

$$\frac{\partial\rho}{\partial n} = -\mu\rho \ . \tag{15}$$

Boundary conditions formally similar to Eq.(15) were first used by Maxwell to describe the phenomenon of viscous slip discovered by Kundt and Warburg in 1875 (Kennard, 1938), and later by Masnou-Seeuws and Bouchiat (1967) in the study of the wall relaxation of alkali metal atoms. Instead of Eq.(9), they assume

$$J_-(\tau_s^B) = (1-\xi_s^B)J_+(0) \ , \tag{16}$$

where τ_s^B is the average time a polarized atom stays on the wall and $0 < \xi_s^B < 1$ represents the relaxation probability of Rb atoms on the wall. Thus, $\mathcal{E} = 1 - \xi_s^B$ is a number, and Eq.(10) becomes

$$\frac{\partial\rho}{\partial n} = -\frac{3\,\xi_s^B}{2\lambda(2-\xi_s^B)}\,\rho \ - \frac{\tau_s^B\bar{v}}{2(2-\xi_s^B)}\frac{\partial^2\rho}{\partial^2 n} \ . \tag{17}$$

Neglecting the second derivative term in Eq.(17) one obtains the boundary condition used by Masnou-Seeuws and Bouchiat (1967).

2. Perturbation theory

Since the coherences $P_{mn} = |m\rangle\langle n|$, where $I_z|m\rangle = m|m\rangle$, are orthonormal in the sense that $\mathrm{Tr}(P^\dagger_{mn}P_{m'n'}) =$

$\delta_{mm'}\delta_{nn'}$, we can expand ρ in terms of P_{mn}

$$\rho(\boldsymbol{r}, t) = \sum_{mn} P_{mn} f_{mn}(\boldsymbol{r}, t) \ . \tag{18}$$

The diffusion equation (2) becomes the following set of equations for the amplitudes $f_{mn}(\boldsymbol{r}, t)$

$$\frac{\partial f_{mn}(\boldsymbol{r}, t)}{\partial t} = (D\nabla^2 + i\Omega_{mn}) f_{mn}(\boldsymbol{r}, t) \ , \tag{19}$$

where $\Omega_{mn} = (m-n)\Omega_0$. Let $f_{mn}(\boldsymbol{r}, t) = f_{mn}(\boldsymbol{r}) e^{-\gamma t}$. Eq.(19) becomes

$$(D\nabla^2 + i\Omega_{mn} + \gamma) f_{mn}(\boldsymbol{r}) = 0 \ . \tag{20}$$

The boundary condition (15) becomes, in terms of the amplitudes $f_{mn}(\boldsymbol{r})$,

$$\frac{\partial f_{mn}(\boldsymbol{r})}{\partial n} = -\sum_{m'n'} \mu_{mn,\, m'n'} f_{m'n'}(\boldsymbol{r}) \ . \tag{21}$$

The matrix elements $\mu_{mn,m'n'}$ of the normal gradient operator μ, functions of position on the cell wall, are defined by

$$\mu_{mn,\, m'n'} = \mathrm{Tr}\,(P^{\dagger}_{mn} \mu P_{m'n'}) \ . \tag{22}$$

The weak quadrupole wall interaction allows one to treat H_{w} as a small perturbation to non-relaxing walls, and solve γ, f_{mn} and $\mu_{mn,m'n'}$ perturbatively. Following the standard procedures of perturbation theory we introduce an expansion parameter $\varkappa$, and write H_{w} as $\varkappa H_{\mathrm{w}}$. We expand γ, f_{mn} and $\mu_{mn,m'n'}$ in Eqs.(20) and (21) as a power series of $\varkappa$, and, equating the coefficients of $\varkappa^l$ ($l = 0, 1, 2, \ldots$), obtain a set of equations and boundary conditions for each order. The zeroth order amplitude $f^{(0)}_{mn}$ is the solution of the diffusion equation subject to the boundary condition $\partial f^{(0)}_{mn}/\partial n = 0$, and can be written as $f^{(0)}_{\alpha;\, mn}$, where α denotes the diffusion mode ϕ_α. The solution that approximately describes the polarization in cells with weakly relaxing walls is the uniform diffusion mode $\phi_0 = 1/\sqrt{V}$, corresponding to polarized ^{131}Xe atoms diffusing freely throughout the cell with no relaxation on the wall. Thus the zeroth order eigenvalue is $\gamma^{(0)}_{0;mn} = -i\Omega_{mn}$, which is purely imaginary and corresponds to unperturbed magnetic resonance frequency. The theory assumes that gas pressures and magnetic fields are sufficiently low that the polarized ^{131}Xe atoms diffuse easily throughout the cell, making many wall collisions in one Larmor period.

For a cylindrical cell of diameter d and height h with its symmetry axis at an angle ψ with the direction of the quantizing magnetic field, the eigenvalue is, including up to second order pressure-independent corrections,

$$\begin{aligned}
\gamma_{0,\, mn} = i\Bigg[&-(m-n)\Omega_0 + \Delta\Omega_0 \frac{m^2 - n^2}{2I-1} P_2(\cos\psi) \\
&- \frac{(\Delta\Omega_0)^2}{8\,\Omega_0 (2I-1)^2} \Big[m\Big((4I^2 + 4I - 8m^2 - 1)\sin^2 2\psi \\
&\qquad - (2I^2 + 2I - 2m^2 - 1)\sin^4\psi \Big) \\
&\qquad - n\Big((4I^2 + 4I - 8n^2 - 1)\sin^2 2\psi \\
&\qquad - (2I^2 + 2I - 2n^2 - 1)\sin^4\psi \Big) \Big] \Bigg] \\
&+ \frac{2v}{45}\langle\theta^2\rangle \Big(\frac{1}{2h} + \frac{1}{d}\Big) \Big[\frac{I(I+1)(2I+3)}{2I-1} \\
&\qquad - \frac{[3m^2 - I(I+1)][3n^2 - I(I+1)]}{(2I-1)^2} \Big] \ ,
\end{aligned} \tag{23}$$

where $P_2(x) = \frac{1}{2}(3x^2 - 1)$ is the second-order Legendre polynomial, and the quadrupole frequency splitting is

$$\Delta\Omega_0 = \frac{v\langle\theta\rangle}{2} \left(\frac{1}{h} - \frac{1}{d} \right) \ . \tag{24}$$

The mean twist angle $\langle\theta\rangle$ and the mean-squared twist angle $\langle\theta^2\rangle$ experienced by the adsorbed atom are

$$\langle\theta\rangle = \langle\dot{\theta}_{nn}\rangle \tau_s \ , \tag{25}$$

and

$$\langle\theta^2\rangle = 5\langle\dot{\theta}^2_{nn}\rangle \frac{\tau_c \tau_s^2}{\tau_c + \tau_s} \ , \tag{26}$$

where the twist-rate tensor $\dot{\theta}_{ij}$ is defined by $\dot{\theta}_{ij} = (3eQ/4I\hbar)(\partial^2 V_{\mathrm{w}}/\partial x_i \partial x_j - \delta_{ij}\nabla^2 V_{\mathrm{w}}/3)$.

By treating μ as an operator, the perturbation theory describes the interplay between diffusion and wall interactions through higher order corrections. For example, the second order correction involving virtual excitations of diffusion modes with nonzero spatial frequencies by μ at the cell surface describes a pressure-dependent relaxation (Wu *et al.*, 1988).

C. Quadrupole wall interaction – experiment

Diamagnetic atoms – ^{201}*Hg* ($I = 3/2$) *and* ^{109}*Cd* ($I = 5/2$)

Early studies of the quadrupole wall interaction were done on optically pumped mercury and cadmium. The wall relaxation mechanisms of these diamagnetic atoms were determined by studying the relaxation times T_1 and T_2 of different isotopes. For example, Cagnac and Brossel (1959) found that ^{201}Hg relaxed almost ten times faster than ^{199}Hg in evacuated quartz cells. Since the isotopes ^{201}Hg and ^{199}Hg have approximately the same magnetic moments but only the former has a nuclear quadrupole moment, they suggested that the faster relaxation rate of ^{201}Hg was due to a quadrupole wall interaction while the slower relaxation rate of ^{199}Hg was due to a magnetic wall interaction, which played a minor role in the relaxation of ^{201}Hg. The exact nature of the wall relaxation of mercury due to the magnetic coupling is unknown.

The theoretical and experimental studies of ^{201}Hg carried out by Cohen-Tannoudji (1963) in cubic quartz cells confirmed that the dominant wall relaxation mechanism for ^{201}Hg was indeed the quadrupole wall interaction. It was found that the relaxation rate of alignment of ^{201}Hg was twice as large as that of orientation, in agreement with the theoretical prediction for quadrupole wall relaxation (Cohen-Tannoudji, 1963). No beating in the precession signal of ^{201}Hg was reported. This is probably because of the use of cubic cells, which, according to Eq.(24), have minimal quadrupole frequency splitting. From the measured relaxation rate of the alignment of ^{201}Hg and the assumption that $\tau_c = 10^{-12}\,\mathrm{s}$ and $\tau_s = 10^{-6}\,\mathrm{s}$, the root mean square of the electric field gradient was estimated to be $\sqrt{\langle q^2\rangle} = 1.7 \times 10^{10}\,\mathrm{C/m^3}$ at the nucleus of the ^{201}Hg atom, where $q = \partial^2 V_{\mathrm{w}}/\partial n^2$ is the electric field gradient along the surface normal.

Wall relaxation of the cadmium isotopes was studied by Leduc and Brossel (1968), who concluded that ^{109}Cd relaxed in the quartz cell mainly through a quadrupole wall interaction whereas ^{111}Cd ($I = 1/2$) through a magnetic wall interaction.

The first experimental observation of the beats in the free precession signals of ^{201}Hg in a fused silica cell was made by Simpson (1978), who also observed the remarkable angular dependence of the beat frequency, which goes to zero when the angle between the symmetry axis of the cell and the magnetic field approaches $\sim 55°$. The relaxation rate of ^{201}Hg depends on the orientation of the cell with respect to the external magnetic field.

^{131}Xe $(I = 3/2)$

Since the discovery of the nuclear polarization of the noble gas atoms by spin exchange collisions with optically pumped alkali metal atoms (Bouchiat *et al.*, 1960; Grover, 1978), the studies of the quadrupole wall interactions have been carried out for the noble gas atoms such as ^{131}Xe, ^{83}Kr and ^{21}Ne. In all these studies, the noble gas atoms were polarized by spin exchange with optically pumped Rb atoms, but the methods for monitoring the nuclear polarization varied among the studies.

The quadrupole wall interaction of ^{131}Xe was first studied in Pyrex glass cells by Kwon *et al.* (1981). After the ^{131}Xe atoms were polarized along a longitudinal field, the field was turned off and replaced by a precessional field in the perpendicular direction. The free precession of the nuclear polarization was monitored using Rb atoms as a magnetometer (Cohen-Tannoudji *et al.*, 1970). Both the beats and the angular dependence of the beat period observed by Simpson (1978) were confirmed. Using $E_a = 0.13\,\mathrm{eV}$ (Volk *et al.*, 1980) and assuming $\tau_0 = 10^{-12}\,\mathrm{s}$, they estimated that $\tau_s = 6.6 \times 10^{-11}\,\mathrm{s}$ (see Eq.(67)), which, when combined with the measured quadrupole splitting, yielded an estimate of the mean electric field gradient $\langle q\rangle = 1.15 \times 10^8\,\mathrm{C/m^3}$ at the ^{131}Xe nucleus (see Eqs. (24) and (25)).

The most quantitative experimental studies of the coherent quadrupole wall interaction of ^{131}Xe were made by Wu *et al.* (1987, 1990) in the rotating coordinate system. A longitudinal static magnetic field B_0 ($\sim 0.1\,\mathrm{G}$) with a long-term stability of $2\,\mu\mathrm{G}$ was along the z-axis, which coincided with the symmetry axis of the cell. This stability made it possible to study the small shift in the nuclear magnetic resonance frequency due to the wall interactions. Once the ^{131}Xe nuclei were polarized by spin

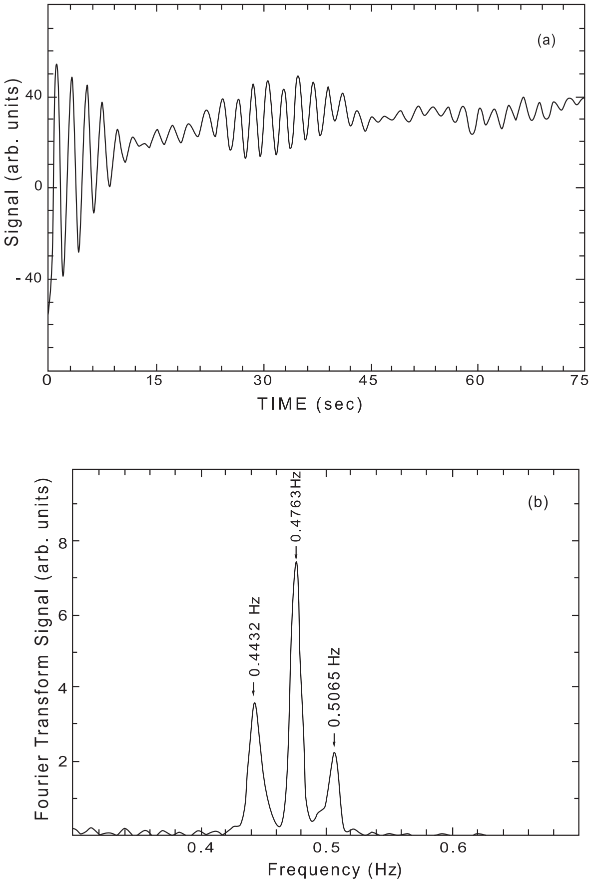

FIG. 1 Precession signal of ^{131}Xe in a cylindrical Pyrex-glass cell of diameter 1.28 cm and height 0.68 cm, which contained a few milligrams of natural Rb metal, 50 Torr of N_2 gas and 5 Torr of xenon, isotopically enriched to an assay of 70 at. % ^{131}Xe and 10 at. % ^{129}Xe. The partial pressures refer to 25°C. The fast oscillation is the Larmor precession in the rotating coordinate system at frequency $\Omega_0 = \omega_1$ since ω was chosen to be equal to ω_0. The signal is proportional to $\langle I_z\rangle$ of ^{131}Xe in the laboratory coordinate system. The Fourier transform of the transient signal of (a) is shown in (b). From Wu *et al.*, 1987.

exchange with optically pumped Rb atoms, the pump beam was blocked. An oscillating magnetic field $2B_1 \cos \omega t$ was applied along the x-axis. Larger values of B_1 were used for cells with larger quadrupole splitting. In a coordinate system rotating at frequency ω about the static field B_0, the ^{131}Xe nuclei precessed at a frequency $\Omega_0 = [(\omega_0 - \omega)^2 + \omega_1^2]^{1/2}$ about the effective magnetic field making an angle $\psi = \cos^{-1}[(\omega_0 - \omega)/\Omega_0]$ with the z-axis, where ω_1 is the Larmor frequency about the field B_1 and ω_0 that about the static field B_0. The nuclear polarization of ^{131}Xe was monitored by passing unpolarized light from a Rb resonance lamp as a probe beam through the cell. The Rb atoms polarized by ^{131}Xe imparted to the probe beam a minute amount of elliptical polarization, which was detected using a photoelastic modulator (Sec. VII.B.1). Since the Rb relaxation time is orders of magnitude shorter than that of ^{131}Xe, the signal is proportional to the longitudinal polarization of ^{131}Xe. A typical transient signal is shown in Fig. 1(a).

From Eq.(23) the transition frequencies between the adjacent Zeeman sublevels of the ^{131}Xe nucleus in the rotating frame are, to first order, $\Omega_{-3/2,\,-1/2} = \Omega_0 + \Delta\Omega_0\, P_2(\cos\psi)$, $\Omega_{-1/2,\,1/2} = \Omega_0$, and $\Omega_{1/2,\,3/2} = \Omega_0 - \Delta\Omega_0\, P_2(\cos\psi)$. The $P_2(\cos\psi)$ dependence of the quadrupole splitting on the angle ψ of the cell symmetry axis with respect to the effective magnetic field direction in the rotating coordinate system was studied by varying the oscillating magnetic field frequency ω instead of physically rotating the cell with respect to the direction of the external magnetic field as was done by Simpson (1978) and Kwon *et al.* (1981).

The three $\Delta m = 1$ Zeeman transition frequencies shown in Fig. 1(b) are not equidistant. This is due to the second order effect of the quadrupole wall interaction. To second order and for $\psi = \pi/2$, the frequencies of the three coherences are given by the imaginary part of the eigenvalue in Eq.(23)

$$\Omega_{-3/2,\,-1/2} = \Omega_0 - \Delta\Omega_0/2\ , \tag{27}$$

$$\Omega_{-1/2,\,1/2} = \Omega_0 - \delta\Omega_0\ , \tag{28}$$

$$\Omega_{1/2,\,3/2} = \Omega_0 + \Delta\Omega_0/2\ , \tag{29}$$

where the second order correction $\delta\Omega_0$ is given by $\delta\Omega_0 = 3(\Delta\Omega_0)^2/16\,\Omega_0$. This relation between the first and second order corrections is confirmed by the measured Zeeman transition frequencies (see, for example, Fig. 1(b)).

The remarkable dependence of the quadrupole splitting $|\Delta\Omega_0|/2\pi$ on the cell asymmetry parameter $1/h - 1/d$ is displayed in Fig. 2 for $\psi = \pi/2$. The mean twist angle $|\langle\theta\rangle| = (3.8 \pm 0.4) \times 10^{-5}$ rad per wall collision of a ^{131}Xe atom is deduced from the slope of Eq.(24). The physical origin of the cell geometry dependence of the quadrupole splitting is the existence of a local symmetry axis, the normal to the local macroscopic surface of the cell, along which the ensemble average value of the fluctuating electric field gradient does not vanish.

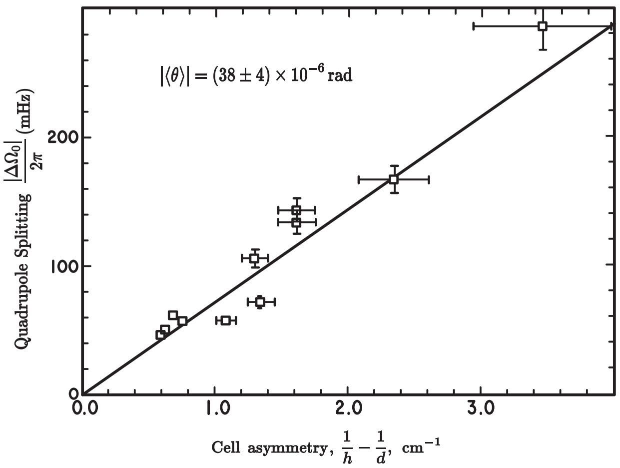

FIG. 2 Measured dependence of the sideband splitting $|\Delta\Omega_0|/2\pi$ on the cell asymmetry parameter $h^{-1} - d^{-1}$. From Wu *et al.*, 1987.

To second order, the real part of the eigenvalue $\gamma'_{0;mn}$, which corresponds to the relaxation rate of the coherence $|m\rangle\langle n|$, is given by Eq.(23),

$$\gamma'_{0;\,-\frac{3}{2},\,-\frac{1}{2}} = \gamma'_{0;\frac{1}{2},\frac{3}{2}} = \frac{3}{2}\gamma'_{0;-\frac{1}{2},\frac{1}{2}} = \frac{3}{5} v \langle\theta^2\rangle \left(\frac{1}{2h} + \frac{1}{d}\right)\ . \tag{30}$$

Since they are not resolved in the experiment, they are assumed to be approximately equal and given by

$$\gamma'_{0;-\frac{1}{2},\frac{1}{2}} = \frac{2}{5} v \langle\theta^2\rangle \left(\frac{1}{2h} + \frac{1}{d}\right)\ . \tag{31}$$

The relaxation time of the precession signal in Fig. 1(a) is 25 s, from which one obtains $\langle\theta^2\rangle = (2.8 \pm 0.3) \times 10^{-6}\,\mathrm{rad}^2$. Thus $\langle\theta^2\rangle \gg \langle\theta\rangle^2$, implying that the instantaneous magnitude of the fluctuating components of the electric field gradient, which cause the nuclear spin polarization to relax, is much larger than the ensemble average value along the direction of the normal to the cell wall, which shifts the $\Delta m = 1$ coherence frequencies of the nucleus by different amount and generates beats in the free precession signal of the nuclear polarization.

The beating signals due to the coherent quadrupole wall interaction are free of any contributions from the isotropic gas phase interactions, and therefore provide an ideal probe of the microscopic nature of the surface. For example, the mean electric field gradients on the surface can be deduced through Eq.(25) from the mean twist angle $\langle\theta\rangle$, which is directly obtained from the quadrupole splitting of the beat signal, provided one knows the dwell time τ_s (Butscher *et al.*, 1994, 1996; Kwon *et al.*, 1981). However, τ_s has not been directly measured for the diamagnetic atoms (Sec.V.B), and therefore reasonable estimate is usually made instead. Similarly, the mean-squared electric field gradient can be deduced through Eq.(26) from the mean-squared twist angle $\langle\theta^2\rangle$ (Butscher *et al.*, 1994, 1996; Cohen-Tannoudji, 1963).

Another study of the quadrupole wall interaction of ^{131}Xe was carried out in Duran glass cells by Butscher *et al.* (1994). The Rb atom are used as a magnetometer to monitor the free precession signals of the ^{131}Xe nuclear polarization in the laboratory coordinate system. The angular dependence as well as the cell geometry dependence of the beat period were confirmed. The Fourier transform of the free precession signal clearly shows that the relaxation rate of the coherence $|{-1/2}\rangle\langle 1/2|$ is slower than those of $|{-3/2}\rangle\langle{-1/2}|$ and $|1/2\rangle\langle 3/2|$ (see Eq.(30)). From the beat period and the relaxation rate of the free precession signal they determined $\langle\theta\rangle = (4.6 \pm 0.5) \times 10^{-5}\,\mathrm{rad}$ and $\langle\theta^2\rangle = (3.4 \pm 0.3) \times 10^{-6}\,\mathrm{rad}^2$, in good agreement with the values obtained by Wu *et al.* (1987). From $\langle\theta\rangle$ and $\langle\theta^2\rangle$, the mean and root mean square quadrupole coupling constant $eQ\langle q_0\rangle(1-\gamma_\infty)/h$ and $eQ\sqrt{\langle q_0^2\rangle}(1-\gamma_\infty)/h$, where q_0 is the electric field gradient on the wall in the absence of the adsorption of noble gas atoms and γ_∞ is the Sternheimer anti-shielding factor, are estimated to be $422 \pm 45\,\mathrm{kHz}$ and $6.17 \pm 0.60\,\mathrm{MHz}$, respectively.

Even though the quadrupole splitting for cubic cells is expected to be minimal (see Eq.(24)), Donley *et al.* (2009), in their studies of the quadrupole wall interaction of ^{131}Xe, used miniature cubic cells of volume $1\,\mathrm{mm}^3$ with four silicon walls and two Pyrex windows. Thus the cubic cells no longer have cubic symmetry, making it possible to observe the quadrupole splitting and consequently the beats in the precession signal. Furthermore the use of miniature cells significantly enhanced the quadrupole splitting (see Eq.(24)). From the quadrupole splitting, it was deduced that the mean twist angle $\langle\theta\rangle = 2.9 \times 10^{-5}\,\mathrm{rad}$ on the silicon surface.

^{83}Kr $(I = 9/2)$

The first study of the quadrupole wall interaction of ^{83}Kr was made by Volk *et al.* (1979). They studied the decay of the transverse nuclear polarization of ^{83}Kr, which was monitored using Rb atoms as a magnetometer (Cohen-Tannoudji *et al.*, 1970). The decay of the precession signal is not exponential, but becomes exponential as the angle between the cell symmetry axis and the external magnetic field approaches the magic angle ($\sim 55^\circ$). The decay time for the precession signal strongly depends on the angle between the cell symmetry axis and the external magnetic field. These observations are in agreement with those of Simpson (1978). Only dephasing but not rephasing of the precession signal was observed, most likely owing to the small quadrupole splitting. A qualitative agreement between the model and observation was obtained.

Butscher *et al.* (1996) also studied the quadrupole wall interaction of ^{83}Kr in Duran glass cell using the same experimental technique as they studied ^{131}Xe (Butscher *et al.*, 1994). The beat period and the relaxation rate of the free precession signal yield $\langle\theta\rangle = (1.02 \pm 0.07) \times 10^{-5}\,\mathrm{rad}$ and $\langle\theta^2\rangle = (4.9 \pm 0.6) \times 10^{-8}\,\mathrm{rad}^2$, from which the mean and root mean square quadrupole coupling constant $eQ\langle q_0\rangle(1-\gamma_\infty)/h$ and $eQ\sqrt{\langle q_0^2\rangle}(1-\gamma_\infty)/h$ are estimated to be $502 \pm 36\,\mathrm{kHz}$ and $5.61 \pm 0.70\,\mathrm{MHz}$, respectively. Combining these results with those of ^{131}Xe (Butscher *et al.*, 1994) and using the nuclear quadrupole moment Q and the Sternheimer anti-shielding factor γ_∞ for ^{83}Kr and ^{131}Xe, it is found that the ratios $\langle q_0\rangle_{\mathrm{Kr}}/\langle q_0\rangle_{\mathrm{Xe}} = 1.10$ and $\sqrt{\langle q_0^2\rangle}_{\mathrm{Kr}}/\sqrt{\langle q_0^2\rangle}_{\mathrm{Xe}} = 0.84$. Physically, that these ratios are close to unity demonstrates that the same information about the microscopic nature of the wall, such as the mean or root mean square electric field gradient on the wall, is obtained regardless of whether ^{83}Kr or ^{131}Xe is used as a probe.

^{21}Ne $(I = 3/2)$

The quadrupole wall interaction of ^{21}Ne was studied by Chupp and Hoare (1990). The ^{21}Ne nuclei were polarized along a static magnetic field (z-axis) by spin exchange with optically pumped Rb atoms. To initiate the free precession of the ^{21}Ne nuclear polarization, a pulse of resonant oscillating magnetic field along the x-axis was applied to rotate the nuclear polarization 20 degrees away from the static magnetic field. The free precession of the ^{21}Ne polarization was monitored by the voltage induced in a pickup coil. The free precession of the ^{21}Ne nuclear polarization for as long as four and a half hours was reported and used for a test of the linearity of quantum mechanics. The washing out of the sharp beat pattern observed in the precession signal was the first confirmation of the theoretical prediction that coherences $|-3/2\rangle\langle{-1/2}|$, $|-1/2\rangle\langle 1/2|$ and $|1/2\rangle\langle{-1/2}|$ do not relax at the same rate (see Eq.(30)).

III. WALL INTERACTIONS OF SPIN-POLARIZED NOBLE GAS ATOMS WITH NUCLEAR SPINS $I = 1/2$

A. The nature of the wall interactions

Wall interactions of spin-polarized noble gas atoms with nuclear spins 1/2, ^{3}He and ^{129}Xe, have been extensively studied. For ^{3}He in glass cells a good understanding of the wall relaxation mechanism has been achieved (Cornaz, 1963; Fitzsimmons and Walters, 1967). The dominant wall interaction of ^{3}He that causes its relaxation is believed to be the scalar magnetic dipole-dipole coupling between the ^{3}He nuclei and the unpaired electrons in the dangling-bond defects in the glass (Mazitov *et al.*, 1993; Schmiedeskamp *et al.*, 2006a). However, a definite proof of the dangling-bond defects being responsible for the ^{3}He relaxation is still lacking.

The nature of the wall interactions responsible for the relaxation of ^{129}Xe on the alkali hydride surface is not fully understood (Nicol, 1984). However, on silicone coatings (dichlorooctamethyltetrasiloxane $Cl[Si(CH_3)_2O]_3Si(CH_3)_2Cl$), it has been unequivocally demonstrated that the dominant wall interaction responsible for the relaxation of ^{129}Xe is the tensorial magnetic dipole-dipole interaction between the nuclear magnetic moments $\boldsymbol{\mu}_I = \gamma_I \hbar \boldsymbol{I}$ of the adsorbed ^{129}Xe atoms and the nuclear magnetic moments $\boldsymbol{\mu}_K = \gamma_K \hbar \boldsymbol{K}$ of the protons in the coating, where $\hbar \boldsymbol{I}$ and $\hbar \boldsymbol{K}$ are respectively their nuclear spins, with γ_I and γ_K being their gyromagnetic ratios (Driehuys *et al.*, 1995). The wall interaction Hamiltonian is

$$H_{\rm w} = \frac{\hbar^2 \gamma_I \gamma_K}{r^3} \left(\boldsymbol{I} \cdot \boldsymbol{K} - 3 \frac{(\boldsymbol{I} \cdot \boldsymbol{r})(\boldsymbol{K} \cdot \boldsymbol{r})}{r^2} \right) , \qquad (32)$$

where $\boldsymbol{r}$ is the radius vector from the proton to the nucleus of the ^{129}Xe atom. Due to the relative motion of the protons and the adsorbed ^{129}Xe atoms, both the direction and magnitude of $\boldsymbol{r}$ fluctuate in time. Therefore $H_{\rm w}$ is a stationary random function.

B. Wall relaxation of ^{3}He

The most important relaxation mechanisms for polarized ^{3}He consist of gas phase nuclear dipole-dipole relaxation, relaxation due to the magnetic field inhomogeneity and wall relaxation. The intrinsic gas phase dipolar relaxation time T_1 for polarized ^{3}He atoms due to magnetic dipole-dipole interaction between the ^{3}He nuclear spins is $T_1 = 744/n$ hours at a temperature of 296 K, where n is the ^{3}He density in amagats (Newbury *et al.*, 1993b). In the early studies the measured relaxation times of ^{3}He were orders of magnitude shorter than the intrinsic gas phase dipolar relaxation limit because of the wall relaxation. Therefore the early studies focused on understanding the nature of the wall interactions of spin-polarized ^{3}He atoms in order to suppress or eliminate wall relaxation. A brief review of the wall relaxation of nuclear spin polarized ^{3}He was recently given by Gentile *et al.* (2017).

The early pioneering work on the wall relaxation of polarized ^{3}He (Bouchiat *et al.*, 1960; Colegrove *et al.*, 1963; Cornaz, 1963; Fitzsimmons and Walters, 1967; Gamblin and Carver, 1965) paved the way to achieving the ultimate dipolar relaxation limit. It has been shown that if the helium gas is sufficiently purified to be free of paramagnetic impurities, if the cell is made with impermeable glass such as aluminosilicate glass and its inner surface is fully blown and coated with Rb or other alkali metal, and if the magnetic field gradient is sufficiently small, one is able to achieve consistently a ^{3}He relaxation time close to the gas phase dipolar limit (Chen *et al.*, 2011; Newbury *et al.*, 1993b; Rich *et al.*, 2002).

In the experimental studies of the wall relaxation of ^{3}He by Fitzsimmons and Walters (1967) and Fitzsimmons *et al.* (1969), the ^{3}He atoms were polarized by metastability exchange optical pumping in low ^{3}He density cells or by spin exchange optical pumping in high ^{3}He density cells. The decay of the ^{3}He polarization was monitored by the adiabatic inversion NMR technique. The wall relaxation mechanism for ^{3}He was determined by studying the temperature dependence of the wall relaxation time of ^{3}He.

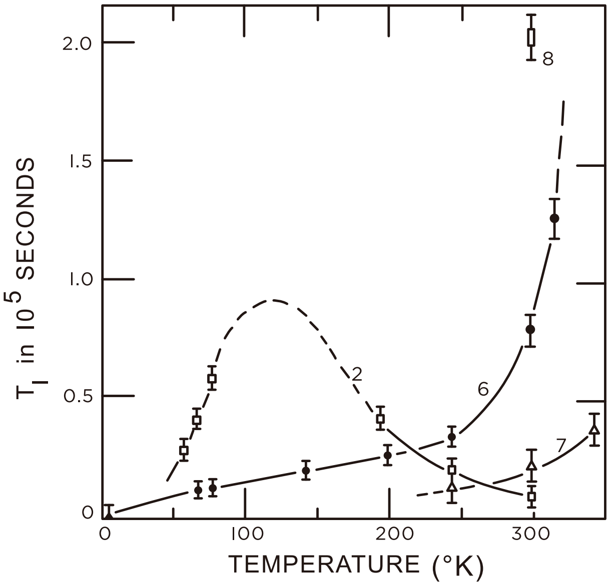

FIG. 3 Nuclear spin relaxation times for ^{3}He measured in spherical cells, about 5 cm in diameter. Curves 6, 7 and point 8 represent measurements in cells made of aluminosilicate glass, with ^{3}He pressures at room temperature of 12, 15 and 10 Torr, respectively. Curve 2 represents measurements in a Pyrex glass cell, with ^{3}He pressure at room temperature of 20 Torr. From Fitzsimmons and Walters, 1967.

Fig. 3 shows the temperature dependence of the wall relaxation time of ^{3}He in Pyrex and aluminosilicate glass cells. The reversal of slope in the Pyrex glass cell, which was also observed in quartz cells, suggests the following wall relaxation mechanisms for ^{3}He. For temperatures below 125 K, the ^{3}He atoms, while adsorbed on the wall, are relaxed by the paramagnetic centers on the glass surface. The relaxation rate, which is proportional to the dwell time τ_s, decreases as temperature increases according to the Arrhenius relation Eq.(67). However, the relaxation rate starts to increase above 125 K, which is interpreted as the onset of a different wall relaxation mechanism. Since it is known that at higher temperatures helium permeates more readily into silica (SiO_2), it is postulated that permeation of ^{3}He into Pyrex and quartz becomes the dominant wall relaxation mechanism at temperatures above 125 K (Fitzsimmons and Walters, 1967). The permeation greatly increases the dwell time τ_s and consequently the relaxation rate, resulting in a reversal of slope.

The permeation mechanism was suggested earlier for the relaxation of ^{3}He in Pyrex cells by Cornaz (1963), who measured T_1 and T_2 for ^{3}He, from which it was estimated that $\tau_c > 10^{-9}$ s at room temperature. The long correlation time led Cornaz to suggest that at room temperature permeation into the Pyrex glass is responsible for the relaxation of ^{3}He in Pyrex cells.

The most convincing experimental evidence for the permeation mechanism is that the reversal of slope is not observed in aluminosilicate glass cells, which is three orders of magnitude less permeable to ^{3}He than Pyrex or quartz (Fig. 3).

Based on the adsorption and permeation mechanisms for the wall relaxation of ^{3}He, several phenomenological models have been suggested. The most quantitative one was proposed by Jacob *et al.* (2003). It calculated the ^{3}He relaxation rates and their temperature dependence on the surface of borosilicate glass. The models assumed the Fe^{+3} ions to be responsible for the relaxation of ^{3}He (Cornaz, 1963; Jacob *et al.*, 2003; Timsit *et al.*, 1971). The existence of the Fe^{3+} ions in glass was indeed demonstrated using paramagnetic resonance absorption (Castner *et al.*, 1960; Sands, 1955). Their typical concentration in the glass is ~ 100 ppm (Timsit *et al.*, 1971). However, there is no convincing evidence that the relaxation sites for ^{3}He are Fe^{3+} ions.

Indeed, a detailed study of the nature of the relaxation centers for ^{3}He by Schmiedeskamp *et al.* (2006a) rules out the possibility that Fe^{+3} ions play any important role in the ^{3}He relaxation because of the lack of dependence of T_1 on the iron content of glasses. For example, the relaxation times T_1 in aluminosilicate glass cells with Fe^{+3} concentrations that differ by more than a factor of four are approximately equal. The influence of the Fe^{+3} concentration on the relaxation time is also found to be minimal in borosilicate glass cells. There is no noticeable difference between the ^{3}He relaxation times in cells made of soda lime glass with Fe^{+3} concentrations that differ by almost one order of magnitude.

A study of the relaxation of ^{3}He dissolved in fused silica using NMR suggests that the ^{3}He relaxation in fused silica is caused by the magnetic dipolar coupling of ^{3}He with the unpaired electrons in the dangling-bond defects, the broken Si–O bonds (Mazitov *et al.*, 1993). The scalar magnetic dipole-dipole interaction between the ^{3}He nuclei and the unpaired electrons in the dangling bond defects is also suggested to be the dominant wall interaction responsible for the relaxation of ^{3}He in Pyrex and aluminosilicate glasses (Schmiedeskamp *et al.*, 2006a).

Physically, the reason dangling-bond defects are expected to play a much more important role in the relaxation of ^{3}He than Fe^{+3} ions is that the scalar magnetic dipole-dipole interaction between the ^{3}He nucleus and the unpaired electron in the dangling bond, which has a significant ($\sim 25\%$) *s*-character (Hochstrasser and Antonin, 1972), is orders of magnitude larger than the tensorial magnetic dipole-dipole interaction between the ^{3}He nucleus and the Fe^{+3} ion (Sec. IV.A).

However, aside from a better fit between the calculations and the measured T_1 data (Schmiedeskamp *et al.*, 2006a), a definite confirmation of the dangling-bond defects being responsible for the relaxation of ^{3}He is yet to emerge.

Nonetheless, the dangling-bond defect hypothesis gives a plausible explanation for the importance of the fully blown procedure, which is widely used in the fabrication of glass cells and can greatly increase the relaxation time T_1 (Chen *et al.*, 2011; Newbury *et al.*, 1993b; Parnell *et al.*, 2009; Rich *et al.*, 2002; Salhi *et al.*, 2014). The fully blown process melts the glass surface and conceivably decreases the paramagnetic dangling bond defects by changing the structure of the glass surface. On the other hand melting of the inner surface of the cell is not likely to change the density of the Fe^{3+} ions on the surface.

Besides the aforementioned wall relaxation sites, the dangling-bond defects, that are intrinsic to the glass, ^{3}He can also be relaxed by the magnetic impurities brought into the cell. One example that has attracted much interest is the following. It was observed that T_1 decreased by a factor of two when the external magnetic field increased from 10 to 225 G in an aluminosilicate glass cell while T_1 increased when the magnetic field increased in a Pyrex cell (Fitzsimmons *et al.*, 1969). The latter case might have had to do with the magnetization history of the cell.

This field dependence of T_1 was later studied in greater detail by Jacob *et al.* (2001). It was reported that T_1^{-1} increased by a factor of 2–20 if the cell was exposed to a magnetic field of a few kG, and had memory of the magnetic field the cell was previously exposed to. The original T_1^{-1} can be restored by demagnetizing the cell. These observations clearly indicate a role played by some ferromagnetic sites. The effect was observed in both Pyrex and aluminosilicate glass cells, but only if the cells had Rb metal in them. This clearly shows that the ferromagnetic impurities that are responsible for the field dependence of T_1 are not intrinsic to the cell glass. In fact, as previously mentioned, the ferromagnetic impurities in the cell glass do not play a significant role in the relaxation of ^{3}He (Schmiedeskamp *et al.*, 2006a). It was speculated that they might be brought into the cell as impurities in the Rb metal.

The field dependence of T_1 was also observed in Cs -coated cells by Hutanu *et al.* (2007a), who determined the saturation field, above which T_1 no longer decreases with increasing field, to be ~ 1 kG, in agreement with what Jacob *et al.* (2001) observed in Rb-coated cells.

The observation of the field dependence of T_1 was also reported for cells that did not contain alkali metal (Hutanu and Rupp, 2005; Schmiedeskamp *et al.*, 2006b), seemingly inconsistent with the earlier observation of the field dependence of T_1, which requires the presence of alkali metal in the cell (Jacob *et al.*, 2001). It was speculated that the ferromagnetic impurities were brought into the cell during the cell fabrication process. It is noted that all those cells seem to have a valve connected with them. Using the superconducting quantum interference device (SQUID) Hutanu *et al.* (2007b) obtained the magnetic field map of a magnetized cell assembly. The contribution to the magnetic field from the valve assembly is found to be more than two orders of magnitude larger than that from the cell itself. Whether the magnetized valve assembly plays any role similar to what Bouchiat and Brossel (1966) called the "reservoir effect" in the relaxation of ^{3}He is not known.

It is also observed that in an external magnetic field of 30 G the relaxation time T_1 changes, and most of the time increases, when the relative orientation of the cell with respect the field changes (Jacob *et al.*, 2004). The orientation dependence is observed only if the cell contains Rb and has been heated. Similar observation was made in cells that contain potassium (Boag *et al.*, 2014).

Thus both the orientation dependence and the field dependence of T_1 seem to be due to the ferromagnetic impurities brought into the cell. It is suggested that the ferromagnetic impurities are Fe_3O_4 particles located at the inner glass surface (Schmiedeskamp *et al.*, 2006b), which, however, is disputed by Hutanu *et al.* (2007a). Thus no definite conclusion has been reached regarding the exact nature of the ferromagnetic impurities responsible for the field dependence and the orientation dependence of T_1. The following study may shed some light on the underlying physical mechanism of the field dependence and the orientation dependence of T_1. The reason that T_1 in both the orientation dependence and the field dependence is so sensitive to the magnetization of the cell is the existence of a correlation among the phase changes experienced by the ^{3}He atom during its collisions with the magnetic sites when the cell is magnetized. This is shown by (Bicout *et al.*, 2013) using a bounded random walk model. Semi-classically, when the cell is magnetized, the rotations experienced by the ^{3}He spin during its collisions with the magnetic sites are coherent, and a spin is easier to be flipped by a sequence of coherent rotations than by a sequence of random ones, corresponding to the demagnetized state of the cell.

C. Wall relaxation of ^{129}Xe

1. Mechanisms

The intrinsic gas phase spin relaxation time T_1 for polarized ^{129}Xe atoms is determined by the spin-rotation interaction between the ^{129}Xe nuclear spin and the rotational angular momentum of two colliding Xe atoms, and is given by $56/n$ hours at a temperature of 298 K, where n is the density of ^{129}Xe in amagats (Brinkmann *et al.*, 1962; Hunt and Carr, 1963). This intrinsic gas phase relaxation time of ^{129}Xe is orders of magnitude longer than what is measured in most experiments due to the existence of other relaxation mechanisms. One of the most important relaxation mechanisms is the relaxation at the cell walls.

Because of the presence of the unknown paramagnetic centers on the uncoated walls, the relaxation times of ^{129}Xe measured in uncoated cells show wide variation from cell to cell (Zeng *et al.*, 1983). Therefore, quantitative studies of the wall interactions of ^{129}Xe are only carried out in coated cells.

The most commonly used anti-relaxation coating for ^{129}Xe is silicone (Surfasil). The experimental studies carried out by Driehuys *et al.* (1995) provide a definite proof about the nature of the dominant wall interaction of ^{129}Xe atoms in silicone-coated cells. Their experiment is based on the double resonance concept (Hartmann and Hahn, 1962). In double resonance, two oscillating magnetic fields $\boldsymbol{B}_{1I}$ and $\boldsymbol{B}_{1K}$ at resonant frequencies $\omega_I = \gamma_I B_0$ and $\omega_K = \gamma_K B_0$ are applied along the x-axis, where B_0 is a static magnetic field along the z-axis. Thus the $\boldsymbol{I}$-spins and $\boldsymbol{K}$-spins rotate in their respective rotating frames around $\boldsymbol{B}_{1I}$ and $\boldsymbol{B}_{1K}$ at frequencies $\omega_{1I} = \gamma_I B_{1I}$ and $\omega_{1K} = \gamma_K B_{1K}$, respectively. Since both rotating frames rotate around the same z-axis, when the Hartmann-Hahn condition $\omega_{1I} = \omega_{1K}$ is satisfied, the components of the magnetic moments $\boldsymbol{\mu}_I$ and $\boldsymbol{\mu}_K$ along the z-axis oscillate at the same frequency, thus allowing angular momentum to be efficiently transferred between $\boldsymbol{I}$ and $\boldsymbol{K}$ (Slichter, 1980).

Due to the exceedingly long correlation time ($\tau_c \sim 10^{-5}$ s) of ^{129}Xe in silicone, Driehuys *et al.* (1995) studied the relaxation rate of ^{129}Xe polarization locked in its rotating frame. They found that the spin-locked relaxation rate $1/T_\rho$ of ^{129}Xe depends strongly on the Hartmann-Hahn matching condition, which determines the efficiency of spin transfer between the ^{129}Xe nuclei and the neighboring protons, thus unmistakably proving that the dipolar interaction between the magnetic moments of ^{129}Xe nuclei and protons in the silicone coating is responsible for the ^{129}Xe relaxation.

Keeping only the terms that are strongly dependent on the fields B_{1I} and B_{1K}, the relaxation rate of the spin-locked ^{129}Xe polarization is given by

$$\frac{1}{T_{1\rho}} = \frac{1}{10\,T_0}\left(\frac{1}{1+(\omega_{1I}+\omega_{1K})^2\tau_c^2} + \frac{1}{1+(\omega_{1I}-\omega_{1K})^2\tau_c^2}\right) . \tag{33}$$

Experimentally the ^{129}Xe polarization was spin-locked to a small B_{1I} (1.1 G) such that $\omega_{1I}\tau_c \ll 1$ so that both terms in Eq.(33) are equal to $1/(1+\omega_{1K}^2\tau_c^2)$. Thus the Hartmann-Hahn matching condition became less and less

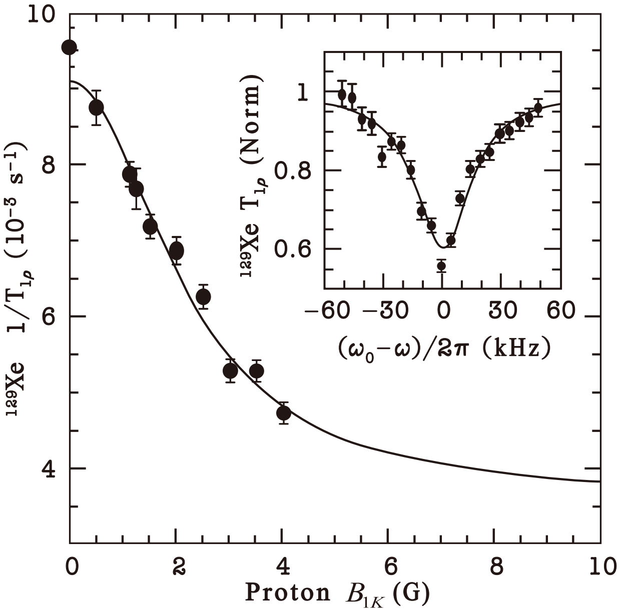

FIG. 4 A double resonance study of the dependence of the spin-locked ^{129}Xe relaxation rate $1/T_{1\rho}$ on the field strength of the resonant proton field. The inset further corroborates the nature of the wall interaction of ^{129}Xe on silicone-coated walls. It shows the dependence of $T_{1\rho}$ on the detuning of the frequency of the proton field from resonance. The detuning rendered the Zeeman splittings in the rotating frames of ^{129}Xe and protons to be even more dissimilar, making the Hartmann-Hahn matching condition even further from being satisfied and leading to an increase in $T_{1\rho}$. The resonance curve was obtained with a constant proton field strength of 4 G while the frequency was varied. Adapted from Driehuys *et al.*, 1995.

satisfied as the proton field increased, causing the relaxation rate of ^{129}Xe to decrease (Fig. 4).

The non-zero asymptotic residual relaxation rate in Fig. 4, which corresponds to the decoupling between the xenon spins and the proton spins, suggests the existence of a second wall interaction, albeit a smaller one, for ^{129}Xe on the silicone surface. The nature of this second wall interaction is not known, but the spin-rotation interaction with the carbon atoms could be a possibility.

The wall relaxation of ^{129}Xe on the rubidium hydride surface was studied by Nicol (1984). It was reported that there was hardly any difference between the ^{129}Xe wall relaxation rates on RbH and RbD. This clearly shows that the magnetic dipole-dipole interaction between the magnetic moments of the ^{129}Xe nuclei and the protons on the RbH surface does not play any significant role in the ^{129}Xe relaxation. This is because the wall relaxation rate due to the magnetic dipole-dipole interaction is proportional to $\gamma_K^2 K(K+1)/R^6$, where K is the proton spin, γ_K its gyromagnetic ratio and R the distance between the ^{129}Xe atoms and the protons, and if the magnetic dipole-dipole interaction were solely responsible for the wall relaxation of ^{129}Xe, one would expect the relaxation rate of ^{129}Xe to be sixteen times smaller on RbD than on RbH (Sec. IV.B.2). Any significant contribution to the ^{129}Xe relaxation from the dipolar interaction between ^{129}Xe and the cations Rb$^+$ is ruled out on the grounds that the distance R between ^{129}Xe and Rb$^+$ is larger than that between ^{129}Xe and H$^-$ or D$^-$. Spin-rotation interaction was suggested as a possible wall relaxation mechanism (Sec. IV.A and B). But no definite identification of the dominant wall relaxation mechanisms for ^{129}Xe on the alkali hydride surface has been made.

2. Theory

The common treatment of the relaxation of the longitudinal polarization $\langle I_z \rangle$ of ^{129}Xe is based on the theory of Abragam (1961) for the relaxation in liquids and gases. Suppose the ^{129}Xe atom is adsorbed on the wall a fraction $f(T)$ of the time, where $f(T)$ depends on the temperature of the wall, and is often taken to be $\tau_s/(\tau_s+\tau_b)$, τ_b being the time between two consecutive wall collisions. The Hamiltonian for the dipolar interaction between the ^{129}Xe atoms and the protons on the silicone coating is given by Eq.(32). We shall use the interaction picture in order to simplify the equation of motion of the density matrix, and to focus on the slow time variation of the observables due to the perturbation $H_{\rm w}$. An operator A in the Schrodinger picture becomes $\widetilde{A} = e^{\frac{i}{\hbar}H_0 t} A e^{-\frac{i}{\hbar}H_0 t}$ in the interaction picture, where $H_0 = \hbar\omega_I I_z + \hbar\omega_K K_z$ represents the Zeeman interaction due to the static magnetic field $\boldsymbol{B}$, with $\omega_I = \gamma_I B$ and $\omega_K = \gamma_K B$. While a ^{129}Xe atom is adsorbed on the wall, it is described by an ensemble-averaged density matrix $\tilde{\rho}_{I,K}(t)$, which, to second order in $\widetilde{H}_{\rm w}(t)$, is governed by the following equation of motion (Abragam, 1961)

$$\frac{d\tilde{\rho}_{I,K}(t)}{dt} = -\frac{1}{\hbar^2}\int_0^\infty dt' \Big\langle \big[\widetilde{H}_{\rm w}(t), [\widetilde{H}_{\rm w}(t-t'), \tilde{\rho}_{I,K}(t)]\big] \Big\rangle \,, \tag{34}$$

where the brackets denote ensemble average for the wall interaction. It is convenient to separate the angular momentum operators in $\widetilde{H}_{\rm w}(t)$ from the random functions that depend on $\boldsymbol{r}$,

$$\widetilde{H}_{\rm w}(t) = \frac{\hbar^2\gamma_K\gamma_I}{r^3}\sum_q F^{(q)}(t)\widetilde{A}^{(q)}(t) \,, \tag{35}$$

where

$$\begin{aligned} F^{(2)}(t) &= F^{(-2)*}(t) = -\frac{3}{4}\sin^2\theta e^{-2i\phi} \,, \\ F^{(1)}(t) &= F^{(-1)*}(t) = -\frac{3}{2}\sin\theta\cos\theta e^{-i\phi} \,, \\ F^{(0)}(t) &= \frac{1}{4}(1-3\cos^2\theta) \,, \end{aligned} \tag{36}$$

$$
\begin{aligned}
\widetilde{A}^{(2)}(t) &= \widetilde{A}^{(-2)\dagger} = I_+ K_+ e^{i(\omega_I+\omega_K)t} \,, \\
\widetilde{A}^{(1)}(t) &= \widetilde{A}^{(-1)\dagger} = I_+ K_z e^{i\omega_I t} + I_z K_+ e^{i\omega_K t} \,, \qquad (37) \\
\widetilde{A}^{(0)}(t) &= 4 I_z K_z - I_+ K_- e^{i(\omega_I-\omega_K)t} - I_- K_+ e^{-i(\omega_I-\omega_K)t} \,.
\end{aligned}
$$

Since we are only interested in the observables of the $\boldsymbol{I}$-spins, we write $\tilde{\rho}_I = \mathrm{Tr}_K \tilde{\rho}_{I,K}$, where $\tilde{\rho}_I$ is the density matrix for the $\boldsymbol{I}$-spins. Taking the trace of Eq.(34) with respect to spin $\boldsymbol{K}$ and neglecting the polarization of the $\boldsymbol{K}$-spins on the wall, one obtains the equation of motion for $\tilde{\rho}_I$, whence the equation of motion of the longitudinal spin polarization $\langle \widetilde{I_z} \rangle = \mathrm{Tr}(I_z \tilde{\rho}_I(t))$ of the ^{129}Xe atoms on the wall in the interaction picture, which agrees with that in the Schrödinger picture because I_z commutes with H_0. Taking into account that the ^{129}Xe atom is adsorbed on the wall only a fraction $f(T)$ of the time, the wall relaxation rate T_{w}^{-1} of ^{129}Xe is given by

$$
\frac{1}{T_{\mathrm{w}}} = \frac{1}{10\, T_{\mathrm{w0}}} \Big[J(\omega_I - \omega_K) + 3J(\omega_I) + 6J(\omega_I + \omega_K) \Big] \,, \quad (38)
$$

where T_{w0}^{-1} is the relaxation rate at zero magnetic field

$$
\frac{1}{T_{\mathrm{w0}}} = \frac{4}{3} f(T) K(K+1) \gamma_I^2 \gamma_K^2 \hbar^2 \tau_c \sum_i r_i^{-6} \,, \quad (39)
$$

and $J(\omega)$ is the spectral density

$$
J(\omega) = 1/(1 + \omega^2 \tau_c^2) \quad (40)
$$

of the correlation function,

$$
\langle F^{(q)}(t) F^{(q')}(t-t') \rangle = \delta_{q,-q'} \langle |F^{(q)}(0)|^2 \rangle \, e^{-|t'|/\tau_c} \,, \quad (41)
$$

where τ_c is the correlation time of the random functions $F^{(q)}(t)$.

Physically, the term $J(\omega_I - \omega_K)$ in Eq.(38), which corresponds to the operators $I_\pm K_\mp$ in Eq.(37), represents a simultaneous flip of one spin up and the other down. Similar meanings can be given to the terms $J(\omega_I)$ and $J(\omega_I + \omega_K)$ in Eq.(38). The sum in Eq.(39) accounts for the fact that the adsorbed ^{129}Xe atom may interact with more than one proton on the wall.

3. Experiments

The first detailed experimental studies on the wall relaxation of ^{129}Xe were carried out in cells coated with silicone (Zeng *et al.*, 1983, 1985). The experiments were performed in low magnetic fields of a few gauss. The nuclei of ^{129}Xe were polarized through spin exchange collisions with optically pumped Rb atoms. The pump beam was then blocked. The relaxation of the longitudinal polarization of ^{129}Xe due to wall interaction was monitored by passing a weak unpolarized $D1$ probe beam through the Rb vapor, which was weakly polarized through spin exchange with the polarized ^{129}Xe. The Rb polarization was proportional to the ^{129}Xe polarization, and imparted to the probe beam a small elliptical polarization, which was measured using a photoelastic modulator (Sec. VII.B.1).

The relaxation rate T_1^{-1} of ^{129}Xe is given by

$$
T_1^{-1} = C\,[\mathrm{Rb}] + T_{\mathrm{w}}^{-1} \,, \quad (42)
$$

where T_W^{-1} is the wall relaxation rate and C[Rb] the relaxation rate due to gas phase Rb atoms, C being a constant and [Rb] the Rb vapor number density. The heat of vaporization of Rb is so much larger than the adsorption energy of ^{129}Xe that T_W^{-1} is commonly assumed to be independent of temperature within the temperature range of the experiment. Thus one obtains T_{w}^{-1} as the intercept of the linear fit of T_1^{-1} to a number of different Rb vapor densities (Fig. 5).

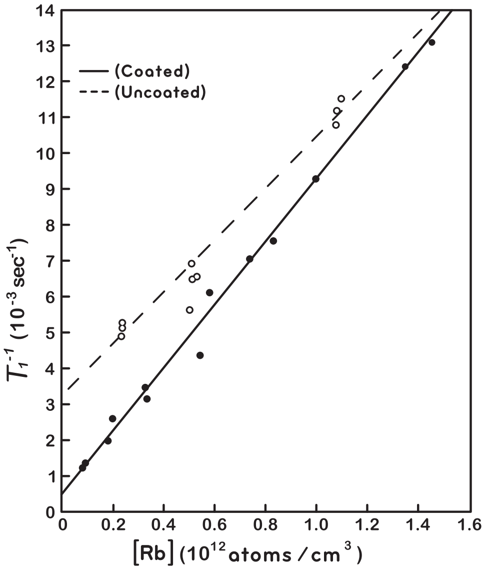

FIG. 5 Dependence of the spin relaxation rate of ^{129}Xe on the ^{87}Rb vapor number density in an uncoated cell and a cell coated with silicone (Surfasil). The different slopes are due to different N_2 pressures in the cells. From Zeng *et al.*, 1985.

D. Cross polarization

The magnetic dipole-dipole interaction transfers the angular momentum from the polarized ^{129}Xe nuclei to the surface protons, resulting in the relaxation of the adsorbed ^{129}Xe nuclei and the polarization of the protons. With a highly polarized ^{129}Xe gas it was observed that this cross polarization increased the surface proton polarization on silicone by a factor of 10^4–10^5 over the thermal equilibrium polarization at 0.2 T (Driehuys *et al.*, 1993) and on Aerosil R812, poly(triarylcarbinol) and poly(tetrabiphenyl silane) by a factor of 10^3 at 90 K and 4.2 T (Gaede *et al.*, 1995).

IV. WALL INTERACTIONS OF SPIN-POLARIZED ALKALI METAL ATOMS

A. The nature of the wall interactions

Unlike diamagnetic atoms with a ${}^1S_0$ ground state, which can collide with uncoated glass walls thousands of times without being depolarized (Happer, 1972), spin-polarized alkali metal atoms can lose their polarization in a single collision on uncoated glass walls (Sec. VI). Therefore quantitative studies of the wall interactions of spin -polarized alkali metal atoms are almost always done in coated cells.

The pioneering studies by Bouchiat and her collaborators (Bouchiat, 1963; Bouchiat and Brossel, 1966) have clearly demonstrated that the wall interactions of spin-polarized Rb atoms in cells coated with paraffin ($\mathrm{C_nH_{2n+2}}$) consist of two types of interactions: the magnetic dipole-dipole interaction, both tensorial and scalar, with the protons on the wall and the spin-rotation interaction with the C atoms, which have zero spin.

Tensorial magnetic dipole-dipole interaction

When the alkali metal atom and the proton on the wall are sufficiently far apart, their interaction is the tensorial magnetic dipole-dipole interaction between the magnetic moment $\boldsymbol{\mu}_K = \gamma_K \hbar \boldsymbol{K}$ of the proton and the magnetic moment $\boldsymbol{\mu}_s = -\gamma_S \hbar \boldsymbol{S}$ of the valence electron of the alkali metal atom, where $\hbar \boldsymbol{S}$ is the electron spin and $\gamma_S > 0$ the gyromagnetic ratio. The Hamiltonian is

$$H = -\frac{\hbar^2 \gamma_K \gamma_S}{r^3}\left(\boldsymbol{S}\cdot\boldsymbol{K} - 3\frac{(\boldsymbol{S}\cdot\boldsymbol{r})(\boldsymbol{K}\cdot\boldsymbol{r})}{r^2}\right) , \tag{43}$$

where $\boldsymbol{r}$ is the radius vector from the proton to the valence electron.

Scalar magnetic dipole-dipole interaction

When the alkali metal atom and the proton on the wall are close, the s-electron wave function is not negligibly small at the proton, and the tensorial magnetic dipole-dipole interaction (43) is replaced by the scalar magnetic dipole-dipole interaction or Fermi contact interaction $V_{\mathrm{Fermi}} = (8\pi/3)\hbar^2\gamma_K\gamma_S\delta(\boldsymbol{r})\,\boldsymbol{S}\cdot\boldsymbol{K}$.

Fermi contact interaction between the s-electron of an alkali metal atom and the nucleus of a noble gas atom has been studied in great detail (Herman, 1965; Walker, 1989; Walker *et al.*, 1987), and will be briefly reviewed here because the theory can be applied as a first approximation to the wall collisions of alkali metal atoms.

To a first approximation the scattering of the valence electron of an alkali metal atom in the Coulomb potential of a noble gas nucleus can be accounted for by orthogonalizing the unperturbed alkali metal valence electron wave function $\phi_1(\boldsymbol{r}+\boldsymbol{R})$ to the occupied core-electron orbitals $\psi_i(\boldsymbol{r})$ of the noble gas atom, where $\boldsymbol{r}$ is the position vector from the noble gas nucleus and $\boldsymbol{R}$ is a vector from the alkali metal atom nucleus to the noble gas nucleus. Thus the orthogonalized valence electron wave function is

$$\phi(\boldsymbol{r}) = \phi_1(\boldsymbol{r}+\boldsymbol{R}) - \sum_i \psi_i(\boldsymbol{r}) \int \psi_i^*(\boldsymbol{r}')\phi_1(\boldsymbol{r}'+\boldsymbol{R})d^3\boldsymbol{r}' \, . \tag{44}$$

Taking the expectation value of V_{Fermi} in the state $\phi(\boldsymbol{r})$ and noting that due to the delta function only the occupied core s-orbitals of the noble gas atom in Eq.(44) contribute, one obtains the Hamiltonian for the scalar magnetic dipole-dipole interaction

$$H = \alpha(R)\boldsymbol{S}\cdot\boldsymbol{K} \, , \tag{45}$$

where the coupling constant $\alpha(R)$ is given by

$$\alpha(R) = \frac{8\pi}{3}\hbar^2\gamma_K\gamma_S\eta^2|\phi_1(R)|^2 \, . \tag{46}$$

The enhancement factor $\eta(R)$ in Eq.(46) is the ratio of the alkali metal valence electron wave function evaluated at $\boldsymbol{R}$ in the presence of the noble gas atom to that in the absence of the noble gas atom. It is given by $\eta = 1 - \sum_n C_{ns}\psi_{ns}(0)$, where $C_{ns} = \int \psi_{ns}(\boldsymbol{r})d^3\boldsymbol{r}$ (Herman, 1965). Thus, to a first approximation, η only depends on the property of the surface atom.

Spin-rotation interaction

During the wall collision of an alkali metal atom, its valence electron can couple to the magnetic field produced by the relative motion of the alkali metal atom and the surface atom in much the same way as in a collision between an alkali metal atom and a noble gas atom in the gas phase (Bernheim, 1962). As a first approximation we assume the spin-rotation interaction between the adsorbed alkali metal atom and the surface atom can be treated by the theory developed for the spin-rotation interaction between an alkali metal atom and a noble gas atom in the gas phase (Wu *et al.*, 1985).

Suppose the noble gas atom is moving at a velocity $\boldsymbol{v}$ relative to the alkali metal atom. The scattering of the alkali metal valence electron in the Coulomb potential $V(r)$ of the noble gas atom can be treated using the same orthogonalized wave approximation Eq.(44) except that one needs to replace the occupied core orbitals $\psi_i(\boldsymbol{r})$ of the noble gas atom by $\psi_i(\boldsymbol{r})e^{im\boldsymbol{v}\cdot\boldsymbol{r}/\hbar}$ to account for the relative motion of the noble gas atom and the alkali metal atom. The spin-orbit interaction is

$$V_{\mathrm{so}} = -\frac{e\hbar}{2mc^2}\nabla V \times \boldsymbol{v}\cdot\boldsymbol{S} \, , \tag{47}$$

where m is the electron mass. Focusing on the contributions of the occupied p-orbitals of the noble gas atom, the expectation value of $V_{\rm so}$ in the orthogonalized valence electron wave function yields the spin-rotation Hamiltonian

$$H = \gamma(R)\boldsymbol{N}\cdot\boldsymbol{S}\ . \tag{48}$$

The coupling constant $\gamma(R)$ in Eq.(48) is

$$\gamma(R) = \frac{mG}{MR}\frac{d\,|\phi_1(R)|^2}{dR}\ , \tag{49}$$

where M is the reduced mass of the alkali metal atom and the noble gas atom, and the factor G is given by

$$G = \frac{1}{2}\left[\frac{\hbar}{mc}\right]^2 \int_0^\infty \left[\sum_n C_{np}R_{np}(r)\right]^2 \frac{1}{r}\frac{dV}{dr}dr\ , \tag{50}$$

and depends only on the spin-orbit interaction of the noble gas atom. The coefficient C_{np} in Eq.(50) is given by $C_{np} = \int z\psi_{np0}(\boldsymbol{r})d^3\boldsymbol{r}$, where $\psi_{np0} = r^{-1}R_{np}(r)Y_{10}(\theta,\phi)$ is the wave function of the noble gas p-electron of principal quantum number n and the sum extends over all occupied p-orbitals of the noble gas atom. Since the ground state of the helium atom does not have occupied p-orbitals, the orthogonalized wave approximation is not applicable, and other methods must be used (Walker and Happer, 1997).

Table I. Calculated values of η (Walker *et al.*, 1987) and G (Wu *et al.*, 1985)

Noble gas	$\lvert\eta\rvert$	$\lvert G\rvert$ (eV $\cdot$ Å^5)
He	9.5	0.00093 [a]
Ne	15	0.26
Ar	21	2.03
Kr	35	12.4
Xe	50	40.6
Rn	63	128

[a] Walker and Happer, 1997

The dependence of η and G on the atomic number Z of the noble gas atoms is shown in Table I. Thus on paraffin surfaces the spin-rotation interaction is expected to be far more important on C atoms than on protons. Because of the enhancement factor η, the scalar magnetic dipole-dipole interaction is generally orders of magnitude larger than the tensorial one (Herman, 1965).

B. Study of the wall interactions of alkali metal atoms in the time domain

1. Relaxation of Rb on paraffin-coated walls – theory

The theory of the wall interactions of spin-polarized Rb atoms in paraffin-coated cells was developed by Bouchiat (1963), who calculated the wall relaxation rates of various observables. These relaxation rates served as a guide to analyze the experimental data, from which the nature of the wall interactions was deduced. For low magnetic fields the electron spin $\hbar\boldsymbol{S}$ and the nuclear spin $\hbar\boldsymbol{I}$ of the alkali metal atom are coupled (hyperfine coupling). It was shown that in the presence of the magnetic dipole-dipole interaction and the spin-rotation interaction, $\langle\boldsymbol{S}\cdot\boldsymbol{I}\rangle$ and $\langle I_z\rangle$ relax with a single time constant $T_{\scriptscriptstyle H}$ and T_n, respectively, whereas $\langle S_z\rangle$ relaxes with two time constants T_e and T_n,

$$T_{\scriptscriptstyle H}^{-1} = C_{dd}J_{dd}(\Delta W) + C_{sr}J_{sr}(\Delta W)\ , \tag{51}$$

$$T_n^{-1} = \frac{C_{dd}}{(2I+1)^2}\left[J_{dd}(\omega_{\scriptscriptstyle F}) + J_{dd}(\Delta W)\right] + \frac{C_{sr}}{(2I+1)^2}\left[J_{sr}(\omega_{\scriptscriptstyle F}) + J_{sr}(\Delta W)\right]\ , \tag{52}$$

$$T_e^{-1} = \frac{C_{dd}}{(2I+1)^2}\left[J_{dd}(\omega_{\scriptscriptstyle F}) + 4I(I+1)J_{dd}(\Delta W)\right] + \frac{C_{sr}}{(2I+1)^2}\left[J_{sr}(\omega_{\scriptscriptstyle F}) + 4I(I+1)J_{sr}(\Delta W)\right]\ , \tag{53}$$

where J_{dd} and J_{sr} are the spectral densities of the correlation function defined in Eq.(40) for the magnetic dipole -dipole interaction and for the spin-rotation interaction, $\omega_{\scriptscriptstyle F} = \gamma_{\scriptscriptstyle F}B$ and ΔW being respectively the Zeeman and hyperfine splittings. The constant C_{dd} for the magnetic dipole-dipole interaction has two contributions, tensorial and scalar,

$$C_{dd} = k\frac{\gamma_{\scriptscriptstyle S}^2\gamma_{\scriptscriptstyle K}^2K(K+1)\hbar^2\tau_s\tau_c}{R^6\left(\tau_b+\tau_s\right)}\ , \tag{54}$$

where k is respectively $16\pi/3$ and $128\pi^2/27$ for tensorial and scalar dipole-dipole interactions, and $R^{-6} = \langle|r_{\scriptscriptstyle SK}(t)|^{-6}\rangle$, $r_{\scriptscriptstyle SK}(t)$ being the distance at time t between the spins $\boldsymbol{S}$ and $\boldsymbol{K}$ (Bouchiat, 1963).

2. Relaxation of Rb on paraffin-coated walls – experiment

The experimental studies of Bouchiat and Brossel (1966) were carried out in the time domain, using the "relaxation in the dark" method first suggested by Franzen (1959). Cells coated with paraffin contained only Rb vapor and no buffer gas. The temperature was below 35°C and the Rb vapor density was $\sim 10^{10}\,\mathrm{cm}^{-3}$. At such low Rb vapor density the Rb atoms bounced from wall to wall with practically no relaxation in the gas phase, thus greatly simplifying the analysis of the experimental data. After the alkali metal vapor was polarized with optical pumping, a weak probe beam passed through the vapor. The relaxation of the observables under study was monitored by the intensity of the transmitted probe beam (Sec. VII.A).

Their experimental observations and analysis provide clear evidence that the relaxation of the longitudinal spin polarization $\langle S_z \rangle$ is mainly caused by the magnetic dipole-dipole interaction whereas the relaxation of the hyperfine polarization $\langle \boldsymbol{S} \cdot \boldsymbol{I} \rangle$ is mainly due to the spin -rotation interaction.

The conclusion that the relaxation of $\langle S_z \rangle$ is caused by the magnetic dipole-dipole interaction and to a lesser extent by the spin-rotation interaction is drawn from the following observations. (1) The relaxation times of $\langle S_z \rangle$ for ^{85}Rb and ^{87}Rb are longer by a factor of 5 on deuterated paraffin $\mathrm{C_nD_{2n+2}}$ than on $\mathrm{C_nH_{2n+2}}$, which clearly shows that magnetic dipole-dipole interaction contribute to the relaxation because the relaxation rate due to the magnetic dipole-dipole interactions is proportional to $\gamma_K^2 K(K+1)$, and we have $\gamma_K = 4.26\,\mathrm{kHz/G}$, $K = 1/2$ for protons and $\gamma_K = 0.65\,\mathrm{kHz/G}$, $K = 1$ for deuterons. However, the fact that the difference is only a factor of 5 instead of 12.8 (the $\mathrm{C_nD_{2n+2}}$ coating has 1.7% H impurity), as one would expect if the magnetic dipole-dipole interaction were the sole type of wall interaction, implies the existence of a second type of wall interaction, which also contributes to the relaxation of $\langle S_z \rangle$, albeit to a lesser extent. (2) The observation that the ratios of T_H^{-1}, T_n^{-1} and T_e^{-1} for a given isotope ^{85}Rb or ^{87}Rb are different for different coatings, $\mathrm{C_nH_{2n+2}}$ and $\mathrm{C_nD_{2n+2}}$, is another indication that there is more than one type of wall interaction (see Eqs. (51)–(53)). (3) The relaxation rate of $\langle S_z \rangle$ for ^{87}Rb on $\mathrm{C_nH_{2n+2}}$, which is dominated by the magnetic dipole-dipole interaction and is proportional to $J_{dd}(\omega_F)$, decreases rapidly from $12\,\mathrm{s}^{-1}$ to an asymptotic residual relaxation rate of about $4\,\mathrm{s}^{-1}$ as the magnetic field increases to over 5000 G. The decrease of the relaxation rate is much less pronounced on $\mathrm{C_nD_{2n+2}}$ due to the much smaller magnetic dipole-dipole interaction on $\mathrm{C_nD_{2n+2}}$. However, the asymptotic residual relaxation rates for ^{87}Rb on $\mathrm{C_nH_{2n+2}}$ and $\mathrm{C_nD_{2n+2}}$ seem to merge at high magnetic fields, lending support to the existence of a second type of wall interaction, which does not depend on the nuclear spins K of the coatings and can therefore be identified as the spin-rotation interaction.

The conclusion that the relaxation of the hyperfine polarization $\langle \boldsymbol{S} \cdot \boldsymbol{I} \rangle$ is mainly due to the spin-rotation interaction with a minor contribution from the magnetic dipole-dipole interaction is drawn from the observation that for ^{87}Rb the ratio of the relaxation rate of $\langle \boldsymbol{S} \cdot \boldsymbol{I} \rangle$ on $\mathrm{C_nH_{2n+2}}$ to that on $\mathrm{C_nD_{2n+2}}$ is 1.3. This clearly shows, firstly, that $\langle \boldsymbol{S} \cdot \boldsymbol{I} \rangle$ is relaxed predominantly by the spin -rotation interaction, which is mainly contributed by carbon atoms, and, secondly, that the magnetic dipole-dipole interaction also played a role, though a lesser one, in relaxing $\langle \boldsymbol{S} \cdot \boldsymbol{I} \rangle$. The minor role of the magnetic dipole -dipole interaction is further corroborated by the observation that on $\mathrm{C_nH_{2n+2}}$ the relaxation rate of $\langle \boldsymbol{S} \cdot \boldsymbol{I} \rangle$ is slightly larger for ^{85}Rb than for ^{87}Rb. This is because $\Delta W_{85} < \Delta W_{87}$ and therefore $J_{dd}(\Delta W_{85}) > J_{dd}(\Delta W_{87})$.

The microscopic parameters that describe the wall interactions of Rb on paraffin such as their strength can be estimated from the measured relaxation data (Eqs. (51)–(53)) by writing the Hamiltonian for the magnetic dipole-dipole interaction and the spin-rotation interaction as $H_\mathrm{w} = \gamma_S \hbar \boldsymbol{S} \cdot \boldsymbol{B}(t)$, where $\boldsymbol{B}(t)$ is the effective random magnetic field on the wall. Its root mean square amplitude is estimated to be 14 G for the magnetic dipole -dipole interaction and 51 G for the spin-rotation interaction (Bouchiat and Brossel, 1966).

C. Study of the wall interactions of alkali metal atoms in the frequency domain

The wall interactions of spin-polarized alkali metal atoms can also be studied in the frequency domain using edge enhanced electron paramagnetic resonance (EPR) of optically pumped alkali metal atoms. Physically the edge enhancement is due to the restricted diffusion near the walls, resulting in an enhanced EPR signal localized near the walls (localized modes). Edge enhancement has been extensively studied in NMR (Callaghan *et al.*, 1993; Grebenkov, 2007; Pütz *et al.*, 1992; Saam *et al.*, 1996; Song *et al.*, 1998; Stoller *et al.*, 1991; de Swiet, 1995; de Swiet and Sen, 1994; Tseng *et al.*, 1998), and a detailed theory of the edge enhancement in NMR for non-relaxing surfaces was developed by Stoller *et al.* (1991). The effects of diffusion and magnetic field gradient on the EPR in optically pumped Rb vapor was first studied by Skalla *et al.* (1997), but edge enhancement was not observed. Edge enhanced EPR in optically pumped Rb vapor was first reported by Zhao *et al.* (2008a), and was found to have both localized and non-localized modes. A detailed theory of edge enhancement in optically pumped alkali metal vapor with wall interactions being taken into account was developed by (Schaden *et al.*, 2007, 2008).

1. Edge enhanced EPR in optically pumped Rb vapor

To observe edge enhanced EPR in optically pumped Rb vapor it is important to use evanescent pump and probe beams (Zhao *et al.*, 2010). The thin cylindrical cells have adjustable length L, and contain Rb vapor and $\mathrm{N_2}$ gas. The z axis is along the cell axis. A magnetic field B is applied along the x-axis, parallel to the cell front ($z = -L/2$) and back ($z = L/2$) surfaces, with a relatively large field gradient $\partial B_x/\partial z$ along the z-axis. The inhomogeneous magnetic field is such that the Larmor frequency $\omega_L(z)$ is given by $\omega_L(z) = \omega_0 + \sigma_\parallel z$, where ω_0 is the Larmor frequency at the center of the cell and $\sigma_\parallel = \gamma_S \partial B_x/\partial z$ is the Larmor frequency gradient associated with the field gradient.

The polarization of the Rb vapor is produced and probed by circularly polarized evanescent pump and probe beams at the front surface. To use phase-sensitive detection, the intensity of the transmitted probe beam, modulated by an amplitude-modulated oscillating magnetic field along the y-axis, is monitored (Sec. VII.A). The EPR curves are obtained by scanning the frequency of the oscillating magnetic field across the Larmor frequency of the Rb atoms. Neglecting gas phase relaxation, the amplitude of the transverse polarization produced by the oscillating magnetic field in the presence of a magnetic field gradient is governed by the Torrey equation (Torrey, 1956)

$$\frac{\partial \psi(t)}{\partial t} = \left(D\nabla^2 - i\sigma_{\parallel} z - i\omega_0\right)\psi(t)\,. \tag{55}$$

Because the cell length is more than one order of magnitude smaller than its radius, the signal is predominantly affected by the wall interactions on the front and back surfaces, and determined by the longitudinal modes $\psi_n(z)$ of the Torrey equation

$$\left(D\frac{d^2}{dz^2} - i\sigma_{\parallel} z - i\omega_0 + \alpha_n\right)\psi_n(z) = 0\,. \tag{56}$$

The real and imaginary parts of the eigenvalues α_n correspond to the width and center frequency of the modes of the magnetic resonance lines. The wall interactions are described by a boundary condition, which in the present case is shown to be (Schaden *et al.*, 2007)

$$0 = \pm\frac{\partial}{\partial z}\psi_n(z) + \mu\psi_n(z) + \eta\frac{\partial^2}{\partial z^2}\psi_n(z)\bigg|_{z=\pm L/2}\,, \tag{57}$$

with

$$\mu = \frac{3(\xi_s + i\phi_s)}{4\lambda} \quad \text{and} \quad \eta = \frac{\tau_s\bar{v}}{4}\,, \tag{58}$$

where ξ_s is the relaxation probability per wall collision, ϕ_s the average phase shift of Zeeman transitions during the wall collision, and τ_s the dwell time. The boundary condition (57) is derived using a binomial model for diffusion (Schaden *et al.*, 2007) and agrees with the boundary condition (10) except that μ and η in (57) are parameters and not operators.

Comparing with Eq.(17) one sees that ξ_s and τ_s are related to the corresponding quantities ξ_s^B and τ_s^B defined by Masnou-Seeuws and Bouchiat (1967) by $\xi_s = 2\,\xi_s^B/(2-\xi_s^B)$ and $\tau_s = 2\,\tau_s^B/(2-\xi_s^B)$. The difference originates from the definition of the dwell time τ_s. Schaden *et al.* (2007) assumed a Poisson process for the adsorption, in which a Rb atom leaves the surface in any equal time interval with equal probability, and τ_s is the average of the Poisson distribution. Masnou-Seeuws and Bouchiat, on the other hand, assumed that the polarized Rb atoms, on average, leave the surface after a relatively sharp time delay τ_s^B, such that Eq.(16) is satisfied. On anti-relaxation coatings, $\xi_s^B \ll 1$, the two definitions agree with each other.

The second derivative term in the boundary condition (57), which contains τ_s, is important and cannot be ignored in some cases. For edge enhanced EPR, the longitudinal mode is $\psi_n(z) \sim A(e_n - 2isz/L)$, where A is the principal Airy function. In dimensionless quantities, the relative orders of magnitude of the three terms on the right-hand side of (57) are 1, $(D/\sigma_{\parallel})^{1/3}\mu$ and $(\sigma_{\parallel}/D)^{1/3}\eta$. Thus, when $(\sigma_{\parallel}/D)^{1/3}\eta \sim 1$, which corresponds to long τ_s, the second derivative term cannot be ignored. When the longitudinal magnetic field gradient is zero or can be neglected as in the case of ultrathin cells, the longitudinal modes are plane waves with wavenumber $k \sim 1/L$. The orders of magnitude of the three terms in (57) are 1, $L\mu$, η/L. Thus, for sufficiently small cell length L or sufficiently long dwell time τ_s such that $\eta/L \sim L\mu$ holds, the second derivative term again is not negligible (Zhao *et al.*, 2010).

The eigenvalue α_n in Eq.(56) can be written as $\alpha_n = (D\sigma_{\parallel}^2)^{1/3}e_n + i\omega_0$, where e_n is the dimensionless longitudinal eigenvalue. Through the boundary conditions (57) and (58), e_n depends on the wall interaction parameters ξ_s, ϕ_s, and τ_s as well as the gas kinetic parameters λ and $\bar{v}$, and in general must be determined numerically.

To understand some general features of the edge enhanced EPR signals, we consider the special case $\mu = \eta = 0$, where analytical solutions can be obtained. The line shape in such cells depends qualitatively on a dimensionless parameter $s = \frac{L}{2}(\sigma_{\parallel}/D)^{1/3}$ (Schaden *et al.*, 2007; Stoller *et al.*, 1991; de Swiet, 1995; de Swiet and Sen, 1994). For $s < 1.31$, all the eigenvalues are real, corresponding to the absence of localized modes. As s increases, the lowest pair of eigenvalues e_0 and e_1 coalesce, and for $s > 1.31$ they form a pair of complex conjugate eigenvalues, corresponding to the appearance of the first two localized modes near the front and back surfaces (edge enhancement). As s increases further, the next pair of eigenvalues e_2 and e_3 begin to coalesce, and for $s > 3.06$ they form another complex conjugate pair, corresponding to the formation of a second pair of localized modes. For small s, there are only nonlocalized modes, and e_n $(n > 0)$ is much larger than e_0. In this case only the lowest mode e_0 contributes significantly to the signal.

This dependence of the EPR curves on the dimensionless parameter s is illustrated in Fig. 6. For OTS (octadecyltrichlorosilane $CH_3(CH_2)_{17}SiCl_3$) coating, the characteristics of the EPR curves are similar to those in a cell with nonrelaxing walls. Thus for $s < 1.31$, the EPR curves consist only of nonlocalized modes. For $s > 1.31$, localized modes start to appear.

From the symmetry point of view, the EPR signal is governed by Eq.(56) with a non-hermitian Hamiltonian, which, however, is PT-symmetric. The boundary conditions (57) at $z = \pm L/2$ are approximately PT-symmetric in cells coated with anti-relaxation coatings. Fig. 6 provides an experimental demonstration of the continuous transition from the unbroken PT-symmetry (nonlocalized modes) to spontaneously broken PT-symmetry (localized modes) in non-hermitian quantum mechanical systems with PT-symmetry. If $L \to \infty$, $s \to \infty$. In that case all the eigenmodes are localized, and PT-symmetry is always spontaneously broken, in agreement with the theoretical studies for infinite space by Bender and Boettcher (1998).

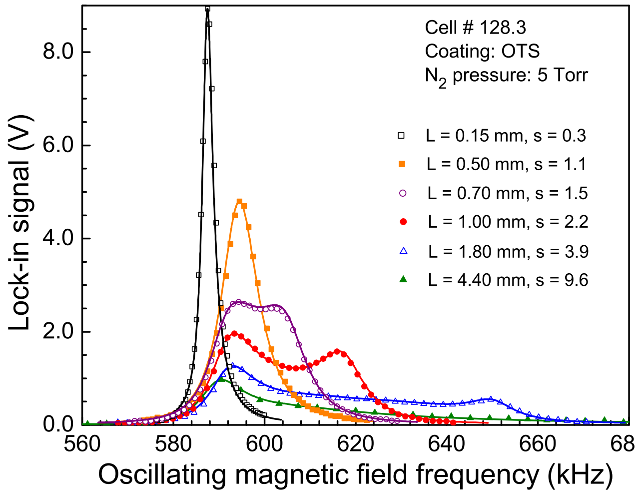

FIG. 6 A representative series of edge enhanced EPR curves. The Larmor frequency gradient $\sigma_\parallel/2\pi$ is 400 kHz/cm. The position of the front cell surface remains fixed as the cell length L is varied. Symbols denote experimental data, and solid lines are calculated from theory (Schaden *et al.*, 2007, 2008; Zhao *et al.*, 2008b). Adapted from Zhao *et al.*, 2010.

2. Study of wall interactions using edge enhanced EPR

The localized modes of the edge enhanced EPR are very sensitive to wall interactions, especially when the edge enhanced peaks are well resolved, and therefore can be used to study the wall interactions of spin-polarized alkali metal atoms. Unlike the symmetric edge enhancement peaks in the traditional NMR experiments, the use of evanescent waves results in an asymmetry between the mode localized near the front wall, where the evanescent pump and probe beams are, and the one at the back wall. This asymmetry strongly depends on surface characteristics.

To determine the microscopic parameters τ_s, ξ_s and ϕ_s for the wall interactions of Rb atoms, it is important to use a cell of adjustable length so that the series of edge enhanced EPR curves obtained for a number of different cell lengths can be fitted by adjusting only the length of the cell and using the same set of surface parameters since the surface properties remain exactly the same when the cell length is varied. This fitting procedure is based on the calculations described in Schaden *et al.* (2007, 2008) and Zhao *et al.* (2008b), and accurately determines the surface parameters (Fig. 7). The parameters τ_s and ξ_s are given in Table II for three representative cells. The Zeeman phase shift ϕ_s on OTS and silicone is too small to be determined reliably. The sensitivity of the fit to surface parameters is demonstrated in Fig. 7(a) for τ_s, illustrating the importance of the second derivative term in the boundary condition (10), which is proportional to τ_s. Using the values of ξ_s and neglecting ϕ_s, one can deduce from Eq.(58) the normal gradient coefficient μ on coated walls as shown in Table II.

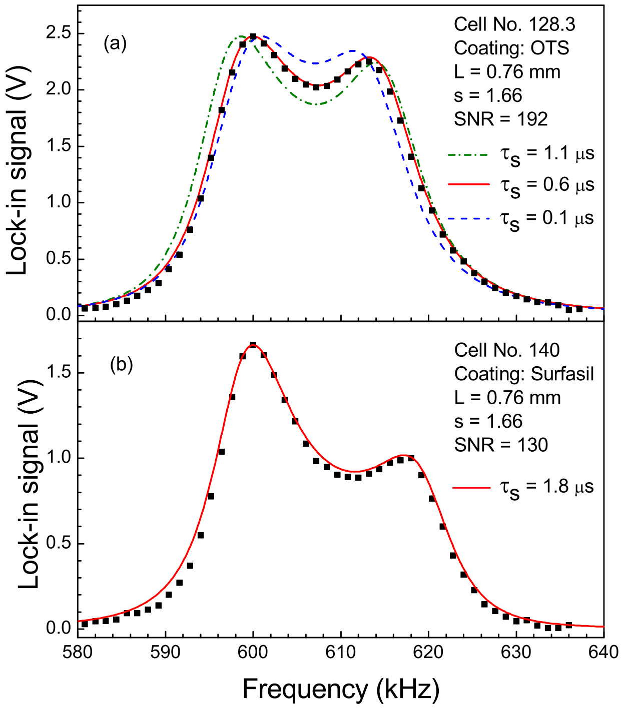

FIG. 7 Representative edge enhanced EPR curves. Filled squares represent experimental data, and solid red lines are the calculated curves corresponding to the best fit. Also shown in (a) are calculated curves (dashed blue and dash-dotted green) that correspond to less optimal values of τ_s, with all other parameters being kept the same. The cell body temperature is 105°C. From Zhao *et al.*, 2008a.

Table II. Representative values of τ_s, ξ_s, ϕ_s, and μ at cell temperature 105°C for three Pyrex glass cells coated with OTS and silicone (Surfasil), the buffer gas (N$_2$) density being 6×10^{-3} amg. Adapted from Zhao *et al.*, 2008a.

Coating	τ_s (μs)	ξ_s (10^{-3})	ϕ_s (mrad)	μ (cm^{-1})
OTS	0.6	1.6	< 1.0	0.40
OTS	0.5	1.0	< 1.0	0.25
Surfasil	1.8	15	< 1.0	3.75

D. Spatial distribution of the polarization of the alkali metal atoms near the wall

1. Normal gradient coefficient

For alkali metal atoms, due to the wall interactions, the polarization near the wall is usually smaller than that far away from the wall, resulting in a layer of inhomogeneous polarization near the wall. When the diffusion equation is applicable, the spatial distribution of the polarization near the wall can be determined as follows (Masnou-Seeuws and Bouchiat, 1967). Consider a one dimensional problem with the cell wall at $z = 0$. The z-axis points out of the cell. Suppose the optical pumping rate P and gas phase relaxation rate $1/T$ are spatially uniform. In the steady state, diffusion equation (2) for the expectation value of an observable Q, such as longitudinal polarization, becomes

$$-D\frac{d^2\langle Q\rangle}{dz^2} = P(q - \langle Q\rangle) - \frac{\langle Q\rangle}{T} \ , \tag{59}$$

where q is related to $\langle Q\rangle_{-\infty}$, the equilibrium value of $\langle Q\rangle$ far away from the wall, by $\langle Q\rangle_{-\infty} = Pq/(P + T^{-1})$. The wall interaction is described by the boundary condition (17), neglecting the second derivative term,

$$\left.\frac{d\langle Q\rangle}{dz}\right|_{z=0} = -\mu\langle Q\rangle_0 \ , \tag{60}$$

where the normal gradient coefficient $\mu = 3\,\xi_s^B/2\lambda(2 - \xi_s^B)$. The solution of Eqs.(59) and (60) is

$$\langle Q\rangle = \langle Q\rangle_0 + \mu\lambda_D\langle Q\rangle_0\,(1 - e^{z/\lambda_D}) \ , \tag{61}$$

where $\lambda_D = \sqrt{D/(P + T^{-1})}$ is the characteristic width of the inhomogeneous layer near the wall. For small z, the boundary condition (60) allows $\langle Q\rangle$ to be written as

$$\langle Q\rangle = \langle Q\rangle_0 - \mu\langle Q\rangle_0\, z \ . \tag{62}$$

From the boundary condition (60) one sees that if the cell wall were displaced backward a distance $1/\mu$ and the slope of $\langle Q\rangle$ at $z = 0$ were to extend to the displaced wall, $\langle Q\rangle$ would be zero at the displaced wall, in analogy with viscous slip in gas kinetic theory (Kennard, 1938). Thus $1/\mu$ describes how close to zero the polarization at the cell wall is. For example, $\mu = \infty$ corresponds to zero polarization at the wall and $\mu = 0$ to uniform polarization in a cell with non-relaxing walls.

2. Zeeman polarization near the wall

Grafström and Suter (1996a,b) used reflection spectroscopy to study the Zeeman polarization near the cell wall. They measured μ and ξ_s^B for Na atoms in both coated and uncoated Pyrex cells. The experiment was done in cells that contained Na and 0.12 amg Ar buffer gas at a temperature of 540 K. The Na vapor was polarized by a horizontal pump beam, the polarization of which was modulated between left and right circular polarizations. A static magnetic field was applied in the vertical direction. The inhomogeneous layer of the vapor polarization near the wall was studied using a linearly polarized horizontal probe beam at an angle of incidence slightly smaller than the critical angle θ_c of total internal reflection. The change in the polarization of the reflected probe beam served as the signal (Sec. VII.B).

The wall interaction parameters were obtained by comparing the measured line shape of the signal with the calculated one. The experiment was carried out using two different but complementary methods. In the first method the polarization of the pump beam was modulated at the Larmor frequency while its frequency was scanned across the resonance. In the second method the frequency of the pump beam was fixed at resonance while the modulation frequency of its polarization was scanned across the Larmor frequency. The former is suitable for large ξ_s^B while the latter for small ξ_s^B. Thus it was found that for uncoated Pyrex glass cells $\xi_s^B = 0.47$ and $\mu = 5.1 \times 10^3\,\text{cm}^{-1}$. The polarization at the wall is 3% of that far away from the wall. For silicone-coated cells it was found that $\xi_s^B = 0.01$ and $\mu = 84\,\text{cm}^{-1}$. The polarization at the wall is 70% of that far away from the wall. Thus the values of ξ_s^B and μ in silicone-coated cells agree with those obtained using edge enhanced EPR in a silicone-coated cell (see Table II) since μ is proportional to the buffer gas density.

3. Hyperfine polarization near the wall

The normal gradient coefficient for the hyperfine polarization in uncoated cells was estimated using evanescent wave spectroscopy (Zhao and Wu, 2003, 2005). The hyperfine polarization of the ground-state Rb atoms is

$$\langle \boldsymbol{S}\cdot\boldsymbol{I}\rangle = \frac{I(I+1)}{n_a + n_b}\left(\frac{n_a}{g_a} - \frac{n_b}{g_b}\right) \ , \tag{63}$$

where n_a and n_b are, respectively, the population densities of the ground-state hyperfine multiplets, with g_a and g_b being their statistical weights. Uncoated Pyrex glass cells were filled with ^{87}Rb vapor and 0.03 amg of N_2 gas. The hyperfine polarization was produced by a pump beam perpendicular to the cell surface and tuned to the transitions $^2S_{1/2}\,F = 1 \rightarrow {}^2P_{1/2}\,F' = 1, 2$, and probed by a weak beam at an angle of incidence slightly larger than the critical angle θ_c of total internal reflection (Sec. VII.C). The frequency ν of the probe beam was scanned across the Rb $D1$ line, and its reflectivity $\mathcal{R}(\nu)$ measured. For each penetration depth d of the probe beam, the average population densities $\overline{n}_a$ and $\overline{n}_b$, determined as the fitting parameters that gave the best fit between the measured $\mathcal{R}(\nu)$ and the calculated one, were used in Eq.(63) to compute the average hyperfine polarization $\overline{\langle \boldsymbol{S}\cdot\boldsymbol{I}\rangle}$. A linear fit of the data points from three uncoated Pyrex cells that correspond to $d \leq 1.0\times10^{-4}\,\mathrm{cm}$ yields an intercept $\langle \boldsymbol{S}\cdot\boldsymbol{I}\rangle_0 = 0.14$ as compared with $\langle \boldsymbol{S}\cdot\boldsymbol{I}\rangle_{-\infty} = 0.73$ and a slope of $-0.9\times10^3\,\mathrm{cm}^{-1}$. From Eq.(62) one obtains $\mu = 6\times10^3\,\mathrm{cm}^{-1}$.

E. Phase shift of hyperfine transitions due to wall collisions

During the wall collision of an alkali metal or hydrogen atom, the van der Waals forces between the colliding atom and the constituent atoms of the wall in most cases outweigh the Pauli exclusion forces, and cause a net reduction of the unpaired electron density at the nucleus of the alkali metal or hydrogen atom, resulting in a downward shift of its hyperfine transition frequency and consequently a negative phase shift. However, for hydrogen atoms, due to their small polarizability, the van der Waals forces in some cases are cancelled or even outweighed by the Pauli exclusion forces. This causes the unpaired electron density at the proton to remain unchanged or even increase, resulting in a null or an upward frequency shift and hence a zero or a positive phase shift. The measured phase shift ϕ_{hfs} per wall collision is the ensemble average of the time-weighted average phase shifts per wall collision of individual atoms.

Zitzewitz and Ramsey (1971) studied the temperature dependence of ϕ_{hfs} for the hyperfine transition of H atoms on Teflon–120, and observed a continuous change of the phase shift from negative to positive values, crossing zero at 374 K. Similar temperature dependence of ϕ_{hfs} for H atoms on Teflon–120 was observed with a slightly different temperature (385 K) for the zero phase shift (Petit *et al.*, 1980). This change of ϕ_{hfs} from negative to positive values with increasing temperature was attributed to the change of the relative importance of the van der Waals forces and the Pauli exclusion forces as a result of phase changes in Teflon. The same physics, that is, the relative importance of the attraction and repulsion forces, also explains the hyperfine frequency shift of H atoms trapped in noble gas matrices, upward shift for Ne, and downward shift for Ar, Kr, and Xe (Adrian, 1960; Foner *et al.*, 1960), and the pressure shift in optical pumping (Anderson *et al.*, 1960; Arditi and Carver, 1958).

In hydrogen masers (Goldenberg *et al.*, 1960; Kleppner *et al.*, 1962a) the hyperfine frequency shift due to wall collisions in the storage bulb constitutes one of the most important factors that affect the long term frequency stability. Due to its importance in atomic frequency standards, the phase shift ϕ_{hfs} for alkali metal and hydrogen atoms on various coatings has been measured. Some representative measured values are listed in Table III.

Table III. Average phase shift ϕ_{hfs} per wall collision of the $0-0$ hyperfine transition in the ground state of the alkali metal atom and hydrogen atom in coated cells. In the study of Robinson and Johnson, $(2,\pm2)\rightarrow(1,\pm1)$ hyperfine transitions were used.

Coating	Isotope	ϕ_{hfs} (mrad)	T (K)	Reference
Paraflint	^{85}Rb	−21	343	Vanier *et al.* (1974)
Paraflint	^{85}Rb	−22	298	Budker *et al.* (2005)
$C_{50}H_{102}$	^{85}Rb	−37	298	Budker *et al.* (2005)
D–Paraffin	^{85}Rb	−49	306	Corsini *et al.* (2013)
Alkene C20–24	^{85}Rb	−32	302	Corsini *et al.* (2013)
Alkene C30	^{85}Rb	−39	303	Corsini *et al.* (2013)
Paraflint	^{87}Rb	−59	303	Brewer (1963)
$C_{40}H_{82}$	^{87}Rb	−58	299	Robinson and Johnson (1982)
Paraflint	^{87}Rb	−65	298	Budker *et al.* (2005)
$C_{40}H_{82}$	^{87}Rb	−50	294	Budker *et al.* (2005)
$C_{40}H_{82}$	^{87}Rb	−43	295	Budker *et al.* (2005)
Alkene C20–24	^{87}Rb	−39	302	Corsini *et al.* (2013)
Paraflint	^{133}Cs	−90		Goldenberg *et al.* (1961)
Paraffin	^{39}K	−2.8	325	Guzman *et al.* (2006)
$(CH_3)_2SiCl_2$	H	0.19		Kleppner *et al.* (1962a)
$(CH_3)_2SiCl_2$	H	−0.076	300	Zitzewitz and Ramsey (1971)
Teflon−120	H	−0.022	150	Desaintfuscien *et al.* (1977)
Teflon−120	H	−0.0016	360	Zitzewitz and Ramsey (1971)
Teflon−120	H	0	374	Zitzewitz and Ramsey (1971)
Teflon−120	H	0.0039	410	Zitzewitz and Ramsey (1971)

The phase shift ϕ_{hfs} is proportional to $\nu_0 E_a$, where ν_0 is the hyperfine frequency of the free atom and E_a the adsorption energy (Goldenberg *et al.*, 1961). The latter is proportional to $\alpha\alpha_s$, with α and α_s being respectively the polarizability of the adsorbed atom and that of the constituent atoms of the wall (see Eq.(68)). For example, the ratio of the measured phase shift for ^{87}Rb to that for ^{85}Rb on Paraflint is approximately equal to the ratio of ν_0 for ^{87}Rb to that for ^{85}Rb since α is the same for isotopes. The small phase shift for hydrogen, especially on flurocarbon surfaces, is due to the small polarizabilities of hydrogen and fluorine.

The average phase shift ϕ_{hfs} per wall collision is deduced from the measured hyperfine frequency shift $\Delta\omega_{\mathrm{hfs}}$, which is related to ϕ_{hfs} by

$$\Delta\omega_{\mathrm{hfs}} = \frac{\phi_{\mathrm{hfs}}}{\tau_b+\tau_s}\,, \tag{64}$$

where τ_b is the average time between two consecutive wall collisions. Since $\tau_s \ll \tau_b$ in most experiments, Eq.(64) can often be written as $\Delta\omega_{\mathrm{hfs}} = \phi_{\mathrm{hfs}}/\tau_b$.

Eq.(64) is the ensemble average of the time-weighted average frequency shifts of individual atoms. It is valid for $\xi_s \ll 1$, in which case the atom undergoes many wall collisions before it relaxes so that the width of the distribution of time-weighted average frequency shifts for individual atoms is sufficiently narrow for an ensemble average frequency shift given by Eq.(64) to be well-defined. The dispersion in the time-weighted average frequency shifts of individual atoms results in a line broadening (Goldenberg *et al.*, 1961).

F. Wall interactions on alkali hydride

On the alkali hydride walls such as CsH, the Cs^+ and H^- are isoelectronic to Xe and He, and therefore both the scalar magnetic dipole-dipole interaction and the spin-rotation interaction of the alkali metal atoms are orders of magnitude larger on Cs^+ than on H^- (Sec. IV.A).

1. Polarization of alkali hydride walls

Even though the polarization of the hydrocarbon or silane coatings due to the wall collisions of polarized alkali metal atoms is negligible (Sec. V.C and Table II), the nuclear polarization of $^{133}Cs^+$ on the CsH coating by the polarized Cs vapor was observed (Ishikawa *et al.*, 2007).

Cells coated with CsH film were filled with Cs vapor and N_2 gas. To facilitate the detection of the nuclear polarization of CsH salt, a magnetic field of 9.4 T was used. At such high fields the electron and nuclear spins of the Cs atom are decoupled to a first approximation. However, optical pumping can still produce a small nuclear polarization of the gas phase Cs atoms through the momentary hyperfine-shift interaction $\delta A\,\hbar^2 \boldsymbol{S}\cdot\boldsymbol{I}$ due to a small change in the valence electron density at the nucleus of the Cs atom during the Cs–N_2 collisions (Adrian, 1960; Arditi and Carver, 1961; Walter *et al.*, 2002).

Either the polarized electrons or the polarized nuclei of the Cs atoms in the vapor can polarize the $^{133}Cs^+$ nuclei on CsH. However, the dependence of the NMR enhancement on the N_2 pressure is different for the two mechanisms, from which it was concluded that at 9.4 T the $^{133}Cs^+$ nuclei were polarized mainly by the electrons of the Cs atoms via the scalar magnetic dipole-dipole interaction. The enhanced NMR signal for the $^{133}Cs^+$ nuclei at 9.4 T is shown in Fig. 8. One possible reason for the modest NMR enhancement is the large energy mismatch of the spin exchange wall interaction between the Cs electron and the Cs^+ nucleus at high fields.

Larger enhancement was observed at a lower magnetic field of 2.7 T. The lower magnetic field allows the hyperfine coupling $A\hbar^2 \boldsymbol{S}\cdot\boldsymbol{I}$ to bring into the decoupled states $|m_S, m_I\rangle$ larger amplitude of admixtures such as $|m_S \pm 1, m_I \mp 1\rangle$ with the same $m_S + m_I$ so that optical pumping can directly excite transitions which change the values of m_I, thus increasing the nuclear polarization of the gas phase Cs atoms, which can therefore also contribute to the nuclear polarization of $^{133}Cs^+$ through the tensorial magnetic dipole-dipole interaction.

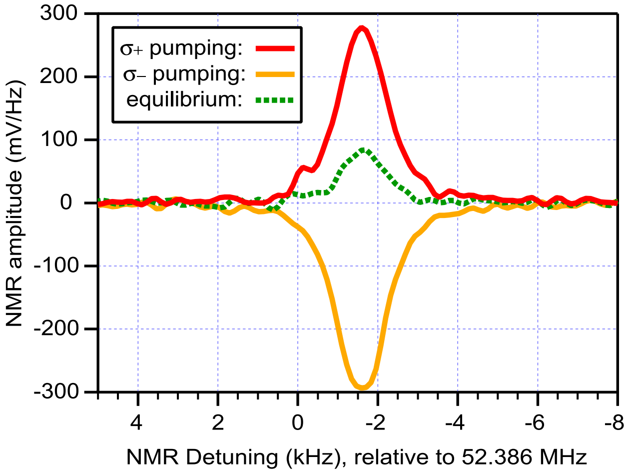

FIG. 8 NMR spectra of $^{133}Cs^+$ in CsH coating. Also shown for comparison is the thermal signal. From Ishikawa *et al.*, 2007.

2. Phase shift of Zeeman transitions on alkali hydride walls

The phase shift of Zeeman transitions for alkali metal atoms due to wall collisions, while being too small to be reliably measured on silane coatings such as OTS because of the negligible wall polarization (Sec. IV.C.2), was measured on RbH-coated walls thanks to the enhanced scalar magnetic dipole-dipole interaction at the Rb^+ sites (Ulanski and Wu, 2014). The phase shift ϕ_s produces a Zeeman frequency shift $\delta\omega_s$. EPR frequency shift of the same origin is also observed for the alkali metal atoms in a gaseous mixture with polarized noble gas atoms (Happer *et al.*, 1984; Newbury *et al.*, 1993a; Schaefer *et al.*, 1989, 1990).

The experiment was performed in two identical cylindrical Pyrex cells of variable length containing ^{87}Rb and N_2, one coated with OTS and the other with RbH. The $\sigma^\pm$ beams optically pumped ^{87}Rb atoms from the $F = 1$ level in order to guarantee that the sign of the light shift $\delta\omega_{\rm light}$ is opposite to that of the wall shift $\delta\omega_s$ (Mathur *et al.*, 1968), thus allowing $\delta\omega_s$ to be unambiguously identified. A weak s-polarized evanescent probe beam was tuned to $5\,^2S_{1/2}\,F = 2 \rightarrow 5\,^2P_{1/2}\,F' = 1, 2$, and its Faraday rotation, which depends on the polarization of the $F = 2$ level, was measured by a Wollaston prism (Sec. VII.B.2) and produced the EPR curve when the frequency of an oscillating magnetic field along the y-axis scanned across the Larmor frequency of the Rb atom.

The EPR frequency is $\omega^{(\pm)} = \omega_0 \pm \delta\omega_{\rm light} \pm \delta\omega_s$ for $\sigma^\pm$ pumping. Thus $\omega^{(+)} - \omega^{(-)} = 2\delta\omega_{\rm light} + 2\delta\omega_s$. The observation that $\omega^{(+)} - \omega^{(-)}$ does not depend on the cell length L and remains negative in the OTS-coated cell whereas in the RbH-coated cell it increases from negative to positive as L decreases shows that the frequency shift due to wall collisions is negligible in the OTS-coated cell but not in the RbH-coated cell. By measuring $\omega^{(+)}-\omega^{(-)}$ in cells coated with OTS and RbH one obtains $\delta\omega_s$.

Including the light shift and considering only the lowest mode $\psi_0(z) \sim \cos 2x_0 z/L$ (Sec. IV.C.1), one obtains from Eq.(56) the eigenvalue $\alpha_0 = i\omega_0 + i\delta\omega_{\text{light}} + 4x_0^2 D/L^2$. The imaginary part of $4x_0^2 D/L^2$ is the EPR frequency shift due to wall collisions

$$\text{Im}\, 4x_0^2 D/L^2 = \delta\omega_s \,. \tag{65}$$

Since τ_s is expected to be short on the alkali hydride wall, the second derivative term can be neglected in the boundary condition (57), which can then be written as

$$x_0 \tan(x_0) = \frac{3L}{8\lambda}(\xi_s + i\phi_s)\,, \quad \text{with } \ 0 < \text{Re}\, x_0 < \pi/2\,. \tag{66}$$

The boundary condition (66) can be used together with Eq.(65) to compute ϕ_s (Zhao *et al.*, 2010), which was found to be about 70 mrad per wall collision.

V. THE TIME SCALE OF WALL INTERACTIONS

A complete microscopic description of the wall interactions of spin-polarized atoms requires the knowledge of three microscopic time parameters τ_c, τ_s and τ_s'. The important roles they play in the wall interactions and the experimental methods for determining them will be discussed in this section.

A. Correlation time τ_c

The wall interaction as a stationary random function is characterized by a correlation time τ_c. Physically τ_c describes the time interval in which the wall interaction is coherent and efficacious in causing the spin relaxation of adsorbed atoms. The correlation time τ_c is most helpful in identifying the type of wall interactions that is responsible for the relaxation of a given observable. The relaxation probability is proportional to the spectral density $J(\omega_{fi})$ of the correlation function of the wall interaction at the transition frequency ω_{fi} (see Eq.(40)). The spectral width of $J(\omega_{fi})$ is $\sim 1/\tau_c$, and consequently the wall interaction is effective in producing transitions of frequency $\omega_{fi} < 1/\tau_c$. Thus, for transitions with large ω_{fi}, wall interactions with shorter τ_c are expected to be more effective in relaxing the spins. For example, in the case of Rb on paraffin, since for the typical magnetic fields used in the experiment, $\omega_F \ll \Delta W$, the relaxation of $\langle S_z \rangle$ is associated with the magnetic dipole-dipole interaction, which has a longer correlation time, whereas the relaxation of $\langle \boldsymbol{S}\cdot\boldsymbol{I} \rangle$ is mainly due to the spin-rotation interaction, which has a much shorter correlation time (Bouchiat and Brossel, 1966).

Vastly different values for τ_c have been reported, ranging from 10^{-12} to 10^{-5} s. For example, for Rb on paraffin, the correlation time is $\sim 10^{-12}$ s for the spin-rotation interaction and 4×10^{-10} s for the magnetic dipole-dipole interaction (Bouchiat and Brossel, 1966). On the other hand, τ_c for the wall interaction of ^{129}Xe on silicone-coated walls is $\sim 10\,\mu$s (Driehuys *et al.*, 1995). One possible explanation for such a long correlation time is that the ^{129}Xe atoms are trapped in clathrates formed by the constituent atoms of the coating (Driehuys *et al.*, 1995; Dybowski *et al.*, 1991). The exceedingly long τ_c also seems to imply that the neighboring protons in the clathrate are polarized, which is consistent with the observation of the proton polarization in the coating (Sec. III.D).

For the wall interactions that cause the relaxation of Zeeman polarization, the transition frequency ω_{fi} is proportional to the external magnetic field B. Thus the relaxation rate, which is proportional to $J(\omega_{fi})$, decreases with increasing B. The magnetic decoupling method utilizes this magnetic field dependence of the relaxation rate to determine τ_c. For example, a fit of the magnetic field dependence of the relaxation rate of $\langle I_z \rangle$ for ^{129}Xe on silicone-coated walls to a sum of two expressions of Eq.(38) yields two correlation times, the longer one being $\tau_c = 8.1 \pm 1.0\,\mu$s (Driehuys *et al.*, 1995). Similarly, the magnetic field dependence of the relaxation rate of $\langle S_z \rangle$ for Rb on paraffin yields a correlation time $\tau_c > 10^{-10}$ s for the magnetic dipole-dipole wall interaction (Bouchiat and Brossel, 1966). For the quadrupole wall interaction of ^{201}Hg in quartz cells, there was little change in the relaxation rate of ^{201}Hg when the magnetic field increased from zero to 350 G, from which an upper limit $\tau_c < 10^{-7}$ s was deduced for the correlation time of the quadrupole wall interaction (Cohen-Tannoudji, 1963).

For the spin-rotation interaction, which causes the relaxation of $\langle \boldsymbol{S}\cdot\boldsymbol{I} \rangle$, one deduces τ_c by comparing the relaxation rate of $\langle \boldsymbol{S}\cdot\boldsymbol{I} \rangle$ for two isotopes which have different ΔW. For example, the observation that the relaxation rate of $\langle \boldsymbol{S}\cdot\boldsymbol{I} \rangle$ on $\mathrm{C_nD_{2n+2}}$ is practically the same for both Rb isotopes implies that $J_{sr}(\Delta W_{85}) = J_{sr}(\Delta W_{87})$ so that $\Delta W \tau_c \ll 1$ for both isotopes, from which one deduces $\tau_c \ll 2.3 \times 10^{-11}$ s (Bouchiat and Brossel, 1966). Physically, the spin-rotation wall interaction has a short correlation time because $\boldsymbol{v}$ in Eq.(47) changes sign in a vibration period ($\sim 10^{-12}$ s).

B. Average dwell time τ_s on the wall

The average dwell time τ_s on the wall is the ensemble average of the time that a spin-polarized atom stays on the wall without losing its polarization. It is one of the most important microscopic parameters of wall interactions. The dwell time τ_s is given by the Arrhenius relation (de Boer, 1953)

$$\tau_s = \tau_0 \, e^{-E_a/kT} \ , \tag{67}$$

where E_a is the adsorption energy and τ_0 describes the migration of adsorbed atoms on or in the wall. When there is diffusion into the wall, τ_0 can be orders of magnitude larger than τ_0' (see Eq.(71)).

Adsorption energy E_a is a negative quantity. Thermodynamically, this is due to the fact that the change of the Gibbs free energy must be negative ($\Delta G = \Delta H - T\Delta S < 0$) for adsorption of gas phase atoms to occur. Since the motion of the atoms is more restricted when they are adsorbed on the wall than when they are in the gas phase, the entropy of the system decreases with adsorption ($\Delta S < 0$). Therefore, adsorption must be exothermic ($\Delta H < 0$), and hence $E_a < 0$.

The microscopic nature of the adsorption is the van der Waals attraction forces between the adsorbed atom and the constituent atoms of the wall. Considering only the dipole-dipole interaction, the adsorption energy E_a is approximately given by (de Boer, 1950)

$$E_a = -\sum \frac{3}{2\,r^6} \alpha \alpha_s \frac{I_s I}{I_s + I} \ , \tag{68}$$

where the summation includes all the constituent atoms of the wall, r is the distance between these wall atoms and the adsorbed atom, I the ionization energy of the adsorbed atom, and I_s that of the constituent atoms.

When the Arrhenius relation (67) holds, E_a and τ_0 can be deduced from the temperature dependence of τ_s. However, in almost all the experimental studies, τ_s is not directly measured. What is measured is the temperature dependence of a quantity that is proportional to τ_s. Therefore only E_a and not τ_0 can be determined. Some of these quantities are the hyperfine frequency shift of alkali metal or hydrogen atoms, the relaxation rate of $\langle S_z \rangle$ of alkali metal atoms, the relaxation rate of $\langle I_z \rangle$ of ^{3}He and ^{129}Xe, and the beat period of the precession signal of ^{131}Xe. For example, the hyperfine frequency shift $\Delta\nu_{\rm hfs}$ due to wall collisions is proportional to the fraction $\tau_s/(\tau_b + \tau_s)$ of time an atom is adsorbed on the wall, which is approximately equal to τ_s/τ_b because in most experiments $\tau_s \ll \tau_b$. Since τ_b is proportional to $T^{-1/2}$, the slope of a plot of $\ln(\Delta\nu_{\rm hfs} T^{-1/2})$, or $\ln(\Delta\nu_{\rm hfs})$, an approximation used in some studies for small temperature ranges, against $1/kT$ yields E_a. Some reported values of E_a for alkali metal atoms, the hydrogen atom and noble gas atoms on various walls are listed in Table IV.

More than one type of adsorption site could exist on the wall. Müller (1965) found that the adsorption of unpolarized helium atoms on the glass surface for temperatures between 13.8 K and 20.4 K could be described by two different adsorption energies, $E_a = -0.01 \pm 0.002$ eV and $E_a = -0.023 \pm 0.001$ eV, with the latter corresponding to only a very small fraction ($\sim 10^{-4}$) of the adsorption sites. Fitzsimmons *et al.* (1969) found that the temperature dependence of the relaxation rate $1/T_1$ for polarized ^{3}He on aluminosilicate glass could be described

Table IV. Some representative measured values of the adsorption energy E_a on various walls.

Coating	Isotope	$\lvert E_a \rvert$ (eV)	Reference
Paraflint	^{85}Rb	0.078	Vanier *et al.* (1974)
Si(CH$_3$)$_2$Cl$_2$	Rb	0.2	Camparo (1987)
Paraflint	^{87}Rb	0.1	Brewer (1963)
Paraffin	^{87}Rb	0.1	Bouchiat and Brossel (1966)
C$_{40}$H$_{82}$	^{87}Rb	0.062 0.076 [a]	Rahman and Robinson (1987)
OTS	^{87}Rb	0.065	Yi *et al.* (2008)
OTS	^{87}Rb	0.19	Zhao *et al.* (2009)
C$_{40}$H$_{82}$	^{87}Rb	0.06	Budker *et al.* (2005)
Sapphire	Na	0.75	Bonch-Bruevich *et al.* (1985)
Pyrex	Na	0.71	Gozzini *et al.* (1992)
Paraflint	Cs	0.09	Liberman and Knize (1986)
Pyrex	Cs	0.53	Stephens *et al.* (1994)
Sapphire	Cs	0.43	Stephens *et al.* (1994)
^{3}He (liquid)	H	3.6×10^{-5}	Jochemsen *et al.* (1981)
^{3}He +^{4} He (liquid)	H	2.9×10^{-5}	van Yperen *et al.* (1981)
^{4}He (liquid)	H	7.7×10^{-5}	Matthey *et al.* (1981)
^{4}He (liquid)	H	8.0×10^{-5}	Morrow *et al.* (1981)
^{4}He (liquid)	D	2.2×10^{-4}	Silvera and Walraven (1980)
Glass	He	0.01	Müller (1965)
Pyrex	^{3}He	0.01	Fitzsimmons *et al.* (1969)
Aluminosilicate glass	^{3}He	0.1, 0.01 [b]	Fitzsimmons *et al.* (1969)
Solid H$_2$	^{3}He	1.0×10^{-3}	Lefevre-Seguin *et al.* (1985)
Solid D$_2$	^{3}He	1.7×10^{-3}	Lefevre-Seguin *et al.* (1985)
Solid Ne	^{3}He	3.3×10^{-3}	Lefevre-Seguin *et al.* (1985)
Solid O$_2$	^{3}He	0.011	Lefevre-Seguin and Brossel (1988)
Solid N$_2$	^{3}He	0.017	Lefevre-Seguin and Brossel (1988)
Cesiated-glass	^{3}He	2.0×10^{-4}	Tastevin (1992)
Duran glass	^{83}Kr	0.095	Butscher *et al.* (1996)
Silicone	^{129}Xe	0.1	Driehuys *et al.* (1995)
Duran glass	Xe	0.3	Ahrens-Botzong *et al.* (1973)
Duran glass	^{131}Xe	0.12	Butscher *et al.* (1994)
Pyrex	^{131}Xe	0.13	Volk *et al.* (1980)
Pyrex (cured)	^{131}Xe	0.03	Wu *et al.* (1990)
RbH	^{131}Xe	0.1	(Wu *et al.*, 1990)

[a] Corresponding to temperatures 72.9 and 81.7°C, respectively.

[b] Corresponding to two kinds of adsorption sites.

by two distinct adsorption energies, $E_a = -0.01\,\mathrm{eV}$ for temperatures below $\sim 240\,\mathrm{K}$ and $E_a = -0.1\,\mathrm{eV}$ for higher temperatures. The exact nature of these sites is unknown.

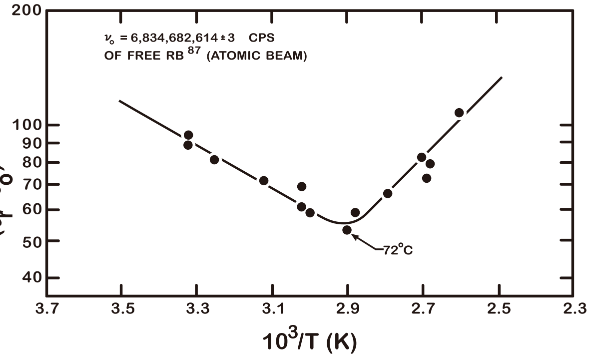

FIG. 9 Wall temperature dependence of the ^{87}Rb hyperfine frequency shift $\nu_r - \nu_0$, where ν_r is the observed hyperfine frequency and ν_0 the hyperfine frequency of the free atom, in a Paraflint-coated cell. The Rb reservoir temperature is fixed at 30°C while the wall temperature T varies. From Brewer, 1963 with the permission of AIP Publishing.

Fig. 9 shows the temperature dependence of the ^{87}Rb $0-0$ hyperfine transition frequency shift due to wall collisions in a Paraflint-coated cell. Since the frequency shift is proportional to τ_s (Brewer, 1963), Fig. 9 shows that τ_s follows the Arrhenius relation (67), decreasing as temperature increases up to 72°C, above which τ_s starts to increase rapidly as temperature further increases. It is known that Paraflint undergoes a structural change around 72°C, becoming more amorphous with increasing temperature (Brewer, 1963; Seltzer *et al.*, 2010). The large increase in τ_s is attributed to the onset of diffusion of Rb atoms into Paraflint as a result of its structural change. This reversal of slope was later observed in numerous experiments. For example, the temperature dependence of the relaxation rate of $\langle S_z \rangle$ for ^{87}Rb in paraffin-coated cells displays a reversal of slope around 60°C, which approximately corresponds to the melting point of paraffin (Bouchiat and Brossel, 1966; Seltzer *et al.*, 2013). The reversal of slope was also observed for diamagnetic atoms such as ^{199}Hg and ^{201}Hg in quartz cells and was attributed to a change in the structure of the wall (Cagnac and Lemeignan, 1967). The underlying physics of the reversal of slope was elucidated by the study of the wall relaxation of ^{3}He as described in Sec. III.B (Fitzsimmons *et al.*, 1969; Fitzsimmons and Walters, 1967). It is demonstrated that the onset of diffusion into the wall is responsible for the rapid increase in τ_s. This is further corroborated by the simultaneous observations of a rapid increase in τ_s for Rb in alkene -coated cells and a sharp decrease in the gas phase Rb density in crossing the melting point (33°C) of alkene (Balabas *et al.*, 2010).

Physically, the reason that diffusion into the coating causes a large increase in τ_s could be twofold. First, as was suggested by Brewer (1963), diffusion into the coating could make E_a more negative. This is probably because the Rb atoms inside the coating are in close proximity to more constituent atoms than when they are on the surface, and since van der Waals forces are additive, one expects a more negative adsorption energy E_a for Rb atoms inside the coating. Second, more importantly, diffusion into the coating causes Rb atoms to visit more sites, resulting in a large increase in τ_0 and hence τ_s. A more negative E_a as a result of diffusion into the coating seems to be supported by the study of Rahman and Robinson (1987), who found that for Rb on tetracontane ($C_{40}H_{82}$) coating $E_a = -0.062\,\mathrm{eV}$ at 72.9°C, below the melting temperature ($\sim$ 81°C) of tetracontane, and $E_a = -0.076\,\mathrm{eV}$ at 81.7°C, slightly above the melting temperature. A direct measurement of τ_s for Rb atoms on OTS coating at temperatures $366\,\mathrm{K} < T < 408\,\mathrm{K}$ yielded $\tau_0 = 2.2 \times 10^{-9}\,\mathrm{s}$ and $E_a = -0.19\,\mathrm{eV}$ (Zhao *et al.*, 2009). That E_a is more negative and τ_0 is much larger than τ_0' is also consistent with the aforementioned physical picture since Rb atoms are known to diffuse into OTS at these temperatures (Rampulla *et al.*, 2009).

The physical meaning of τ_0 is further illustrated by the following. The values of τ_s span several orders of magnitude. For example, for Rb on paraffin (24°C $< T <$ 35°C), it was estimated that $\tau_s \sim 10^{-9}\,\mathrm{s}$ (Seltzer *et al.*, 2013) whereas for ^{129}Xe on silicone-coated walls ($170\,\mathrm{K} < T < 300\,\mathrm{K}$), it was found that $\tau_s > 10\,\mu s$ (Driehuys *et al.*, 1995). Since $E_a = -0.1\,\mathrm{eV}$ is the same for Rb on paraffin and ^{129}Xe on silicone (see Table IV), the most obvious explanation for such a large difference in τ_s is that τ_0 is vastly different. Physically, this means that, compared with Rb, the ^{129}Xe atoms, due to their high solubility in silicone and their much weaker wall interaction, on average visit far more sites in the coating before leaving the wall without losing their polarization. In Paraflint-coated cells the exceedingly long τ_s for the Rb atoms suggested by Brewer (1963) to account for the disappearance of the hyperfine signal when Paraflint completely melts above 105°C can naturally be explained by the exceedingly large τ_0 in liquid Paraflint.

Since the adsorption energy E_a is relatively easy to measure, the uncertainty in τ_s is mainly due to τ_0, which usually is not directly measured, but is taken to be equal to $\tau_0' \sim 10^{-12}\,\mathrm{s}$, that is, the migration on the wall or the diffusion into the wall is ignored, and τ_s is underestimated. For example, using $E_a = -0.1\,\mathrm{eV}$ and $\tau_0 = 10^{-12}\,\mathrm{s}$, Brewer (1963) deduced $\tau_s = 5 \times 10^{-11}\,\mathrm{s}$ for ^{87}Rb on hydrocarbon-coated walls at 30°C, about two orders of magnitude smaller than the value reported by Seltzer *et al.* (2013).

The dwell time τ_s has not been directly measured for polarized diamagnetic atoms. For polarized alkali metal atoms, the following two direct measurements of τ_s have been reported.

Determination of τ_s using edge enhanced EPR

The dwell time τ_s as well as other wall interaction parameters can be determined from the best fit between the measured localized edge enhanced EPR lines and the calculated ones (Sec. IV.C.2). As can be seen in Fig. 7, as dwell time τ_s increases, the peaks localized near the front and back surfaces shift in frequency space further toward front and back surfaces, illustrating vividly the role of τ_s.

Determination of τ_s using light shift

The experimental arrangement is the same as that described in Sec. IV.C.1 except that the magnetic field along the x-axis is uniform throughout the cell (Zhao *et al.*, 2009). The cylindrical cell has a diameter of 25 mm and an adjustable length between 70 and 500 μm. The method owes its sensitivity to the use of thin cells of variable length in which the average time a Rb atom spends on the surface is comparable to the time it spends in the bulk. For a uniform magnetic field one only needs to consider the lowest mode $\psi_0(z) \sim \cos 2x_0 z/L$ of Eq.(56) and its eigenvalue $\alpha_0 = i\omega_0 + 4x_0^2 D/L^2$. The Rb Larmor frequency ω, which is given by $\operatorname{Im}\alpha_0$, can be written as

$$\omega = \omega_0 + \frac{\phi_s}{2L/\bar{v} + \tau_s} \,, \tag{69}$$

where we have used the boundary condition (57), which on anti-relaxation coatings ($\xi_s \ll 1$) can be approximated as $x_0^2 = L^2\mu/2(L+2\eta)$.

Since the length of the cell is approximately two orders of magnitude smaller than the diameter, the collisions of Rb atoms with the side walls can be neglected. From kinetic theory, the average time between two consecutive collisions of a Rb atom with the front or back surface is $\tau_b = 2L/\bar{v}$. Thus the boundary condition with the second derivative term reproduces the ensemble average frequency shift due to wall collisions given by Eq.(64).

Evanescent beams with $\sigma^{\pm}$ polarizations are used to pump and probe the ^{87}Rb atoms in the vicinity ($\sim 10^{-4}$ cm) of the cell wall. The negligible phase shift ϕ_s in Eq.(69) due to wall collisions is now replaced by $\phi_s + \phi_e^{(\pm)}$, where $\phi_e^{(\pm)}$ is the average light shift (Mathur *et al.*, 1968) due to the evanescent $\sigma^{\pm}$ pump beam. Let the difference between the EPR frequencies for σ^- and σ^+ pumping be $\Delta = \omega^{(-)} - \omega^{(+)}$. We have

$$\frac{2L}{\bar{v}} = (\phi_e^{(-)} - \phi_e^{(+)})\frac{1}{\Delta} - \tau_s \,. \tag{70}$$

Due to the use of evanescent pump beam, the light induced phase shift $\phi_e^{(-)} - \phi_e^{(+)}$ remains unchanged while the cell length L is varied. Thus the intercept of a plot of $2L/\bar{v}$ against $1/\Delta$ is equal to $-\tau_s$ (Fig. 10). The dwell times on the OTS coating determined using this method agree with those obtained using edge enhanced EPR (see Table II). By directly measuring τ_s for a number of different wall temperatures in an OTS-coated cell and fitting the temperature dependence of τ_s to the Arrhenius relation (67), one obtains both $\tau_0 = 2.2^{+5.1}_{-1.4} \times 10^{-9}$s and $E_a = -\,0.19 \pm 0.03$ eV.

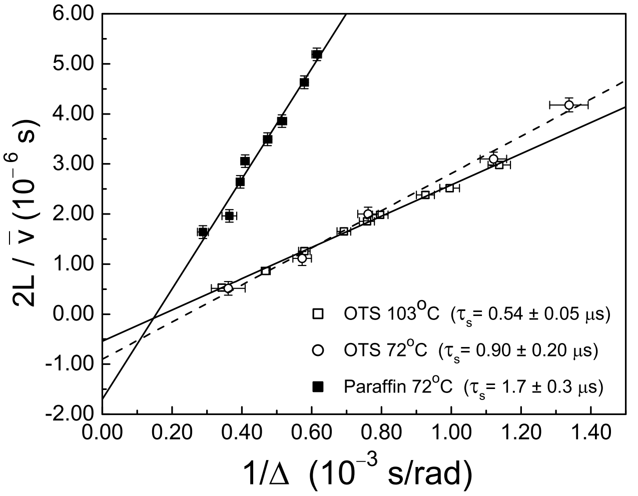

FIG. 10 Representative plots of $2L/\bar{v}$ against $1/\Delta$ for a cell coated with OTS (□) at 103°C, and cells coated with OTS (◯) and paraffin (■) at 72°C. Adapted from Ulanski and Wu, 2011 with the permission of AIP Publishing and Zhao *et al.*, 2009.

C. Average dwell time τ_s' at a given site

While the atoms are adsorbed on the wall, they hop from site to site. The physical reason for this hopping instead of sliding behavior of the adsorbed atoms on the surface is that the adsorption energy E_a at different surface sites tends to be slightly different because of the sightly different atomic environment at different sites. The adsorbed atom hops from a site to a neighboring one whenever its thermal kinetic energy exceeds the difference between the adsorption energies E_a at the two sites. If we let ΔE_a, sometimes referred to as the activation energy, be the average difference of the adsorption energies E_a at neighboring sites, the average dwell time τ_s' at a given site is (de Boer, 1953)

$$\tau_s' = \tau_0'\, e^{-\Delta E_a/kT} \,, \tag{71}$$

where τ_0' is commonly taken to be of the order of the vibration period ($\sim 10^{-12}$ s). The vibration period of an adsorbed atom in the surface potential well is proportional to the square root of the mass of the adsorbed atom, and therefore the vibration period can be an order of magnitude smaller for hydrogen than, for example, for caesium (Goldenberg *et al.*, 1961).

For Rb on paraffin-coated walls it was reported that $\tau_s' = 4 \times 10^{-10}$ s, which is equal to the correlation time τ_c for the magnetic dipole-dipole wall interaction (Bouchiat and Brossel, 1966). This implies that the dipole-dipole interaction at different sites on the wall is not coherent. Physically, this is because of the negligible proton polarization on the paraffin surface.

The potential importance of ΔE_a in the wall interactions of spin-polarized atoms was pointed out in a study by Corsini *et al.* (2013). It was reported that the Zeeman relaxation rate of Rb atoms in cells coated with alkene ($\mathrm{C_nH_{2n}}$) is almost two orders of magnitude smaller than in cells coated with alkane whereas the hyperfine frequency shifts of Rb in alkene- and alkane-coated cells are comparable. Since the hyperfine frequency shift due to wall collisions is proportional to dwell time τ_s, which in turn has an Arrhenius dependence on E_a, it was suggested that the small Zeeman relaxation rate in alkene -coated cells was not owing to a small $|E_a|$ but to a small $|\Delta E_a|$ on alkene-coated walls. Physically, a small $|\Delta E_a|$ would make the motion of the Rb atoms more like sliding on the wall, resulting in a shorter interaction time (τ_s') at each site. Hence a smaller relaxation rate.

VI. ANTI-RELAXATION COATINGS

Experiments involving polarized atoms are usually carried out in glass cells. However, due to the presence of paramagnetic centers on the glass walls, in most applications the inner walls of the cells are coated with anti-relaxation coatings to mitigate the spin relaxation and frequency shift due to the wall collisions.

The most commonly used anti-relaxation coatings are alkanes such as paraffin and silane compounds such as dimethyldichlorosilane, silicone, and OTS. Alkane coating eicosane ($\mathrm{C_{20}H_{42}}$) was first used by Robinson *et al.* (1958). Silane coating dimethyldichlorosilane ($\mathrm{(CH_3)_2SiCl_2}$) was first used by Bouchiat *et al.* (1960) and Alley (1961). The difference between the alkanes and the silane compounds is that the former is physisorbed whereas the latter is chemisorbed on the glass surfaces. Therefore the silane coatings such as OTS can be operated at much higher temperatures up to 170°C than the alkane coatings such as paraffin (Seltzer and Romalis, 2009). The silane compounds tend to polymerize, resulting in a more uniform coating on the glass surface. The outmost layer of both the alkane coatings and the silane coatings is composed of the inert methyl groups $-\mathrm{CH_3}$, which are responsible for the anti-relaxation property of the coatings (Camparo, 1987). The methyl groups $-\mathrm{CH_3}$ do not react chemically with alkali metal atoms, which are physisorbed on these coatings. This is corroborated by x-ray photoelectron spectroscopy, which indicates that there are no Rb−C bonds on the coatings (Seltzer *et al.*, 2010). More recently it was reported that the spin relaxation probability on the alkene that has 20 carbon atoms per molecule is more than one order of magnitude smaller than on the paraffin coating (Balabas *et al.*, 2010; Balabas and Tretiak, 2013). The melting temperature of the alkene coating is 33°C. However, the alkenes with a longer chain ($\sim$ 30 carbon atoms per molecule) can be operated at higher temperatures (> 100°C) but with an anti-relaxation property comparable to OTS (Seltzer *et al.*, 2013). The reason that the unsaturated $\mathrm{C=C}$ bonds result in a much smaller spin relaxation probability is not fully understood.

Cells freshly coated with anti-relaxation coatings often require to be cured. For example, silicone-coated cells are usually baked at 85°C for a few days (Zeng *et al.*, 1985). In paraffin-coated cells filled with Rb, there is no absorption of the D lines until the cells are baked for four to five days at 40°C, after which the coating would reach a stable state (Bouchiat and Brossel, 1966). The anti-relaxation property tends to improve once the cells are cured. For example, the curing process results in a decrease of the wall relaxation rate of Rb hyperfine polarization (Camparo *et al.*, 1987). A closely related phenomenon is that in coated cells the alkali vapor number density is always lower than one would expect from the vapor-liquid equilibrium number density (Bouchiat and Brossel, 1966; Gozzini *et al.*, 1993; Grafström and Suter, 1996a; Meucci *et al.*, 1994; Zeng *et al.*, 1983). The curing process tends to decrease the discrepancy between the alkali vapor density and the saturated number density.

The microscopic nature of the curing process is not completely understood, but the following studies have shed some light on the nature of the curing process. For a freshly prepared dimethyldichlorosilane coating, Camparo *et al.* (1987) showed that the residual silanol groups (Si−OH) were removed from the glass surface by chemical reactions with Rb atoms, making the surface more uniformly covered with the methyl $-\mathrm{CH_3}$ groups and resulting concomitantly in a reduction of Rb vapor number density. Tretiak *et al.* (2016) studied the curing process in the alkene-coated cells using NMR and Raman spectroscopy, and showed that, during the curing process, the alkene molecules, in the presence of the alkali metal (Cs), were converted to trans- and cis-isomers of non-terminal alkene molecules. It is also known that alkali metal atoms diffuse into the coatings (Bouchiat and Brossel, 1966; Liberman and Knize, 1986), which is responsible for the phenomenon of light induced atomic desorption (Gozzini *et al.*, 1993). Diffusion of Rb atoms into OTS coating at 120°C (Rampulla *et al.*, 2009) and into tetracontane at 60°C (Seltzer *et al.*, 2010) was confirmed by x-ray photoelectron spectroscopy. Raman spectra taken at 21°C as a function of the distance from the cell wall in a potassium cell coated with alkene showed that the K atoms permeated through the entire 180 μm-thick alkene coating (Tretiak *et al.*, 2016).

The curing process also happens in bare glass cells.

For example, in bare Pyrex glass cells, the relaxation time for ^{129}Xe can be lengthened by one order of magnitude by exposing the inner cell walls to Rb vapor at 80°C for a few weeks (Zeng *et al.*, 1983). For ^{131}Xe the beat period and relaxation rate in bare Pyrex glass cells reach a value that depends only on the cell geometry and temperature after the cell surface has been exposed to Rb vapor at about 80°C for several days. The curing process in those cells probably corresponds to the inner cell walls being gradually coated by the Rb atoms. This assumption is supported by the observation that the adsorption energy of ^{131}Xe on cured walls is found to be $E_a = -0.03\,\mathrm{eV}$ (Wu *et al.*, 1990), significantly smaller in magnitude than $E_a = -0.3\,\mathrm{eV}$ for xenon on Pyrex glass walls not exposed to alkali metal (Ahrens-Botzong *et al.*, 1973). It is also in agreement with the observation that the adsorption energy for ^{3}He on cesiated Pyrex glass walls is $E_a = -2 \times 10^{-4}\,\mathrm{eV}$ (Tastevin, 1992), much smaller in magnitude than $E_a = -0.01\,\mathrm{eV}$ on Pyrex glass walls not exposed to alkali metal (Fitzsimmons *et al.*, 1969).

A more quantitative study concludes that at 94 °C the inner wall of cured bare Pyrex glass cells that contain Rb metal is covered with 6–7 layers of liquid Rb (Ma *et al.*, 2009). This is consistent with the observation that, unlike the Pyrex glass cells coated with anti-relaxation coatings, the Rb vapor density in bare Pyrex cells is well described by the equilibrium density even in the vicinity ($\sim 10^{-4}\,\mathrm{cm}$) of the cell wall (Zhao *et al.*, 2001).

The presence of a Rb film on the cell wall in cured bare glass cells containing Rb metal also explains why in those cells a Rb atom becomes depolarized in a single wall collision, *i.e.* the relaxation probability per wall collision $\xi_s^B = 1$ (Happer, 1972; Seltzer *et al.*, 2013). In steady state, when a polarized Rb atom collides with the Rb film on the wall, it is replaced by an unpolarized Rb atom released from the film into the gas phase. In contrast, the fact that a Rb atom can collide with the walls in cured paraffin-coated cells many times before losing its polarization clearly indicates that the paraffin -coated walls are not covered with a thin film of Rb even though the Rb atoms diffuse into the paraffin coating (Bouchiat and Brossel, 1966). Physically, this difference most likely appertains to the different adsorption energies of Cs on the bare glass surface and on the paraffin-coated surface (see Table IV).

The following observation seems to suggest that the alkali metal layers on the cured bare glass surface are slightly fragmented, resulting in an incomplete coverage of the cell surface by the alkali metal. The relaxation time T_1 of ^{3}He in bare aluminosilicate glass cells is about one order of magnitude longer than in bare Pyrex glass or fused silica cells, and is about 10% longer in Cs-coated aluminosilicate glass cells than in Cs-coated Pyrex or fused silica cells (Heil *et al.*, 1995). This seems to imply that, to some degree, ^{3}He atoms in Cs-coated cells still come in contact with the glass surface probably because of the incomplete coverage of the glass surface by Cs (Deninger *et al.*, 2006; Heil *et al.*, 1995).

The assumption of the incomplete coverage of the bare glass surface by the alkali metal also seems to be consistent with the observation that $\xi_s^B < 1$ for the alkali metal atoms on the bare glass surface. For example, Grafström and Suter (1996a) studied the Zeeman polarization of Na near the bare glass surface (Sec.IV.D.2). They found $\xi_s^B = 0.47$, which implies that the bare glass surface is not fully covered with Na and that $\xi_s^B < 0.47$ on the parts of the bare glass surface that are not covered with Na. In a study by Horsley *et al.* (2013) the Franzen's "relaxation in the dark" technique was used to perform spatially resolved imaging of T_1 of the hyperfine polarization of Rb in a cell with glass windows and silicon side walls. They deduced that $\xi_s^B = 0.05 \pm 0.01$ for Rb atoms on the silicon wall, which indicates that the silicon wall is partially covered with Rb and that $\xi_s^B < 0.05$ on the parts of the silicon surface that are not covered with Rb. The silicon surface is covered with a thin layer ($\sim 2\,\mathrm{nm}$) of native SiO_2 (Mang *et al.*, 1996), and therefore is similar to the Pyrex glass surface, possessing dangling bond defects. It is not clear why for Rb atoms the relaxation probabilities per wall collision on the silicon surface uncoated with Rb and on the Pyrex glass surface coated with silicone have the same order of magnitude (see Table II).

The curing process was also reported in bare fused silica cells that contain ^{199}Hg (Lehmann and Brossel, 1966). The T_1 and T_2 in a 4 cm cubic fused silica cells increased from $\sim$ 0.1 s to 15 s and 5 s, respectively, after the cell inner surface was exposed to the ^{199}Hg vapor at room temperature for several days. Thus the curing process in the ^{199}Hg cells is different from that in the Rb cells because the curing process in the ^{199}Hg cells leads to a two orders of magnitude increase in the relaxation time T_1 of ^{199}Hg, which clearly is not consistent with the presence of a ^{199}Hg film on the inner cell surfaces. The physics of the curing process in the ^{199}Hg cells is yet to be understood.

The performance of anti-relaxation coatings varies widely. For example, a spin-polarized Rb atom can, on average, collide more than 10^5 times with alkene-coated walls before being depolarized (Balabas *et al.*, 2010; Balabas and Tretiak, 2013). This number goes down to $\sim 10^4$ for cell walls coated with paraffin (Bouchiat and Brossel, 1966), to $\sim 10^3$ for cell walls coated with multilayer OTS (Seltzer *et al.*, 2007; Zhao *et al.*, 2008a) and to $\sim 10^2$ for silicone-coated walls (Zhao *et al.*, 2008a). Despite numerous studies using different techniques (Camparo *et al.*, 1987; Rampulla *et al.*, 2009; Seltzer *et al.*, 2010, 2008; Yi *et al.*, 2008; Zhao and Wu, 2004), the large variation of the anti-relaxation property of these coatings remains to be understood.

The performance of anti-relaxation coatings depends on the coating temperature because the dwell time τ_s depends on the physical state of the coating (Sec. V.B). For example, for rubidium, the reason for the degradation of the performance of paraffin above its melting point 60°C is the increase in τ_s due to the onset of rapid diffusion of Rb into the paraffin.

Even though alkane and silane coatings are very effective for alkali metal and ^{129}Xe, they are not for ^{3}He. In fact, it was reported that uncoated Pyrex glass cells and cells coated with dimethyldichlorosilane yielded the same relaxation time for ^{3}He (Gamblin and Carver, 1965). The most obvious explanation is that the ^{3}He atoms, due to their small size, can readily diffuse through the dimethyldichlorosilane coating and reach the Pyrex glass surface.

In search of effective coatings for ^{3}He to be used in, for example, compressors, neutron spin filters, target cells and others, the relaxation times of ^{3}He have been measured on a wide variety of materials, including semiconductors, metals, salts, oxides and plastics (Deninger *et al.*, 2006; Heil *et al.*, 1999, 1995; Hussey *et al.*, 2005; Katabuchi *et al.*, 2005; Timsit *et al.*, 1971). For example, silicon windows are often used in neutron spin filters because of their high neutron transmission, but the relaxation time T_1 of ^{3}He on the Si surface is more than one order of magnitude shorter than on the aluminosilicate glass surface, and is comparable to that on the Pyrex glass surface (Heil *et al.*, 1999). This is consistent with the observation that the mean twist angle $\langle\theta\rangle$ for the quadrupole wall interaction of ^{131}Xe on the silicon surface is comparable to that on the Pyrex surface (Donley *et al.*, 2009). Physically, this is because of the native SiO_2 layer on the silicon surface. Of all the materials studied, only a handful of them have turned out to be good coatings for ^{3}He. They include diamagnetic metal bismuth, alkali metals, and cesium oxide. For example, a four-fold increase in the relaxation time of ^{3}He was reported in aluminosilicate glass cells coated with bismuth (Heil *et al.*, 1995). The physical reason for the increase in the relaxation time on bismuth is the lack of the s-state coupling between the ^{3}He nuclear spins and the electron spins at the Fermi surface of bismuth, resulting in a small Korringa relaxation rate (Deninger *et al.*, 2006; Slichter, 1980) and also because the metal coatings, due to their compact packing, can prevent ^{3}He atoms from coming in contact with the paramagnetic sites on the glass surface. On the other hand, the relaxation time of ^{3}He on a clean diamagnetic metal mercury surface is about the same as on the Pyrex glass surface (Gamblin and Carver, 1965; Timsit *et al.*, 1971). Alkali metals such as Cs, Rb and K, which in fact in spin exchange optical pumping cells would automatically coat the inner cell walls, are found to be excellent anti-relaxation coatings for ^{3}He. The relaxation time T_1 of ^{3}He was found to be one order of magnitude longer in Cs-coated Pyrex cells than in uncoated Pyrex cells, and a similar increase in T_1 was observed in aluminosilicate glass cells, albeit by a smaller amount (Deninger *et al.*, 2006; Heil *et al.*, 1995). The increase in T_1 in Cs-coated cells is attributed to the exceedingly small magnitude of the adsorption energy E_a of ^{3}He on Cs-coated surface (Heil *et al.*, 1999, 1995), which is the physical reason for the non-wetting of cesium surface by superfluid helium (Nacher and Dupont-Roc, 1991). It was also reported that the relaxation time T_1 for ^{3}He increased by more than one order of magnitude in fused silica cells coated with the suboxide Cs_7O of cesium (Deninger *et al.*, 2006).

It was reported that a relaxation time T_1 close to the gas phase dipole-dipole limit was obtained in a Pyrex glass cell coated with high-purity sol-gel (Hsu *et al.*, 2000). Pyrex glass cells coated with sol-gel have an advantage over the GE180 (boron-free aluminosilicate glass) cells in that the latter produce more neutron background events because of the rich content of barium in the aluminosilicate glass (Ye *et al.*, 2010).

At low temperatures ($\sim 4\,$K) the ^{3}He polarization in uncoated Pyrex glass cells is undetectable due to the long dwell time τ_s on the cell wall and hence the short relaxation time. Probably for the same reason a ^{3}He polarization consistent with zero was reported at $\sim 6\,$K in a target cell made of ultra-pure aluminum (99.999%) (Korsch *et al.*, 1997). However, relaxation times of ^{3}He longer than 2 days were obtained at 4.2 K in a Pyrex glass cell of 3 cm in diameter and coated with solid H_2 film about 30 layers thick (Barbé *et al.*, 1975).

For the relaxation of the hyperfine transitions in the ground state of hydrogen in atomic hydrogen masers, Teflon, a synthetic polymerized fluorocarbon, is often used as the anti-relaxation coating instead of hydrocarbon because of the lower polarizability, the much smaller phase shift $|\phi_{\rm hfs}|$, the considerably smaller wall relaxation rate, and the substantially higher activation energy for surface recombination of H atoms on fluorocarbon than on hydrocarbon surfaces (Kleppner *et al.*, 1962b; Zitzewitz and Ramsey, 1971).

VII. INSTRUMENTATION

Wall interactions of spin-polarized alkali metal atoms are studied by their effect on the polarization of the alkali metal atoms. For noble gas atoms, the effect of wall interactions on their polarization can be studied using NMR techniques such as free induction decay and adiabatic passage or using as a magnetometer the repolarization of the alkali metal atoms through spin exchange interaction with the noble gas atoms. A detailed discussion of monitoring the polarization of alkali metal atoms is given in the classic review by Happer (1972). A brief review was given by Knize *et al.* (1988). Here we will focus on the transmission monitoring, commonly used in the study of wall interactions of polarized atoms, in which the change in the intensity or polarization of the transmitted probe beam is studied.

A. Absorption monitoring

The intensity of the transmitted probe beam is determined by the polarization of the alkali metal vapor, as well as the polarization and spectral profile of the probe beam. If the alkali metal vapor is optically thin and its polarization is uniform along the path length l of the probe beam, the absorption of the probe beam is given by (Bhaskar *et al.*, 1980; Happer, 1972)

$$I_0 - I = I_0 l (k_0 + k_1\, s_z \langle S_z \rangle + k_2 \langle \boldsymbol{S} \cdot \boldsymbol{I} \rangle)\ , \tag{72}$$

where I_0 and I are respectively the intensities of the incident and transmitted probe beams, k_0 is the attenuation coefficient of unpolarized vapor and s_z is the component of the mean photon spin $\boldsymbol{s} = i\boldsymbol{e} \times \boldsymbol{e}^*$, $\boldsymbol{e}$ being the polarization vector of the probe beam. The coefficients k_1 and k_2 represent the contributions from the longitudinal spin polarization $\langle S_z \rangle$ and hyperfine polarization $\langle \boldsymbol{S} \cdot \boldsymbol{I} \rangle$, respectively, and depend on the polarization and spectral profile of the probe beam, which can be chosen to make the absorption signal depend on only one particular type of polarization.

B. Polarization monitoring – Poincaré sphere

Consider an elliptically polarized light beam propagating along the z-axis, which is taken to be horizontal. For convenience, the x- and y-axes are respectively taken to be vertical and horizontal. The polarization of the light can be characterized by two angles, χ and ψ, where χ is the ellipticity defined by $\tan\chi = b/a$ $(-\pi/4 \le \chi \le \pi/4)$, with $2a$ and $2b$ being the major and minor axes of the ellipse, and ψ is the azimuth defined as the angle the major axis makes with the x-axis $(0 \le \psi \le \pi)$. The positive (negative) value of χ corresponds to the positive (negative) helicity of the photons.

The polarization of a light beam is best described using Poincaré sphere, an elegant geometric representation of the polarization of light (Ramachandran and Ramaseshan, 1961). For example, the elliptical polarization of a light beam characterized by χ and ψ is represented by a point P on the Poincaré sphere, with a latitude 2χ and a longitude 2ψ (see Fig. 11). The points on the equator represent linear polarizations $(\chi = 0)$. Thus point V $(\chi = 0,\ \psi = 0)$ represents vertical linear polarization and point H $(\chi = 0,\ \psi = \pi/2)$ horizontal linear polarization. The north pole corresponds to left circular polarization (σ^+ or positive helicity) and the south pole right circular polarization (σ^- or negative helicity).

A polarized alkali metal vapor is birefringent, with left and right circular polarizations being its eigenpolarizations. The change in the polarization of the transmitted probe beam provides a sensitive way to study the polarization of the alkali metal vapor. Here we shall use the Poincaré sphere to illustrate the use of two instruments, photoelastic modulator and Wollaston prism, that are commonly used for measuring the polarization of light. For simplicity we shall assume the probe beam to be linearly polarized along the vertical direction, and therefore is represented by point V $(\chi = 0,\ \psi = 0)$ on the Poincaré sphere. After passing through the polarized alkali metal vapor, it becomes elliptically polarized, characterized by χ and ψ, and is represented by point P on the Poincaré sphere. For a weakly polarized alkali metal vapor, both χ and ψ are very small.

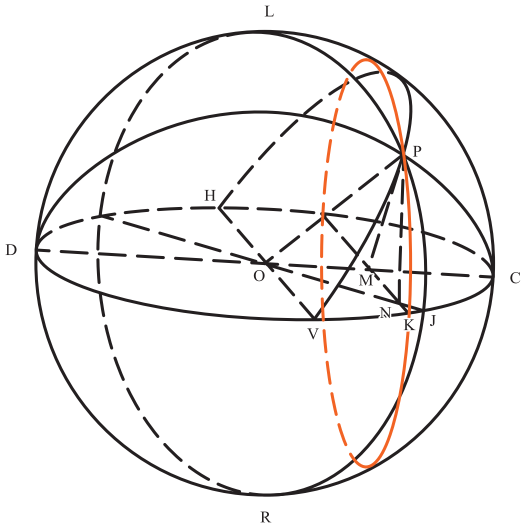

FIG. 11 Poincaré sphere, a sphere of unit radius, as a geometric representation of the polarization of light. Polarization characterized by angles χ and ψ is represented by a point P on the Poincaré sphere, which has a latitude 2χ $(\angle POJ)$ and a longitude 2ψ $(\angle VOJ)$.

1. Photoelastic modulator

A photoelastic modulator is a device that modulates the polarization of an incident beam, and when used in combination with an analyzer, allows phase sensitive detection of the polarization of the incident beam. It is based on photoelastic effect, which refers to the phenomenon, first discovered by Brewster in 1815, that an isotropic transparent material becomes birefringent under mechanical stress. The isotropic optical element used in a photoelastic modulator is typically made of fused silica or crystalline materials with cubic symmetry such as calcium fluoride (CaF_2), and is made to vibrate at its natural resonant frequency Ω, typically several tens of kHz, by a piezoelectric transducer. The periodic compression and stretching of the optical element cause it to be linearly birefringent with its optic axis along the direction of the compression and stretching, and introduce a time-varying phase retardation $\beta \sin\Omega t$ between the two polarizations, one parallel and one perpendicular to the optic axis, where β denotes the magnitude of the retardation. These two polarizations are represented by points C and D on the equator of the Poincare sphere if the optic axis is at 45° with respect to the vertical direction (see Fig. 11).

Geometrically the phase difference $\beta \sin \Omega t$ between the polarizations C and D is equivalent to a rotation of the point P around the axis CD, looking from C to D, clockwise or counterclockwise, depending on whether C lags or leads D, by an angle $\beta \sin \Omega t$, changing $\angle PCV$ to $\angle PCV - \beta \sin \Omega t$. The periodic phase retardation $\beta \sin \Omega t$ between the polarizations C and D causes the point P to move back and forth along the orange small circle in Fig. 11. Let the linear analyzer transmit completely light linearly polarized in the horizontal direction (point H on the equator). It can be shown that the fraction of the intensity I_0 of the probe beam that passes through the analyzer is given by $\cos^2(\widehat{PH}/2)$, where $\widehat{PH}$ is the length of the arc that connects the two points P and H on the Poincare sphere. Since $\widehat{PH} = \pi - \widehat{PV}$, one has $\cos^2(\widehat{PH}/2) = \sin^2(\widehat{PV}/2) = (1 - \cos \widehat{PV})/2$. Using the law of cosines of sides for the spherical triangle $\triangle PCV$, one finds for the intensity of the probe beam after passing through the analyzer

$$I = \frac{I_0}{2}\Big[1 - \cos 2\chi \cos 2\psi \cos(\beta \sin \Omega t) - \sin 2\chi \sin(\beta \sin \Omega t)\Big] \; . \qquad (73)$$

Thus the phase sensitive detection for this configuration measures the ellipticity χ in the first order and the azimuth ψ, sometimes referred to as the Faraday rotation angle, in the second order.

2. Wollaston prism

Wollaston prism is usually made up of two right triangle calcite prisms cemented together on their base. The optic axes of the front and rear prisms are perpendicular to each other, and both are parallel to the front surface of the prism. The calcite crystal is a negative uniaxial crystal with the indices of refraction for ordinary and extraordinary rays being respectively $n_o = 1.6584$ and $n_e = 1.4864$. Suppose the Wollaston prism is oriented such that the optic axis of the front right angle prism is at 45° with respect to the vertical direction. For an elliptically polarized incident beam characterized by χ and ψ, or point P on the Poincaré sphere, the difference between the intensities of the two beams exiting from the Wollaston prism with e- and o-polarizations is $I_e - I_o = I_0 \cos^2(\widehat{PC}/2) - I_0 \cos^2(\widehat{PD}/2)$. Therefore we have

$$I_e - I_o = I_0 \, \cos 2\chi \sin 2\psi \; . \qquad (74)$$

Thus the intensity difference of the two exiting beams is proportional to the first order of the azimuth ψ.

C. Evanescent wave monitoring

Both absorption monitoring and polarization monitoring as described above can also be performed using evanescent waves, which have some advantages in the study of the wall interactions of spin-polarized alkali metal atoms because they only probe the atoms in the vicinity ($\sim 10^{-4}$ cm) of the cell wall.

The evanescent wave is an inhomogeneous wave propagating along the wall. That is, the surfaces of constant amplitude of the wave do not coincide with the surfaces of constant phase. Whereas the former are parallel to, the latter are perpendicular to the wall. The evanescent wave is not transversal. Depending on its polarization, the component of the electric vector in the direction of propagation is not necessarily zero. The polarization of the evanescent wave is in general different from that of the incident wave. For example, while for s-polarized incident wave the evanescent wave is also s-polarized, for p-polarized incident wave the evanescent wave is elliptically polarized in the plane of incidence and thus the electric field vector has a component in the direction of propagation (Born and Wolf, 1980; Józefowski *et al.*, 2007; Kawalec *et al.*, 2007). Therefore s-polarized probe beam is most commonly used. Due to the exceedingly small penetration depth, which is of the order of the wavelength of the probe beam, typically $\sim 10^{-4}$ cm, relatively high alkali metal vapor densities ($> 10^{12}\,\mathrm{cm}^{-3}$) are often used.

VIII. SUMMARY

We have presented a critical review of the studies done in the past six decades of the wall interactions of spin-polarized atoms. The theoretical studies have shown that wall interactions can be described by a boundary condition, which, when combined with the diffusion equation or the Torrey equation, depending on whether the magnetic field is uniform or there is a field gradient, also describes the interplay between wall interactions and diffusion in the gas phase. This boundary value problem has been studied in great detail using different methods. When analytical solutions are not available, perturbation theory or numerical method is used, as demonstrated in the studies of the wall interactions of diamagnetic atoms ($I \geq 1$) and alkali metal atoms. The eigenvalues of the boundary value problem allow the information about the microscopic nature of the walls to be deduced from the experimental data. The real part of the eigenvalue determines the spin relaxation rate and the imaginary part the frequency shift due to wall collisions.

We have reviewed the experimental studies that elucidate the nature of wall interactions on a number of different surfaces. The understanding of the nature of wall interactions helps to determine the physical mechanisms of the spin relaxation and frequency shift due to wall collisions. Studies that determine the microscopic parameters that characterize wall interactions are also described in some detail.

Due to the presence of paramagnetic centers on the glass walls, uncoated glass cells in most cases do not give optimal performance. Various anti-relaxation coatings have therefore been used to coat the inner walls of the cells. Coatings such as alkanes, alkenes and silane compounds are used for spin-polarized alkali metal atoms. Silane coatings such as silicone are commonly used for ^{129}Xe. The most effective and common anti-relaxation coatings for ^{3}He are the alkali metals such as Cs, Rb and K. Other effective anti-relaxation coatings for ^{3}He include bismuth film, suboxide Cs_7O of Cs, and solid H_2 film for low temperatures ($\sim 4\,K$). For the hyperfine polarization of the ground state H atoms in hydrogen masers, fluorocarbon coating is used.

A good understanding of the nature of wall interactions has been achieved on most of the practically important surfaces. For polarized diamagnetic atoms with $^1S_0$ ground states and nuclear spins $I \geq 1$, such as ^{21}Ne ($I = 3/2$), ^{83}Kr ($I = 9/2$), ^{109}Cd ($I = 5/2$), ^{131}Xe ($I = 3/2$), and ^{201}Hg ($I = 3/2$), their dominant wall interaction on the glass surface is the coupling of their nuclear electric quadrupole moment to the electric field gradients on the wall. For ^{129}Xe ($I = 1/2$) on silicone -coated walls the dominant wall interaction is the tensorial magnetic dipole-dipole interaction with the protons on the wall. The dominant wall interaction of spin-polarized ^{3}He ($I = 1/2$) on the glass surface is believed to be the scalar magnetic dipole-dipole interaction between the ^{3}He nuclei and the unpaired electrons in the dangling bond defects although a definite proof is still lacking. For spin-polarized alkali metal atoms on paraffin-coated walls, the wall interactions consist of the magnetic dipole -dipole interaction, both tensorial and scalar, with the protons and the spin-rotation interaction with the carbon atoms on the wall.

In spite of the significant progress, there are still many issues in the wall interactions of spin-polarized atoms that remain to be understood, such as the underlying physics for the orders of magnitude difference in the performance of various anti-relaxation coatings. A good understanding of these issues will help develop optimum coatings with reproducible quality. More studies are needed.

ACKNOWLEDGMENTS

I would like to thank Dr. Will Happer for his invaluable comments. I would also like to acknowledge the support by the Office for Naval Research and the National Science Foundation.

REFERENCES

Abragam, A (1961), *The Principles of Nuclear Magnetism* (Clarendon Press, Oxford).

Adrian, F J (1960), “Matrix effects on the electron spin resonance spectra of trapped hydrogen atoms,” J. Chem. Phys. **32**, 972–981.

Ahrens-Botzong, Rudolf, Peter Hess, and Klausr Schäfer (1973), “Messung der Adsorption von Xenon an Duran und an Gold,” Ber. Bunsenges. Phys. Chem. **77**, 1157–1159.

Albert, M S, G D Cates, B Driehuys, W Happer, B Saam, C S Springer, and A Wishnia (1994), “Biological magnetic resonance imaging using laser-polarized ^{129}Xe,” Nature **370**, 199–201.

Alley, C O (1961), “Wall coatings of alkyl-chloro-silanes for the inhibition of spin relaxation,” in *Advances in Quantum Electronics*, pp. 120–127.

Anderson, L W, F M Pipkin, and J C Baird (1960), “Precision determination of the hyperfine structure of the ground state of atomic hydrogen, deuterium, and tritium,” Phys. Rev. Lett. **4**, 69–71.

Appelt, S, G Wäckerle, and M Mehring (1994), “Deviation from Berry’s adiabatic geometric phase in a ^{131}Xe nuclear gyroscope,” Phys. Rev. Lett. **72**, 3921–3924.

Arditi, M, and T R Carver (1958), “Frequency shift of the zero-field hyperfine splitting of ^{133}Cs produced by various buffer gases,” Phys. Rev. **112**, 449.

Arditi, M, and T R Carver (1961), “Pressure, light, and temperature shifts in optical detection of $0-0$ hyperfine resonance of alkali metals,” Phys. Rev. **124**, 800–809.

Balabas, M V, D Budker, J Kitching, P D D Schwindt, and J E Stalnaker (2006), “Magnetometry with millimeter-scale antirelaxation-coated alkali-metal vapor cells,” J. Opt. Soc. Am. B **23**, 1001–1006.

Balabas, M V, T Karaulanov, M P Ledbetter, and D Budker (2010), “Polarized alkali-metal vapor with minute-long transverse spin-relaxation time,” Phys. Rev. Lett. **105**, 070801.

Balabas, Mikhail Vladlenovich, and O Yu Tretiak (2013), “Comparative study of alkali-vapour cells with alkane-, alkene and 1-nonadecylbenzene-based antirelaxation wall coatings,” Sov. J. Quantum Electron. **43** (12), 1175–1178.

Barbé, R, F Laloë, and J Brosse (1975), “Very long ^{3}He nuclear relaxation times at 4 K using cryogenic coatings,” Phys. Rev. Lett. **34**, 1488–1491.

Bender, C M, and S Boettcher (1998), “Real spectra in non-Hermitian Hamiltonians having PT symmetry,” Phys. Rev. Lett. **80**, 5243–5246.

Bernheim, R A (1962), “Spin relaxation in optical pumping,” J. Chem. Phys. **36**, 135–140.

Bhaskar, N D, M Hou, M Ligare, B Suleman, and W Happer (1980), “Role of Na−Xe molecules in spin relaxation of optically pumped Na in Xe gas,” Phys. Rev. A **22**, 2710–2716.

Bicout, D J, E I Kats, A K Petukhov, and R S Whitney (2013), “Size independence of statistics for boundary collisions of random walks and its implications for spin-polarized gases,” Phys. Rev. Lett. **110**, 010602.

Bloch, D, and M Ducloy (2005), “Atom-wall interaction,” in *Advances in atomic, molecular, and optical physics*, Vol. 50, pp. 91–154.

Boag, S, C Y Jiang, X Tong, and S R Parnell (2014), “Lifetime behaviour and polarization stability in ^{3}He neutron spin filter cells,” in *Journal of Physics: Conference Series*, Vol.

528, p. 012019.

de Boer, J H (1950), in *Advances in Colloid Science*, edited by H. Mark and E. J. W. Verwey.

de Boer, J H (1953), *The Dnamical Character of Adsorption* (Oxford University Press, London).

Böhi, Pascal, Max F Riedel, Theodor W Hänsch, and Philipp Treutlein (2010), "Imaging of microwave fields using ultracold atoms," Appl. Phys. Lett. **97** (5), 051101.

Böhi, Pascal, and Philipp Treutlein (2012), "Simple microwave field imaging technique using hot atomic vapor cells," Appl. Phys. Lett. **101** (18), 181107.

Bonch-Bruevich, A M, Yu M Maksimov, and V V Khromov (1985), "Variation of the absorption spectrum of sodium atoms when they are adsorbed on a sapphire surface," Opt. Spectrosc. (USSR) **58** (6), 854–856.

Born, M, and E Wolf (1980), *Principles of Optics* (Pergamon Press, Oxford).

Bouchiat, M A (1963), "Relaxation magnétique d'atomes de rubidium sur des parois paraffinées," J. Phys. (Paris) **24**, 379–390, 611–621.

Bouchiat, M A, and J Brossel (1966), "Relaxation of optically pumped Rb atoms on paraffin-coated walls," Phys. Rev. **147**, 41–54.

Bouchiat, M A, T R Carver, and C M Varnum (1960), "Nuclear polarization in ^{3}He gas induced by optical pumping and dipolar exchange," Phys. Rev. Lett. **5**, 373–375.

Bouchiat, M A, J Guena, L Hunter, and L Pottier (1982), "Observation of a parity violation in cesium," Phys. Lett. B **117**, 358–364.

Brewer, R G (1963), "Study of atom–wall collisions by optical pumping," J. Chem. Phys. **38**, 3015–3020.

Brinkmann, D, E Brun, and H H Staub (1962), "Kernresonanz im gasformigen Xenon," Helv. Phys. Acta **35**, 431–436.

Brossel, J, J Margerie, and A Kastler (1955), "Augmentation du taux d'orientation atomique de la vapeur de sodium en présence d'hydrogène," C. R. Acad. Sci. Ser. B **241**, 865–867.

Budker, D, L Hollberg, D F Kimball, J Kitching, S Pustelny, and V V Yashchuk (2005), "Microwave transitions and nonlinear magneto-optical rotation in anti-relaxation-coated cells," Phys. Rev. A **71**, 012903.

Budker, D, and M Romalis (2007), "Optical magnetometry," Nature physics **3**, 227–234.

Budker, Dmitry, Wojciech Gawlik, D F Kimball, S M Rochester, V V Yashchuk, and A Weis (2002), "Resonant nonlinear magneto-optical effects in atoms," Rev. Mod. Phys. **74** (4), 1153–1201.

Budker, Dmitry, Valeriy Yashchuk, and Max Zolotorev (1998), "Nonlinear magneto-optic effects with ultranarrow widths," Phys. Rev. Lett. **81** (26), 5788–5791.

Butscher, R, G Wäckerle, and M Mehring (1994), "Nuclear quadrupole interaction of highly polarized gas phase ^{131}Xe with a glass surface," J. Chem. Phys. **100**, 6923–6933.

Butscher, R, G. Wäckerle, and M. Mehring (1996), "Nuclear quadrupole surface interaction of gas phase ^{83}Kr: comparison with ^{131}Xe," Chem. Phys. Lett. **249**, 444–450.

Cagnac, B, and J Brossel (1959), "Orientation nucleaire par pompage optique des isotopes ^{201}Hg et ^{199}Hg et mesure de leurs moments magnetiques par resonance magnetique nucleaire," C. R. Acad. Sci. Ser. B **249**, 77–79.

Cagnac, B, and G Lemeignan (1967), "Relaxation nucleaire de la vapeur de mercure sur des parois en silice," C. R. Acad. Sci. Ser. B **264**, 1850–1853.

Callaghan, P T, A Coy, L C Forde, and C J Rofe (1993), "Diffusive relaxation and edge enhancement in NMR microscopy," J. Magn. Reson. A **101**, 347–350.

Camparo, J C (1987), "Alkali $\langle$S·I$\rangle$ wall relaxation in dichlorodimethylsilane coated resonance cells," J. Chem. Phys. **86**, 1533–1539.

Camparo, J C, R P Frueholz, and B Jaduszliwer (1987), "Alkali reactions with wall coating materials used in atomic resonance cells," J. Appl. Phys. **62**, 676–681.

Campbell, E J, L W Buxton, M R Keenan, and W H Flygare (1981), "^{83}Kr and ^{131}Xe nuclear quadrupole coupling and quadrupolar shielding in KrHCl and XeDCl," Phys. Rev. A **24**, 812–821.

Castner, T, G S Newell, W C Hilton, and C P Slichter (1960), "Note on the paramagnetic resonance of iron in glass," J. Chem. Phys. **32**, 668–673.

Chen, W C, T R Gentile, C B Fu, S Watson, G L Jones, J W McIver, and D R Rich (2011), "Polarized ^{3}He cell development and application at NIST," in *Journal of Physics: Conference Series*, Vol. 294, p. 012003.

Chupp, T E, and R J Hoare (1990), "Coherence in freely precessing ^{21}Ne and a test of linearity of quantum mechanics," Phys. Rev. Lett. **64**, 2261–2264.

Chupp, T E, R J Hoare, R A Loveman, E R Oteiza, J M Richardson, Mark E Wagshul, and A K Thompson (1989), "Results of a new test of local Lorentz invariance: A search for mass anisotropy in ^{21}Ne," Phys. Rev. Lett. **63**, 1541–1544.

Chupp, T E, M E Wagshul, K P Coulter, A B McDonald, and W Happer (1987), "Polarized, high-density, gaseous ^{3}He targets," Phys. Rev. C **36**, 2244–2251.

Cohen-Tannoudji, C (1963), "Relaxation quadrupolaire de l'isotope ^{201}Hg sur des parois de quartz," J. Phys. (Paris) **24**, 653–660.

Cohen-Tannoudji, C, J DuPont-Boc, S Haroche, and F Laloe (1970), "Diverses résonances de croisement de niveaux sur des atomes pompés optiquement en champ nul I. Théorie," Revue de physique appliquée **5**, 95–101.

Cohen-Tannoudji, Claude, Jacques Dupont-Roc, Serge Haroche, and Franck Laloë (1969), "Detection of the static magnetic field produced by the oriented nuclei of optically pumped ^{3}He gas," Phys. Rev. Lett. **22**, 758–760.

Colegrove, F D, L D Schearer, and G K Walters (1963), "Polarization of ^{3}He gas by optical pumping," Phys. Rev. **132**, 2561–2572.

Cornaz, P (1963), "Relaxation nucleaire de l'helium 3 gazeux a la surface du verre pyrex," Phys. Lett. **7**, 123–124.

Corsini, E P, T Karaulanov, M Balabas, and D Budker (2013), "Hyperfine frequency shift and zeeman relaxation in alkali-metal-vapor cells with antirelaxation alkene coating," Phys. Rev. A **87**, 022901.

Coulter, K P, T E Chupp, A B McDonald, C D Bowman, J D Bowman, J J Szymanski, V Yuan, G D Cates, D R Benton, and E D Earle (1990), "Neutron polarization with a polarized ^{3}He spin filter," Nucl. Instrum. Methods Phys. Res. A **288**, 463–466.

Dang, H B, A C Maloof, and M V Romalis (2010), "Ultrahigh sensitivity magnetic field and magnetization measurements with an atomic magnetometer," Appl. Phys. Lett. **97** (15), 151110.

Deninger, A, W Heil, E W Otten, M Wolf, R K Kremer, and A Simon (2006), "Paramagnetic relaxation of spin polarized ^{3}He at coated glass walls," Eur. Phys. J. D **38**, 439–443.

Desaintfuscien, M, J Viennet, and C Audoin (1977), "Discussion of temperature dependence of wall and spin exchange effects in the hydrogen maser," Metrologia **13**, 125.

Donley, E A, J L Long, T C Liebisch, E R Hodby, T A Fisher, and J Kitching (2009), "Nuclear quadrupole resonances in compact vapor cells: The crossover between the NMR and the nuclear quadrupole resonance interaction regimes," Phys. Rev. A **79**, 013420.

Driehuys, B, G D Cates, and W Happer (1995), "Surface relaxation mechanisms of laser-polarized ^{129}Xe," Phys. Rev. Lett. **74**, 4943–4946.

Driehuys, B, G D Cates, W Happer, H Mabuchi, B. Saam, M S Albert, and A Wishnia (1993), "Spin transfer between laser-polarized ^{129}Xe nuclei and surface protons," Phys. Lett. A **184**, 88–92.

Dybowski, C, N Bansal, and T M Duncan (1991), "NMR spectroscopy of xenon in confined spaces: clathrates, intercalates, and zeolites," Annu. Rev. Phys. Chem. **42**, 433–464.

Farooq, Midhat, Timothy Chupp, Joe Grange, Alec Tewsley-Booth, David Flay, David Kawall, Natasha Sachdeva, and Peter Winter (2020), "Absolute magnetometry with ^{3}He," Phys. Rev. Lett. **124**, 223001.

Fitzsimmons, W A, L L Tankersley, and G K Walters (1969), "Nature of surface-induced nuclear-spin relaxation of gaseous ^{3}He," Phys. Rev. **179**, 156–179.

Fitzsimmons, W A, and G K Walters (1967), "Very long nuclear spin relaxation times in gaseous ^{3}He by suppression of ^{3}He-surface interactions," Phys. Rev. Lett. **19**, 943–946.

Foner, S N, E L Cochran, V A Bowers, and C K Jen (1960), "Multiple trapping sites for hydrogen atoms in rare gas matrices," J. Chem. Phys. **32**, 963–971.

Franzen, W (1959), "Spin relaxation of optically aligned rubidium vapor," Phys. Rev. **115**, 850–856.

Gaede, H C, Y Q Song, R E Taylor, E J Munson, J A Reimer, and A Pines (1995), "High-field cross polarization NMR from laser-polarized xenon to surface nuclei," Appl. Magn. Reson. **8**, 373–384.

Gamblin, R L, and T R Carver (1965), "Polarization and relaxation processes in ^{3}He gas," Phys. Rev. **138**, A946–A960.

Gentile, T R, P J Nacher, B Saam, and T G Walker (2017), "Optically polarized ^{3}He," Rev. Mod. Phys. **89**, 045004.

Goldenberg, H M, D Kleppner, and N F Ramsey (1960), "Atomic hydrogen maser," Phys. Rev. Lett. **5**, 361–362.

Goldenberg, H M, D Kleppner, and N F Ramsey (1961), "Atomic beam resonance experiments with stored beams," Phys. Rev. **123**, 530–537.

Gozzini, A, F Mango, J H Xu, G Alzetta, F Maccarrone, and R A Bernheim (1993), "Light-induced ejection of alkali atoms in polysiloxane coated cells," Il Nuovo Cimento D **15**, 709–722.

Gozzini, S, G Nienhuis, E Mariotti, G Paffuti, C Gabbanini, and Moi. L (1992), "Wall effects on light-induced drift," Opt. Commun. **88**, 341–346.

Grafström, S, and D Suter (1995), "Wall relaxation of spin-polarized sodium measured by reflection spectroscopy," Opt. Lett. **20**, 2134–2436.

Grafström, S, and D Suter (1996a), "Interaction of spin-polarized atoms with a surface studied by optical-reflection spectroscopy," Phys. Rev. A **54**, 2169–2179.

Grafström, S, and D Suter (1996b), "Optically enhanced magnetic resonance for the study of atom-surface interaction," Z. Phys. D **38**, 119–132.

Grebenkov, D S (2007), "NMR survey of reflected Brownian motion," Rev. Mod. Phys. **79**, 1077–1137.

Griffith, W C, M D Swallows, T H Loftus, M V Romalis, B R Heckel, and E N Fortson (2009), "Improved limit on the permanent electric dipole moment of ^{199}Hg," Phys. Rev. Lett. **102**, 101601.

Grover, B C (1978), "Noble-gas NMR detection through noble-gas-rubidium hyperfine contact interaction," Phys. Rev. Lett. **40**, 391–392.

Guzman, J S, A Wojciechowski, J E Stalnaker, K Tsigutkin, V V Yashchuk, and D Budker (2006), "Nonlinear magneto-optical rotation and zeeman and hyperfine relaxation of potassium atoms in a paraffin-coated cell," Phys. Rev. A **74**, 053415.

Hallin, A L, F P Calaprice, D W MacArthur, L E Piilonen, M B Schneider, and D F Schreiber (1984), "Test of time-reversal symmetry in the β decay of ^{19}Ne," Phys. Rev. Lett. **52**, 337–340.

Happer, W (1972), "Optical pumping," Rev. Mod. Phys. **44**, 169–249.

Happer, W, E Miron, S Schaefer, D Schreiber, W A van Wijngaarden, and X Zeng (1984), "Polarization of the nuclear spins of noble-gas atoms by spin exchange with optically pumped alkali-metal atoms," Phys. Rev. A **29**, 3092–3110.

Hartmann, S, and E L Hahn (1962), "Nuclear double resonance in the rotating frame," Phys. Rev. **128**, 2042–2053.

Heil, W, J Dreyer, D Hofmann, H Humblot, E Lelievre-Berna, and F Tasset (1999), "^{3}He neutron spin-filter," Physica B **267**, 328–335.

Heil, W, H Humblot, E Otten, M Schafer, R Sarkau, and M Leduc (1995), "Very long nuclear relaxation times of spin polarized helium 3 in metal coated cells," Phys. Lett. A **201**, 337–343.

Herman, R M (1965), "Theory of spin exchange between optically pumped rubidium and foreign gas nuclei," Phys. Rev. **137**, A1062–A1065.

Hochstrasser, G, and J F Antonin (1972), "Surface states of pristine silica surfaces: I. ESR studies of E_s' dangling bonds and of CO_2-adsorbed radicals," Surf. Sci. **32**, 644–664.

Horsley, A, G X Du, M Pellaton, C Affolderbach, G Mileti, and P Treutlein (2013), "Imaging of relaxation times and microwave field strength in a microfabricated vapor cell," Phys. Rev. A **88**, 063407.

Hsu, M F, G D Cates, I Kominis, I A Aksay, and D M Dabbs (2000), "Sol-gel coated glass cells for spin-exchange polarized ^{3}He," Appl. Phys. Lett. **77**, 2069–2071.

Hunt, E R, and H Y Carr (1963), "Nuclear magnetic resonance of ^{129}Xe in natural xenon," Phys. Rev. **130**, 2302–2305.

Hussey, Daniel S, D R Rich, A S Belov, X Tong, H Yang, C Bailey, C D Keith, J Hartfield, G D R Hall, Timothy C Black, W M Snow, T R Gentile, W C Chen, G L Jones, and E Wildman (2005), "Polarized ^{3}He gas compression system using metastability-exchange optical pumping," Rev. Sci. Instrum. **76**, 053503.

Hutanu, V, and A Rupp (2005), "Research on ^{3}He spin filter cells made of quartz glass," Physica B **356**, 91–95.

Hutanu, V, A Rupp, J Klenke, W Heil, and J Schmiedeskamp (2007a), "Magnetization of ^{3}He spin filter cells," J. Phys. D: Appl. Phys. **40** (15), 4405–4412.

Hutanu, V, B A Ruppa, and T Sander-Thömmes (2007b), "SQUID measurements of remanent magnetisation in refillable ^{3}He spin-filter cells (SFC)," Physica B **397**, 185–187.

Ishikawa, K, B Patton, Y Y Jau, and W Happer (2007), "Spin transfer from an optically pumped alkali vapor to a solid," Phys. Rev. Lett. **98**, 183004.

Jacob, R E, B Driehuys, and B Saam (2003), "Fundamental mechanisms of ^{3}He relaxation on glass," Chem. Phys. Lett. **370**, 261–267.

Jacob, R E, S W Morgan, B Saam, and J C Leawoods (2001), "Wall relaxation of ^{3}He in spin-exchange cells," Phys. Rev. Lett. **87**, 143004.

Jacob, R E, J Teter, B Saam, W C Chen, and T R Gentile (2004), "Low-field orientation dependence of ^{3}He relaxation in spin-exchange cells," Phys. Rev. A **69**, 021401(R).

Jochemsen, H, M Morrow, A J Berlinsky, and W N Hardy (1981), "Interaction of hydrogen atoms with helium films: Sticking probabilities for H on ^{3}He and ^{4}He, and the binding energy of H on ^{3}He," Phys. Rev. Lett. **47**, 852–855.

Jones, G L, T R Gentile, A K Thompson, Z Chowdhuri, M S Dewey, W M Snow, and F E Wietfeldt (2000), "Test of ^{3}He-based neutron polarizers at NIST," Nucl. Instrum. Methods Phys. Res. A **440**, 772–776.

Józefowski, L, J Fiutowski, T Kawalec, and H Rubahn (2007), "Direct measurement of the evanescent-wave polarization state," J. Opt. Soc. Am. B **24**, 624–628.

Julsgaard, Brian, Jacob Sherson, J Ignacio Cirac, Jaromír Fiurášek, and Eugene S Polzik (2004), "Experimental demonstration of quantum memory for light," Nature **432** (7016), 482–486.

Kastler, A (1950), "Quelques suggestions concernant la production optique et la détection optique d'une inégalité de population des niveaux de quantifigation spatiale des atomes. Application à l'expérience de stern et gerlach et à la résonance magnétique," J. Phys. Radium **11**, 255–265.

Katabuchi, T, S Buscemi, J M Cesaratto, T B Clegg, T V Daniels, M Fassler, R B Neufeld, and S Kadlecek (2005), "Spin-exchange optically pumped polarized ^{3}He target for low-energy charged particle scattering experiments," Rev. Sci. Instrum. **76**, 033503.

Kawalec, T, L Józefowski, J Fiutowski, M J Kasprowicz, and T Dohnalik (2007), "Spectroscopic measurements of the evanescent wave polarization state," Opt. Commun. **274**, 341–346.

Kennard, E H (1938), *Kinetic Theory of Gases* (McGraw-Hill, New York).

Kitano, M, M Bourzutschky, F P Calaprice, J Clayhold, W Happer, and M Musolf (1986), "Measurement of magnetic dipole moments of $^{129}\mathrm{Xe}^{\mathrm{m}}$ and $^{131}\mathrm{Xe}^{\mathrm{m}}$ by spin exchange with optically pumped Rb," Phys. Rev. C **34**, 1974–1979.

Kitching, J (2018), "Chip-scale atomic devices," Appl. Phys. Rev. **5**, 031302.

Kitching, John, Svenja Knappe, and Elizabeth A Donley (2011), "Atomic sensors–a review," IEEE Sensors Journal **11** (9), 1749–1758.

Kleppner, D, H M Goldenberg, and N F Ramsey (1962a), "Properties of the hydrogen maser," Appl. Opt. **1**, 55–60.

Kleppner, D, H M Goldenberg, and N F Ramsey (1962b), "Theory of the hydrogen maser," Phys. Rev. **126**, 603–615.

Knappe, Svenja, Vishal Shah, Peter D D Schwindt, Leo Hollberg, John Kitching, Li-Anne Liew, and John Moreland (2004), "A microfabricated atomic clock," Appl. Phys. Lett. **85** (9), 1460–1462.

Knize, R J, Z Wu, and W Happer (1988), "Optical pumping and spin exchange in gas cells," in *Advances in atomic and molecular physics*, Vol. 24, pp. 223–267.

Kominis, I K, T W Kornack, J C Allred, and Michael V Romalis (2003), "A subfemtotesla multichannel atomic magnetometer," Nature **422** (6932), 596–599.

Korsch, W, R W Carr, D DeSchepper, A Dvoredsky, L H Kramer, Y Li, R D McKeown, R G Milner, S F Pate, M L Pitt, and T Shin (1997), "Temperature dependence of ^{3}He polarization in aluminum storage cells," Nucl. Instrum. Methods Phys. Res., Sect. A **389**, 389–397.

Kuzmich, A, L Mandel, and N P Bigelow (2000), "Generation of spin squeezing via continuous quantum nondemolition measurement," Phys. Rev. Lett. **85**, 1594–1597.

Kwon, T M, J G Mark, and C H Volk (1981), "Quadrupole nuclear spin relaxation of ^{131}Xe in the presence of rubidium vapor," Phys. Rev. A **24**, 1894–1903.

Lamoreaux, S K, J P Jacobs, B R Heckel, FJ Raab, and E N Fortson (1986), "New limits on spatial anisotropy from optically-pumped ^{201}Hg and ^{199}Hg," Phys. Rev. Lett. **57**, 3125–3128.

Leduc, M, and J Brossel (1968), "Comparative study of relaxation on silica walls of nuclei of ^{109}Cd and ^{111}Cd oriented by optical pumping," C. R. Acad. Sci. Ser. B **266**, 287–290.

Lefevre-Seguin, V, and J Brossel (1988), "Attempts to increase the nuclear relaxation time of a ^{3}He gas at low temperatures," J. Low Temp. Phys. **72**, 165–188.

Lefevre-Seguin, V, P J Nacher, J Brossel, W N Hardy, and F Laloë (1985), "Relaxation nucléaire de ^{3}He gazeux sur H_2 solide," J. Phys. (Paris) **46**, 1145–1172.

Lehmann, J C, and J Brossel (1966), "Etude comparee de la relaxation sur des parois de silice datomes de mercure et de cadmium orientes nucleairement par pompage optique," C. R. Acad. Sci. Ser. B **262**, 624–627.

Liberman, V, and R Knize (1986), "Relaxation of optically pumped Cs in wall-coated cells," Phys. Rev. A **34**, 5115–5118.

Ma, J, A Kishinevski, Y Y Jau, C Reuter, and W Happer (2009), "Modification of glass cell walls by rubidium vapor," Phys. Rev. A **79**, 042905.

Mang, K M, Y Khang, Y J Park, Y Kuk, S M Lee, and C C Williams (1996), "Direct imaging of SiO_2 thickness variation on Si using modified atomic force microscope," J. Vac. Sci. Technol. B **14**, 1536–1539.

Masnou-Seeuws, F, and M A Bouchiat (1967), "Theoretical study of the relaxation of alkali atoms by collisions against a wall and with a gas," J. Phys. (Paris) **28**, 406–420.

Mathur, B S, H. Tang, and W Happer (1968), "Light shifts in the alkali atoms," Phys. Rev. **171**, 11–19.

Matthey, A P M, J T M Walraven, and I F Silvera (1981), "Measurement of pressure of gaseous $H_\downarrow$: Adsorption energies and surface recombination rates on helium," Phys. Rev. Lett. **46**, 668–671.

Mazitov, R K, P Diehl, and R Seydoux (1993), "Nuclear magnetic resonance of ^{3}He dissolved in vitreous silica," Chem. Phys. Lett. **201**, 543–549.

Meucci, M, E Mariotti, P Bicchi, C Marinelli, and L Moi (1994), "Light-induced atom desorption," Europhys. Lett. **25**, 639.

Middleton, Hunter, Robert D Black, Brian Saam, Gordon D Cates, Gary P Cofer, Robert Guenther, William Happer, Lawrence W Hedlund, G Alan Johnson, Kim Juvan, and John Swartz (1995), "MR imaging with hyperpolarized ^{3}He gas," Magn. Reson. Med. **33**, 271–275.

Morrow, M, R Jochemsen, A J Berlinsky, and W N Hardy (1981), "Zero-field hyperfine resonance of atomic hydrogen for $0.18 \le T \le 1$ K: The binding energy of H on liquid ^{4}He," Phys. Rev. Lett. **46**, 195–198.

Müller, D (1965), "Messung der Verweilzeit von He-Atomen an Glasoberflächen," Z. Phys. **188**, 326–338.

Nacher, P J, and J Dupont-Roc (1991), "Experimental evidence for nonwetting with superfluid helium," Phys. Rev. Lett. **67**, 2966–2969.

Newbury, N R, A S Barton, P Bogorad, G D Cates, M Gatzke, H Mabuchi, and B Saam (1993a), "Polarization-dependent frequency shifts from Rb –^{3}He collisions," Phys. Rev. A **48**, 558–568.

Newbury, N R, A S Barton, G D Cates, W Happer, and H Middleton (1993b), "Gaseous ^{3}He –^{3}He magnetic dipolar spin relaxation," Phys. Rev. A **48**, 4411–4420.

Nicol, A T (1984), "Effect of several surface treatments on xenon nuclear polarization and relaxation in optically pumped Rb – Xe systems," Phys. Rev. B **29**, 2397–2403.

Parnell, S R, E Babcock, K Nünighoff, M W A Skoda, S Boag, S Masalovich, W C Chen, R Georgii, J M Wild, and C D Frost (2009), "Study of spin-exchange optically pumped ^{3}He cells with high polarisation and long lifetimes," Nucl. Instrum. Methods Phys. Res., Sect. A **598**, 774–778.

Petit, P, M Desaintfuscien, and C Audoin (1980), "Temperature dependence of the hydrogen maser wall shift in the temperature range 295 – 395 K," Metrologia **16**, 7–14.

Phillips, G C, R R Perry, P M Windham, G K Walters, L D Schearer, and F D Colegrove (1962), "Demonstration of a polarized ^{3}He target for nuclear reactions," Phys. Rev. Lett. **9**, 502–504.

Pütz, B, D Barsky, and K Schulten (1992), "Edge enhancement by diffusion in microscopic magnetic resonance imaging," J. Magn. Reson. **97**, 27–53.

Raftery, D, H Long, T Meersmann, P J Grandinetti, L Reven, and A Pines (1991), "High-field nmr of adsorbed xenon polarized by laser pumping," Phys. Rev. Lett. **66**, 584–587.

Rahman, C, and H G Robinson (1987), "Rb 0 – 0 hyperfine transition in evacuated wall-coated cell at melting temperature," IEEE J. Quantum Electron. **23**, 452–454.

Ramachandran, G N, and S Ramaseshan (1961), *Handbuch der Physik. Vol. XXV/1*, edited by S. Flugge (Springer-Ver1ag, Berlin).

Rampulla, D M, N Oncel, E Abelev, Y W Yi, S Knappe, and S L Bernasek (2009), "Effects of organic film morphology on the formation of Rb clusters on surface coatings in alkali metal vapor cells," Appl. Phys. Lett. **94**, 041116.

Rich, D R, T R Gentile, T B Smith, A K Thompson, and G L Jones (2002), "Spin exchange optical pumping at pressures near 1 bar for neutron spin filters," Appl. Phys. Lett. **80**, 2210–2212.

Robinson, H G, E S Ensberg, and H G Dehmelt (1958), "Preservation of spin state in free atom-inert surface collisions," Bull. Am. Phys. Soc **3**, 9.

Robinson, H G, and C E Johnson (1982), "Narrow ^{87}Rb hyperfine-structure resonances in an evacuated wall-coated cell," Appl. Phys. Lett. **40** (9), 771–773.

Rosenberry, M A, and T E Chupp (2001), "Atomic electric dipole moment measurement using spin exchange pumped masers of ^{129}Xe and ^{3}He," Phys. Rev. Lett. **86**, 22–25.

Saam, B, N Drukker, and W Happer (1996), "Edge enhancement observed with hyperpolarized ^{3}He," Chem. Phys. Lett. **263**, 481–487.

Salhi, Z, E Babcock, P Pistel, and A Ioffe (2014), "^{3}He neutron spin filter cell development program at JCNS," in *J. Phys. Conf. Ser.*, Vol. 528, p. 012015.

Sands, R H (1955), "Paramagnetic resonance absorption in glass," Phys. Rev. **99**, 1222–1226.

Savukov, Igor M, S J Seltzer, M V Romalis, and K L Sauer (2005), "Tunable atomic magnetometer for detection of radio-frequency magnetic fields," Phys. Rev. Lett. **95**, 063004.

Schaden, M, K F Zhao, and Z Wu (2007), "Effects of diffusion and surface interactions on the line shape of electron paramagnetic resonances in the presence of a magnetic field gradient," Phys. Rev. A **76**, 062502.

Schaden, M, K F Zhao, and Z Wu (2008), "Erratum: Effects of diffusion and surface interactions on the line shape of electron paramagnetic resonances in the presence of a magnetic field gradient [Phys. Rev. A **76**, 062502 (2007)]," Phys. Rev. A **77**, 049903.

Schaefer, S R, G D Cates, Ting-Ray Chien, D Gonatas, W Happer, and T G Walker (1989), "Frequency shifts of the magnetic-resonance spectrum of mixtures of nuclear spin-polarized noble gases and vapors of spin-polarized alkali-metal atoms," Phys. Rev. A **39**, 5613–5623.

Schaefer, S R, G D Cates, and W Happer (1990), "Determination of spin-exchange parameters between optically pumped rubidium and ^{83}Kr," Phys. Rev. A **41**, 6063–6070.

Schmiedeskamp, J, W Heil, E W Otten, R K Kremer, A Simon, and J Zimmer (2006a), "Paramagnetic relaxation of spin polarized ^{3}He at bare glass surfaces," Eur. Phys. J. D **38**, 427–438.

Schmiedeskamp, Jörg, H-J Elmers, W Heil, EW Otten, Yu Sobolev, W Kilian, H Rinneberg, T Sander-Thömmes, F Seifert, and J Zimmer (2006b), "Relaxation of spin polarized ^{3}He by magnetized ferromagnetic contaminants," Eur. Phys. J. D **38**, 445–454.

Schori, C, B Julsgaard, J L Sørensen, and E S Polzik (2002), "Recording quantum properties of light in a long-lived atomic spin state: Towards quantum memory," Phys. Rev. Lett. **89**, 057903.

Schwindt, Peter D D, Svenja Knappe, Vishal Shah, Leo Hollberg, John Kitching, Li-Anne Liew, and John Moreland (2004), "Chip-scale atomic magnetometer," Appl. Phys. Lett. **85**, 6409–6411.

Seltzer, S J, M A Bouchiat, and M V Balabas (2013), "Surface coatings for atomic magnetometry,".

Seltzer, S J, P J Meares, and M V Romalis (2007), "Synchronous optical pumping of quantum revival beats for atomic magnetometry," Phys. Rev. A **75**, 051407.

Seltzer, S J, D J Michalak, M H Donaldson, M V Balabas, S K Barber, S L Bernasek, M A Bouchiat, A Hexemer, A M Hibberd, D FJ Kimball, C Jaye, T Karaulanov, F A Narducci, S A Rangwala, H G Robinson, A K Shmakov, D L Voronov, V V Yashchuk, A Pines, and D Budker (2010), "Investigation of antirelaxation coatings for alkali-metal vapor cells using surface science techniques," J. of Chem. Phys. **133**, 144703.

Seltzer, S J, D M Rampulla, S Rivillon-Amy, Y J Chabal, S L Bernasek, and M V Romalis (2008), "Testing the effect of surface coatings on alkali atom polarization lifetimes," J. Appl. Phys. **104**, 103116.

Seltzer, S J, and M V Romalis (2009), "High-temperature alkali vapor cells with antirelaxation surface coatings," J. Appl. Phys. **106**, 114905.

Silvera, I F, and J T M Walraven (1980), "Spin-polarized atomic deuterium: stabilization, limitations on density, and adsorption energy on helium," Phys. Rev. Lett. **45**, 1268–1271.

Simpson, J H (1978), "NMR frequency splitting of ^{201}Hg signals due to collisions with a fused silica surface," Bull. Am. Phys. Soc. **23**, 394–395.

Skalla, J, G Wäckerle, and M Mehring (1997), "Optical magnetic resonance imaging of atomic diffusion and laser beam spatial profiles," Opt. Comm. **143**, 209–213.

Slichter, C P (1980), *Principles of Magnetic Resonance* (Springer-Verlag, Berlin).

Song, Y Q, B M Goodson, B Sheridan, T M de Swiet, and A Pines (1998), "Effects of diffusion on magnetic resonance imaging of laser-polarized xenon gas," J. Chem. Phys. **108**, 6233–6239.

Steinberg, M, and B Manowitz (1959), "Recovery of fission product noble gases," Ind. Eng. Chem. **51**, 47–50.

Stephens, M, R Rhodes, and C Wieman (1994), "Study of wall coatings for vapor-cell laser traps," J. Appl. Phys. **76**, 3479–3488.

Stoller, S D, W Happer, and F J Dyson (1991), "Transverse spin relaxation in inhomogeneous magnetic fields," Phys. Rev. A **44**, 7459–7477.

de Swiet, T (1995), "Diffusive edge enhancement in imaging," Journal of Magnetic Resonance, Series B **109**, 12–18.

de Swiet, T, and P Sen (1994), "Decay of nuclear magnetization by bounded diffusion in a constant field gradient," J. Chem. Phys. **100**, 5597–5604.

Tastevin, G (1992), "Investigation of adsorption and wetting of ^{3}He on cesium and cesiated glass," J. of Low Temp. Phys. **89**, 669–672.

Timsit, R S, J M Daniels, and A D May (1971), "Nuclear relaxation of ^{3}He gas on various solid surfaces," Can. J. Phys. **49**, 560–575.

Torrey, H C (1956), "Bloch equations with diffusion terms," Phys. Rev. **104**, 563–565.

Tretiak, O Yu, J W Blanchard, D Budker, P K Olshin, S N Smirnov, and M V Balabas (2016), "Raman and nuclear magnetic resonance investigation of alkali metal vapor interaction with alkene-based anti-relaxation coating," J. Chem. Phys. **144**, 094707.

Tseng, C H, G P Wong, V R Pomeroy, R W Mair, D P Hinton, D Hoffmann, R E Stoner, F W Hersman, D G Cory, and R L Walsworth (1998), "Low-field MRI of laser polarized noble gas," Phys. Rev. Lett. **81**, 3785–3788.

Ulanski, E, and Z Wu (2011), "Measurement of dwell times of spin polarized rubidium atoms on octadecyltrichlorosilane- and paraffin-coated surfaces," Appl. Phys. Lett. **98**, 201115.

Ulanski, E, and Z Wu (2014), "Observation of large frequency shifts of the electron paramagnetic resonance of ^{87}Rb atoms due to collisions with cell walls coated with RbH salt," Phys. Rev. A **89**, 053431.

Vanier, J, and C Audoin (1989), *The quantum physics of atomic frequency standards* (Adam Hilger, Bristol).

Vanier, Jacques, Jean-F Simard, and Jean-S Boulanger (1974), "Relaxation and frequency shifts in the ground state of ^{85}Rb," Phys. Rev. A **9**, 1031–1040.

Vasilakis, G, J M Brown, T W Kornack, and M V Romalis (2009), "Limits on new long range nuclear spin-dependent forces set with a K$-^3$He comagnetometer," Phys. Rev. Lett. **103**, 261801.

Vold, T G, F J Raab, B Heckel, and E N Fortson (1984), "Search for a permanent electric dipole moment on the ^{129}Xe atom," Phys. Rev. Lett. **52**, 2229–2232.

Volk, C H, T M Kwon, J G Mark, Y B Kim, and J C Woo (1980), "Measurement of the Rb$-^{131}$Xe spin-exchange cross section in ^{131}Xe relaxation studies," Phys. Rev. Lett. **44**, 136.

Volk, C H, J G Mark, and B Grover (1979), "Spin dephasing of ^{83}Kr," Phys. Rev. A **20**, 2381–2388.

Walker, T (1989), "Estimates of spin-exchange parameters for alkali-metal–noble-gas pairs," Phys. Rev. A **40**, 4959–4964.

Walker, T, and W Happer (1997), "Spin-exchange optical pumping of noble-gas nuclei," Rev. Mod. Phys. **69**, 629–642.

Walker, T G, K Bonin, and W Happer (1987), "Electron–noble-gas spin-flip scattering at low energy," Phys. Rev. A **35**, 3749–3752.

Walter, D K, W M Griffith, and W Happer (2002), "Magnetic slowing down of spin relaxation due to binary collisions of alkali-metal atoms with buffer-gas atoms," Phys. Rev. Lett. **88**, 093004.

Walters, G K, F D Colegrove, and L D Schearer (1962), "Nuclear polarization of ^{3}He gas by metastability exchange with optically pumped metastable ^{3}He atoms," Phys. Rev. Lett. **8**, 439–442.

Watanabe, S F, and H G Robinson (1977), "Motional narrowing of zeeman resonance lineshapes. I. Theoretical development," J. Phys. B **10**, 931–939.

Wu, Z, W Happer, and J Daniels (1987), "Coherent nuclear-spin interactions of adsorbed ^{131}Xe gas with surfaces," Phys. Rev. Lett. **59**, 1480–1483.

Wu, Z, W Happer, M Kitano, and J Daniels (1990), "Experimental studies of wall interactions of adsorbed spin-polarized ^{131}Xe nuclei," Phys. Rev. A **42**, 2774–2784.

Wu, Z, S Schaefer, G D Cates, and W Happer (1988), "Coherent interactions of the polarized nuclear spins of gaseous atoms with the container walls," Phys. Rev. A **37**, 1161–1175.

Wu, Z, T G Walker, and W Happer (1985), "Spin-rotation interaction of noble-gas alkali-metal atom pairs," Phys. Rev. Lett. **54**, 1921–1924.

Ye, Q, G Laskaris, W Chen, H Gao, W Zheng, X Zong, T Averett, G D Cates, and W A Tobias (2010), "A high-pressure polarized ^{3}He gas target for nuclear-physics experiments using a polarized photon beam," Eur. Phys. J. A **44**, 55–61.

Yi, Y W, H G Robinson, S Knappe, J E Maclennan, C D Jones, C. Zhu, N A Clark, and J Kitching (2008), "Method for characterizing self-assembled monolayers as antirelaxation wall coatings for alkali vapor cells," J. Appl. Phys. **104**, 023534.

van Yperen, G H, A P M Matthey, J T M Walraven, and I F Silvera (1981), "Adsorption energy and nuclear relaxation of $H_\downarrow$ on ^{3}He$-^4$He mixtures," Phys. Rev. Lett. **47**, 800–803.

Zeng, X, E Miron, W A Van Wijngaarden, D Schreiber, and W Happer (1983), "Wall relaxation of spin polarized ^{129}Xe nuclei," Phys. Lett. A **96**, 191–194.

Zeng, X, Z Wu, T Call, E Miron, D Schreiber, and W Happer (1985), "Experimental determination of the rate constants for spin exchange between optically pumped K, Rb, and Cs atoms and ^{129}Xe nuclei in alkali-metal–noble-gas van der waals molecules," Phys. Rev. A **31**, 260–278.

Zhao, K, and Z Wu (2003), "Hyperfine polarization and its normal gradient coefficient of ^{87}Rb atoms in the vicinity ($\sim 10^{-5}$cm) of coated and uncoated pyrex glass surfaces," Phys. Rev. Lett. **91**, 113003.

Zhao, K, and Z Wu (2004), "Mapping surfaces using regionally specific hyperfine polarization," Phys. Rev. A **70**, 010901.

Zhao, K, and Z Wu (2005), "Regionally specific hyperfine polarization of Rb atoms in the vicinity ($\sim 10^{-5}$cm) of surfaces," Phys. Rev. A **71**, 012902.

Zhao, K, Z Wu, and H M Lai (2001), "Optical determination of alkali metal vapor number density in the vicinity ($\sim 10^{-5}$cm) of cell surfaces," J. Opt. Soc. Am. B **18**, 1904–

1910.

Zhao, K F, M Schaden, and Z Wu (2008a), "Method for measuring surface-interaction parameters of spin-polarized Rb atoms on coated pyrex glass surfaces using edge enhancement," Phys. Rev. A **78** (3), 034901.

Zhao, K F, M Schaden, and Z Wu (2008b), "Nonperturbative broadening of paramagnetic resonance lines by transverse magnetic field gradients," Phys. Rev. A **78**, 013418.

Zhao, K F, M Schaden, and Z Wu (2009), "Method for measuring the dwell time of spin-polarized Rb atoms on coated pyrex glass surfaces using light shift," Phys. Rev. Lett. **103** (7), 073201.

Zhao, K F, M Schaden, and Z Wu (2010), "Enhanced magnetic resonance signal of spin-polarized Rb atoms near surfaces of coated cells," Phys. Rev. A **81**, 042903.

Zhao, K F, and Z Wu (2006), "Evanescent wave magnetometer," Appl. Phys. Lett. **89**, 261113.

Zitzewitz, P W, and N F Ramsey (1971), "Studies of the wall shift in the hydrogen maser," Phys. Rev. A **3**, 51–61.